The University Of Sheffield.

White Rose Mechanistic Biology DTP

Universities of Leeds, Sheffield & York

Dissecting the Interplay between TREX and the N^6-methyladenosine Epitranscriptomic Machinery

Simon Lesbirel

A thesis submitted in partial fulfilment of the requirements for the degree of Doctor of Philosophy

The Department of Molecular Biology and Biotechnology

The University of Sheffield

Sheffield

United Kingdom

Acknowledgements

First and foremost I would like thank my supervisor Professor Stuart Wilson for giving me the opportunity to work within his group. I am grateful of the support and advice offered over the course of my project. I also extend great thanks to Dr Ian Sudbury and Matt Parker for providing all the bioinformatics analysis throughout this project.

I would also like to thank the people I have had the pleasure of sharing my time in the lab with over the past four years, Arthur, Marcus, Cath, Victoria, Janet, James, Dani and ~~llewylwn~~ ~~llwellyn~~ Llywelyn. We formed a number of world leading clubs, most notably the award winning gin club with expertise and experience in over 100 gins. Yet this was not our greatest achievement, the formation of PCRcelona a football team built on the triangle ethos consistently ending the league in the top 3. I would also like to extend my gratitude to Dr Nicolas Vipakone. The experimental and lifestyle advices he offered helped greatly throughout this work, although not always followed. Thanks guys, you made the past 4 years a fantastic experience.

Who could forget Abbie Cooke sticking by me for over 7 years whilst at Sheffield and not getting bored. Thank you for providing me with a great deal of happiness over the years and also the occasional payday treat. Finally, I am greatly indebted to my Mum who has provided a great deal of support throughout my life and education. I cannot thank her enough for all of her help over the years.

Cheers.

Table of Contents

List of Abbreviations

AP	-	Alkaline Phosphatase
ATP	-	Adenosine triphosphate
Bp	-	Base pair
CBC	-	Cab binding complex
CC	-	Control siRNA cytoplasmic cell fraction
CN	-	Control siRNA nuclear cell fraction
Co-IP	-	Co immunoprecipitation
DNA	-	Deoxyribonucleic acid
EJC	-	Exon junction complex
GDP	-	Guanosine-5'-diphosphate
GTP	-	Guanosine-5'-triphosphate
iCLIP	-	Individual nucleotide resolution crosslinking-Immunoprecipitation
m^{6}A	-	N^6-Methyladenosine
m^{6}am	-	*N*^{6},2′-*O*-dimethyladenosine
m^{6}A-RIP SEQ	-	m^{6}A RNA immunoprecipitation sequencing
m^{7}G	-	7-methylguanosine
mRNA	-	Messenger ribonucleic acid
mRNP	-	Messenger ribonucleoparticle
Nt	-	Nucleotide
PABP	-	PolyA binding protein
PAR-CLIP	-	Photoactivatable ribonucleoside-enhanced crosslinking-Immunoprecipitation
RISC	-	RNA induced silencing complex
RNAi	-	RNA interference
rRNA	-	Ribosomal ribonucleic acid

RIP	-	RNA immunoprecipitation
RIP-SEQ	-	RNA immunoprecipitation sequencing
snRNA	-	Small nuclear ribonucleic acid
TREX	-	Transcription export complex
tRNA	-	Transfer ribonucleic acid
siRNA	-	Small interfering RNA
VMN	-	Kiaa1429(Virilizer)/Mettl3 siRNA nuclear cell fraction
VMC	-	Kiaa1429(Virilizer)/Mettl3 siRNA cytoplasmic cell fraction
VWN	-	Kiaa1429(Virilizer)/Wtap siRNA nuclear cell fraction
VWC	-	Kiaa1429(Virilizer)/Wtap siRNA cytoplasmic cell fraction

Abstract

N^6-methyladenosine (m^6A) is an abundant internal modification of eukaryotic mRNA. Recently the details of the methyladenosine pathway and function have been unravelled. Methylation occurs via a Writer complex consisting of Wtap, Kiaa1429 and Mettl3/14. The final components of the pathway are Reader proteins, Ythdc1 in the nucleus and Ythdf1/2/3 in the cytoplasm. Methylation readers can cause mRNA destabilisation, cap-independent translation and alter alternative splice site selection. Perturbation of the m^6A writers and erasers can result in mRNA nuclear export phenotypes, though the molecular basis for this phenotype was unknown.

Here we show the m^6A writer complex and reader (Ythdc1) associates with TREX and within this complex, Wtap and Kiaa1429 are essential for the interaction. This association leads to loading of TREX onto m^6A modified mRNAs. Knockdown of Wtap and Kiaa1429 leads to inefficient TREX loading and nuclear export of m^6A modified mRNAs, whereas non-methylated mRNA export is unaffected. This observation extends transcriptome wide with transcripts harbouring greater m^6A more susceptible to nuclear accumulation upon Wtap/Kiaa1429 knockdown. Further evidence of a cooperative pathway between m^6A machinery and TREX was identified with the reader Ythdc1.

Chapter 1: Introduction

The central dogma of eukaryotic gene expression states that DNA is transcribed to RNA, in the nucleus, and subsequently translated to protein in the cytoplasm. Therefore, a core step within gene expression is the export of mature mRNA from the nucleus to the cytoplasm. Progression of an mRNA through the maturation pathway is coupled with strict surveillance mechanisms, successful processing grants a licence allowing nuclear export of the molecule. Intertwined with these maturation steps is the deposition of the Transcription export (TREX) complex. The mature mRNA is escorted through the nuclear pore loaded with TREX and bound by the heterodimeric export receptor Nxf1:p15.

The details of epitranscriptomic regulation upon mRNA maturation have recently come to light, and play an essential role in maintaining and transcribing a specific subset of mRNAs. Methyladenosine (m^6A) is one of the most prevalent chemical modification on mammalian mRNA. The addition of this modification can result in multiple outcomes for individual mRNAs, such as alternative splicing, degradation and increased translational initiation.

1.1 The Nuclear Pore Complex

In eukaryotic cells RNAs, proteins and ribonucleoprotein (RNP) particles are exported through large (125MDa with a 125nm diameter) aqueous channels known as the nuclear pore complexes (NPC). These multimeric complexes are embedded in a double nuclear membrane/nuclear envelope and facilitate nucleocytoplasmic transport. The NPC is a dynamic macromolecular structure that consists of multiple copies of around 30 different proteins, referred to as nucleoporins (Nups), present in multiple copies totalling to 500-1000 Nups per NPC (Cronshaw *et al.*, 2002). The Nups create distinct structural elements, illustrated in Figure 1.1, that form the overall NPC. These elements are defined as

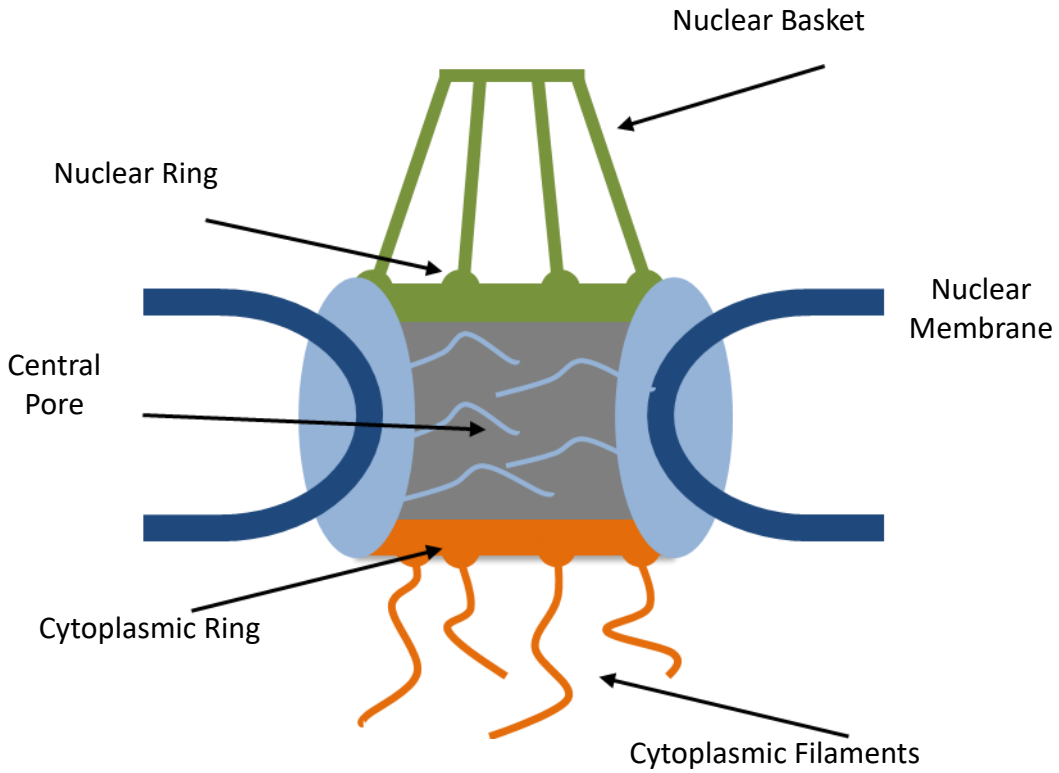

Figure 1.1 The nuclear pore complex (NPC). The NPC is constructed from 30 different proteins, known as Nups. These Nubs form distinct structural elements, an inner pore, nuclear basket and cytoplasmic filaments.

an inner pore ring, nuclear basket and an intrinsically discorded, highly flexible cytoplasmic domain (classically referred to as cytoplasmic filaments) (Fahrenkrog and Aebi, 2003; Beck and Hurt, 2016). Nups can be categorised into three functional groups, pore membrane Nups, used to anchor the NPC to the nuclear envelope, FG Nups containing short hydrophobic stretches rich in phenylalanine and glycine residues. A final class of Nups acts in an architectural role, providing stable folded protein domains (Tran *et al*., 2006; Amlacher *et al*., 2011).

Interactions between the NPC and cargo receptors facilitate transport through the pore. More specifically transport receptors, also known as karyopherins, interact with FG nucleoporins. Evidence for this interaction was generated by crystal structures illustrating FG peptides in complex with multiple transport receptors (Bayliss *et al*., 2002). Upon FG interactions the cargo must translocate the NPC, currently three models exists to describe this action, the Brownian affinity-gating model, the affinity gradient model and the selective phase model (Hülsmann *et al*., 2012). The selective phase model dictates that permeability barriers are generated due to FG Nups self-interaction. This model is akin to a sieve, it allows selective translocation of transport receptors and cargo upon their binding to FG peptides. The energy for translocation is provided by a small Ras-related GTPase, Ran, that exists in two states GTP bound and GDP bound.

1.2 RanGTP/GDP Nuclear Translocation Cycle

The RanGTP/GDP system drives the nucleocytoplasmic shuttling of macromolecules in conjunction with a superfamily (21 members) of mobile transport receptors (Moore and Blobel, 1994; Görlich *et al*., 1997). The general consensus dictates karyopherins responsible for import of cargo to the nucleus are called importins, and karyopherins responsible for exporting cargo are exportins. A short peptide is employed for karyopherin cargo recognition, a nuclear localisation signal (NLS) or nuclear export signal (NES) (Güttler and Görlich, 2011).

The Karyopherins are regulated by Ran, a small GTPase. Ran exists in two states GTP bound within the nucleus and GDP bound in the cytoplasm (Deursen, *et al.*, 1997; Görlich *et al.*, 1997). The cell actively maintains a gradient of each Ran state. Maintenance of this gradient requires the action of two Ran activating proteins. RanGTP undergoes cytoplasmic hydrolysis via RanGAP (Ran GTPase activating protein) conversely nuclear RanGDP exchanges GDP for GTP once acted upon by RanGEF (guanosine exchange factor) (Pemberton *et al*., 1998). The paradigm, depicted in Figure 1.2, states importins form a receptor-cargo dimer in the cytoplasm prior to commencing NPC translocation. Once in the nucleus importins interact with RanGTP inducing a reduced binding affinity for their cargo and subsequent dissociation (Floer *et al*., 1997). Ran dependent nuclear export occurs with the initial formation of a trimeric complex, consisting of exportin-RanGTP-cargo. The whole complex translocates the NPC into the cytoplasm where association with RanGAP concludes in GTP hydrolysis and dissociation of the complex (Kutay *et al.*, 1997).

RanGTP export is required for the export of multiple RNA species. snRNA, rRNA, tRNA and miRNA all require RanGTP:Exportin for their export (Pemberton, *et al*., 1998; Güttler and Görlich, 2011). However the bulk of spliced and intronless mRNA nuclear export undergoes Ran independent export. Spliced mRNA export is mediated by the nuclear export factor Nxf1 and is regulated via a myriad of mRNA processing protein factors (Hautbergue *et al.*, 2008). The array of RNA export pathways is displayed in Figure 1.3.

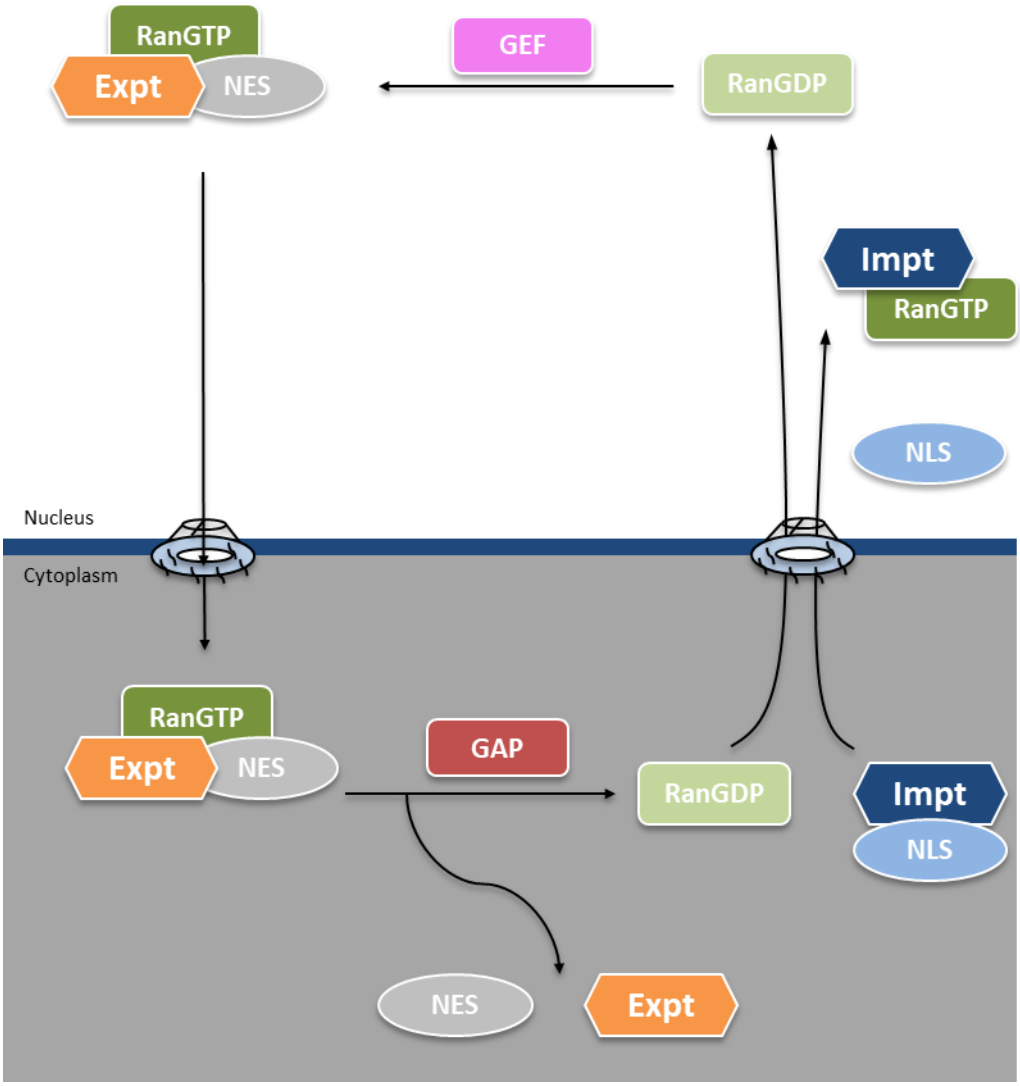

Figure 1.2 The Ran GTP cycle. The energy for nuclear export and import is provided by a RanGTP gradient. Nuclear export receptors (Orange) associate with RanGTP and their NES containing cargo prior to export. Conversely nuclear import receptors (Navy) form a dimer with their NLS containing cargo. RanGTP is hydrolysed in the cytoplasm by Ran GTPase activating protein (Red). GDP-GTP exchange occurs in the nucleolus facilitated by Ran guanosine exchange factor (Pink).

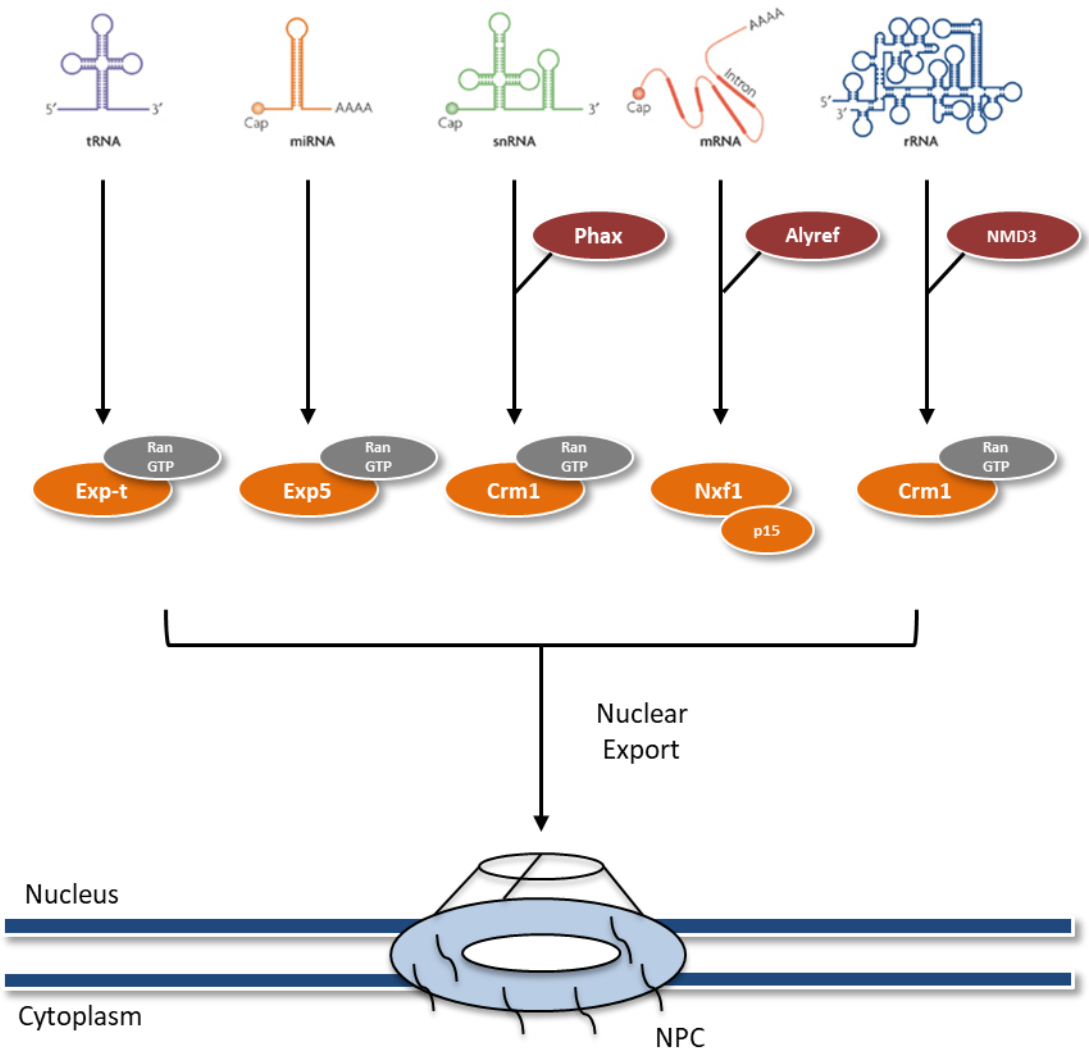

Figure 1.3 RNA nuclear export pathways. The major factors for each RNA export pathway. Export adaptors (Red), export receptors (Orange) and RanGTP (Grey). The bulk of mRNA export does not require RanGTP for nuclear translocation. Diagram adapted from (Köhler & Hurt 2007).

1.2.1 Crm-1 Pathway

The karyopherin Chromosome Region Maintenance 1 (Crm-1) interacts with RanGTP in the nucleus and is responsible for the passage of multiple RNA species, these include ribosomal RNAs (rRNA) and several U small nuclear RNAs (snRNA). Crm1 does not bind RNA cargo directly but acts in conjunction with export adapter proteins. The association of Crm1 and export adaptors is dependent on a leucine rich NES (Fornerod *et al.*, 1997).

Spliceosomal snRNAs require the export adapter Phosphorylated adapter for RNA export (PHAX) (Segref *et al*., 2001). The initial phase of snRNA biogenesis requires precursor synthesis using RNA polymerase II, note this is for U1, U2, U4 and U5, U6 is synthesised in a RNA polymerase III manner and does not participate in nuclear export for complete maturation. Post synthesis the pre-snRNAs associate with their export adapter PHAX, this enables targeting of Crm1 to the 5' cap binding complex (CBC). The heterodimeric complex Crm1:pre-snRNA:PHAX also associates with RanGTP, facilitating nuclear translocation. There are no direct RanGTP-cargo contacts, yet it is required to drive Crm1 complex formation. Upon entering the cytoplasm dephosphorylation of PHAX and hydrolysis of RanGTP results in dissociation of the complex (Segref *et al*., 2001). Survival of motor neurons (SMN) complex facilitates the maturation of the snRNAs prior to their nuclear import. The reasons for exporting snRNAs for maturation are not entirely clear, however it is reasonable to assume it acts as a failsafe therefore preventing a build-up of non-functioning snRNA within the nucleus.

Crm1 also acts as the receptor for the export of ribosomal subunits 40S and 60S. rRNAs are synthesised as a large pre-rRNA by RNA polymerase I, subsequent processing yields three mature rRNAs (28S, 18S and 5.8S). Once processed, rRNAs associate with ribosomal proteins forming the 60S and 40S subunits (Zemp and Kutay, 2007). Export of the 60S subunit, but not the 40S, requires Nmd3, an adapter protein which contains two C-terminal NES peptides. Nmd3 is essential for the final stages of 60S biogenesis and Crm1 interaction (Trotta *et al.*, 2003). However, multiple 60S maturation factors have been implicated in its export.

Current literature implicates the zinc-finger protein Bud20 (Baßler *et al.*, 2012), Mex67 (yeast homologue of Nxf1) in direct surface binding of 60S and facilitation of its export. A recent maturation protein Arx1 has been identified binding the Phe-Gly repeats of FG nucleoporins (Bradatsch *et al.*, 2007). Although it does not look like a typical export receptor its presence in 60S export is required. The 40S pre-ribosomal subunit is also exported in a Crm1 dependant manner but requires a different set of maturation-complex proteins for export (Faza *et al.*, 2012).

The final Crm1 dependant species of RNA to be exported is small subsets of mRNAs containing 3' AU-rich element (ARE). The ARE element indirectly interacts with two proteins, Pp32 and APRIL. These two proteins contain multiple NESs, complexing with Crm1 and leading to export (Brennan *et al.*, 2000)

1.2.3 Exportin-t

The export of tRNAs is co-ordinated via a Karyopherin family member exportin-t and RanGTP. Initially RNA polymerase III synthesises tRNAs as large precursors that undergo multiple processing steps, trimming of the 5' and 3' ends, base modifications and removal of a short intron if present (Lipowsky *et al.*, 1999). These maturation steps culminate in a complex clover leaf structure.

Post maturation, the process of exporting tRNA begins with exportin-t which forms a trimeric complex with its tRNA cargo and Ran-GTP. The formation of the heterotrimeric complex requires a conformational change within exportin-t that is triggered upon RanGTP binding (Arts *et al.*, 1998). The distinctive shape and charge of a tRNA molecule is needed for recognition, however the hypervariable and anticodon loops are not part of this recognition process as they can differ greatly between tRNAs. This secondary structure recognition mechanism means the NES of a tRNA is not constructed from a primary peptide motif but by its secondary and tertiary structure. Recognition of the structural NES acts as a quality control step, ill-formed or incomplete tRNAs will not display the correct NES therefore exportin-t will not bind (Cook *et al.*, 2005). Further checking

of complete and correct maturation exists in the binding affinity of exportin-t to modified and unmodified tRNA, binding to modified is 10 times greater than unmodified (Lipowsky *et al.*, 1999).

The tRNA-exportin-t-RanGTP shuttles to the cytoplasm and again activation of Ran's GTPase activity causes hydrolysis of GTP and subsequent dissociating of the complex releasing tRNA into the cytoplasm. It is worth noting that exportin-t may not be the sole pathway for tRNA export. For example yeast Los1, the exporting-t orthologue, is not essential for viability (Hellmuth *et al.*, 1998). A recent genome-wide *Saccharomyces cerevisiae* screen revealed the karyopherin Crm1/Xpo1 as members of the Ran GTPase-dependent nuclear export pathway for tRNAs (Wu *et al.*, 2015).

1.2.4 Exportin-5

Exportin-5 is required for the nuclear export of precursor-micro RNAs (pre-miRNAs). Initially RNA polymerase II synthesises primary miRNAs (pri-miRNA), followed by 5' capping and polyadenylation. Nuclear processing of the pre-miRNAs via Drosha, a type III nuclear RNase, and an RNA binding protein Dgcr8 yields a ~70bp double stranded loop pre-miRNA. Dgcr8 is thought to act as a molecular ruler, measuring the precise position for Drosha to act. A typical pre-miRNA consists of a 2 nucleotide overhang at the 3'end (Bartel, 2004). The processed pre-miRNA is the target for exportin-5. The 2 nucleotide overhang is essential for exportin-5 recognition of a processed miRNA whilst 5' overhangs result in impaired exportin-5 binding (Lund *et al.*, 2004). Exportin-5 binds 16 nucleotides of the double stranded pre-mRNA, the complex is locked together upon RanGTP binding to the N-terminal Ran-binding interface of exportin-5 (Okada *et al.*, 2009). Truncated processed miRNAs ≤14 nucleotides in length do not bind exportin-5 efficiently. The trimeric complex acts to protect the pre-miRNA from degradation (Yi *et al.*, 2003). Once exported to the cytoplasm and post Ran GTP hydrolysis and release of the pre-miRNA, it undergoes further maturation steps resulting in a ~22

nucleotide single stranded miRNA. Association of the Pre-miRNA with the RNA induced silencing complex (RISC) complex helps unwind the duplex to generate the 22 nucleotide ssRNA required to carry out post translational gene regulation. (Bartel *et al*., 2004).

Exportin-5 has also been implicated in an auxiliary tRNA export pathway (Calado *et al*., 2002). Comparisons of the RNA binding interface of exportin5 and exportin-t revealed a 2 fold greater RNA interaction site for exportin-5. The functional consequence results in flexible cargo recognition allowing double stranded RNA with varied stem loop structures and extrusions to become export targets (Okada *et al.*, 2009).

1.3 mRNA Maturation and Nuclear Export

The bulk of mRNA export is undertaken in a Ran-independent manner via the transcription export complex (TREX) and the heterodimeric export receptor Nxf1-p15. RNA Polymerase II synthesises pre-mRNA that is then subject to multiple co- and post-transcriptional processing events, such as 5' capping, splicing and 3' polyadenylation (Shatkin and Manley, 2000). The culmination of these maturation events grants an export license to the mRNA allowing export receptor guided nuclear pore translocation.

The initial addition of the 5' m^7guanasine (m^7G) cap onto nascent pre-mRNAs protects them from the action of 5'-3' exonucleases (Shatkin and Manley, 2000). Moreover the m^7G cap confers binding of Cbp80 and Cbp20 that form the cap-binding complex (CBC). The action of CBC binding allows for deposition of TREX components onto the 5' end of the mRNA (Reed and Hurt, 2002; Cheng *et al.*, 2006).

Pre-mRNAs containing introns undergo co- and post-transcriptional splicing. During transcription, spliceosome assembly begins with U1 small nuclear RNA complex association with the 5' splice site followed by U2 and U4,5,6 small nuclear ribonucleoprotein complex's (snRNPs) (Lacadie and Rosbash, 2005). The

subsequent excision of introns and fusing of exons results in the formation of an exon junction complex (EJC) upon the exon-exon boundary. The EJC associates with TREX subunits whilst TREX member Uap56 is involved in spliceosome assembly (M. Luo *et al.*, 2001; Gromadzka *et al.*, 2016).

Polyadenylation of pre-mRNAs at the 3' terminus is another maturation event that commits the mRNA for nuclear export. A hexanucleotide cleavage signal is bound by cleavage and polyadenylation factors responsible for removal of the downstream RNA (Proudfoot *et al.,* 1977; West, Gromak and Proudfoot, 2004). Post cleavage, PolyA polymerase catalysis the addition of adenosine repeats upon the 3' terminal cleaved mRNA. The adenosine repeats are then bound by polyadenine binding proteins (PABP), again protecting the mRNA from degradation by 3'-5' exonuclease (Libri *et al.*, 2002). The combination of these processing events leads to the formation of a correctly packaged messenger ribonucleoparticle (mRNP) that contains all the licencing signals for nuclear pore translocation orchestrated by Nxf1-p15.

1.3.1 The Transcription Export Complex (TREX)

Akin to the spliceosome, the TREX complex undergoes multiple conformational and compositional changes. TREX is conserved from yeast to humans and is required for messenger ribonucleoprotein particles (mRNP) nuclear export (Reed and Hurt., 2002; Strässer *et al.*, 2002). At the core of the TREX complex sits the multimeric THO complex comprised of Thoc1-Thoc7 (metazoans) and Dead box RNA helicase, Uap56 (Masuda *et al.,* 2005; Chi *et al.*, 2013).

Export adapters Alyref, UIF and LuzP4 aid in the loading and handover of the packaged mRNA to the nuclear export receptor Nxf1 (Viphakone *et al.*, 2012) (Hautbergue *et al.*, 2009). Co adapters, Chtop and Thoc5, also play a role in Nxf1 loading (Chang *et al.*, 2013). Several new TREX subunits, Cip29, Erh, Skar, Elg and Zc3h11a, have also recently been identified (Dufu *et al.*, 2010). Elg is also known

as Ncbp3 and is implicated in the export of mRNA under stress conditions (Gebhardt *et al.*, 2015)

With the current known constituents the export of the mRNP is as follows; 1.Co-transcriptional deposition of the TREX complex during the maturation of a pre-mRNA (Luo *et al.*, 2001). 2. Once complete recruitment of TREX has occurred adapter and co-adapter proteins interact with Nxf1-p15. 3. The mRNA is handed over to the Nxf1-p15 dimer as a result of a conformational change induced via adapter and co adapter binding (Hautbergue *et al.*, 2009; Viphakone *et al*., 2012; Herold *et al.*, 2001). Upon handover Uap56 is displaced form the mRNA. 4. Subsequent interaction of mRNA-Nxf1-p15 with the TREX-2 complex and nucleoporins, facilitates translocation through the nuclear pore. 5. During translocation export adapters are released from the mRNP. See Figure 1.4 for an illustration of the above process.

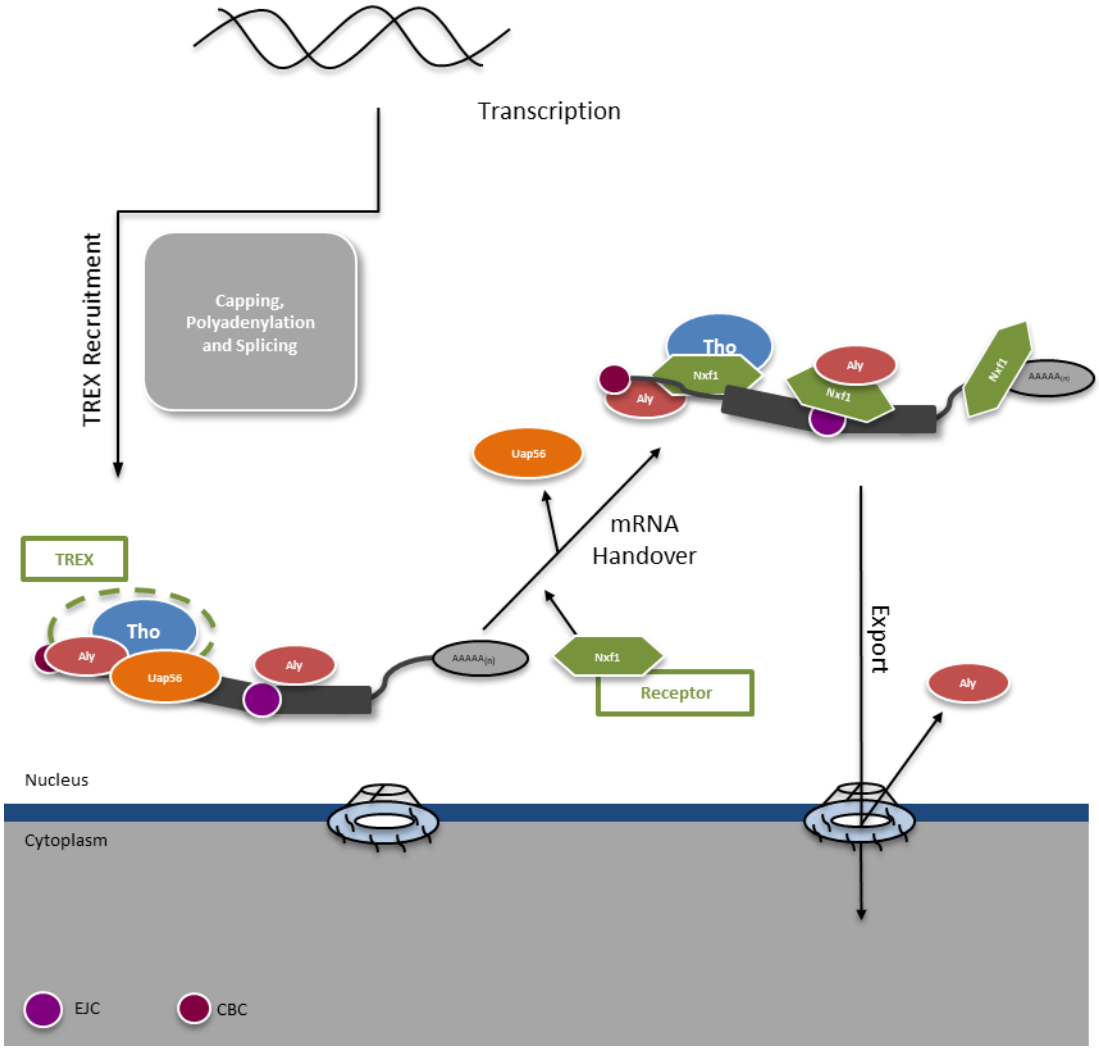

Figure 1.4 mRNA export. The mRNA export pathway. The TREX complex is recruited during processing/maturation of the pre-mRNA. Following maturation TREX recruits the heterodimeric export receptor Nxf1-p15. An mRNA hand over event occurs, displacing Uap56, following an Nxf1 conformational change. The mRNP is then shuttled to the nuclear pore were it is guided to the cytoplasm.

1.3.2 Export Adaptors and Co-adaptors

A key stage in export of the mRNP is the handover of the mRNA to the export receptor Nxf1-p15. However Nxf1 has a low RNA binding affinity, therefore export adaptors/ co-adaptors are required to induce an intramolecular conformational change increasing Nxf1 affinity for mRNA.

Alyref is recruited to the mRNP via Uap56 during splicing in an ATP dependent manner (Masuda *et al.*, 2005; Dufu *et al.*, 2010). It contains two Uap56-binding motifs (UBM) at its N and C-terminus. The core of the adapter consist of an RNA recognition motif and a principle RNA binding site, constructed from two disordered arginine rich regions (Gromadzka *et al.*, 2016). The arginine rich regions are also the Nxf1 binding site. The recruitment of Nxf1-p15 to the mRNP occurs via its N-terminal domain binding to Alyref and the Nxf1 NTF2 like domain binding to a co-adaptor such as Thoc5 or Chtop. The Alyref-coadaptor-Nxf1-p15 complex has a ~10 fold greater RNA binding affinity compared with Nxf1-p15, thereby initiating the handover of RNA from the adaptor/co-adaptor proteins to Nxf1 (Hautbergue *et al.*, 2008). Further studies have also implicated arginine methylation within the RNA binding regions of Alyref reducing its binding affinity form RNA, aiding in the Nxf1 mRNA hand over process (Hung *et al.*, 2010).

Uap56 interacting factor (UIF) is a second export adapter that contains a UBM. Although UIF interacts with Alyref, the interaction is RNA-dependent, therefore it has been theorised UIF may exist in an alternative TREX complex populating the same mRNA as an Alyref containing TREX. UIF recruitment to the mRNA differs to that of Alyref. The FACT chromatin remodelling complex is required for the co-transcriptional loading of UIF but not Alyref. Furthermore the knockdown of Uap56 has a drastic effect on Alyref mRNA loading but a lesser phenotype was observed for UIF mRNA deposition (Hautbergue *et al.*, 2009). The RNAi of Alyref results in a modest block of mRNA nuclear export, this could be due to the functional redundancy between export adapters. The knock down of both adapter proteins (UIF and Alyref) leads to a catastrophic mRNA export block resulting in cell death (Hautbergue *et al.*, 2009).

A third export adaptor, Luzp4, is a cancer testis antigen – a group of proteins normally restricted to testis which are commonly upregulated in cancer cells. Luzp4 displays the classical adapter characteristics mentioned above, contains a UBM and Nxf1-p15s mRNA binding affinity increases upon association. It was identified that efficient growth of melanoma cells requires Luzp4 (Viphakone *et al.*, 2015). Members of the serine/arginine (SR) rich family of proteins can act as a mRNA export adaptor when in a hypophosphorylated state (Muller-McNicoll *et al.*, 2016).

Thoc5 and Chtop have been identified as co-adaptor proteins binding to an NTF2-like domain of Nxf1 (Katahira *et al.*, 2009; Chang *et al.*, 2013). The co-adaptors bind to Nxf1 co-operatively with Alyref. It is also worth noting that Chtop and Thoc5 bind to Nxf1 in a mutually exclusive manner, competing for the NTF2-like domain (Chang *et al.*, 2013). The presence of multiple adaptors and co-adaptors illustrates the dynamic changes and redundancy within the TREX complex dependent mRNA export pathway.

1.3.3 Nxf1-p15 Export receptor

The major export receptor for mRNA nuclear export is Nxf1-p15. Nxf1 is constructed form five distinct domains (depicted in Figure 1.5), RNA binding domain (RBD), pseudo-RNA recognition motif (ΨRRM), leucine rich region (LRR), NTF2-like (NTF2L) domain and ubiquitin associated domain (UBA) (Liker *et al.*, 2000). The receptor heterodimer is found associated with the same mRNA as TREX complex (Sträßer and Hurt, 2000). This association is vital for the recruitment of Nxf1 (Hautbergue *et al.*, 2008). An N-terminal arginine rich RBD is responsible for Nxf1 RNA recognition, however it shows no sequence specificity (Zolotukhin *et al.*, 2002). To prevent the export of non-/incorrectly processed mRNA Nxf1 sequesters its own RNA binding action via intramolecular association of the NTF2L and RBD (Viphakone *et al.*, 2012). Therefore an mRNA is only handed to Nxf1 once inhabited by the TREX complex. The mRNA handover is conducted via export

adaptors binding RBD and ΨRRM whilst export co-adaptors associate with the NTF2L domain (Figure 1.5) (Viphakone *et al.*, 2012). The association of TREX components releases the RBM increasing Nxf1 binding affinity for the mRNA. Nxf1-p15 escorts the mRNA to the nuclear pore where it interacts with nucleoporins via NTF2L and Ubiquitin associated domain on its C-terminus. p15 is essential for the stabilisation of NTF2L and its interaction with NPC members, RNAi of p15 results in nuclear accumulation of mRNA (Braun *et al.*, 2001; Fribourg *et al.*, 2001).

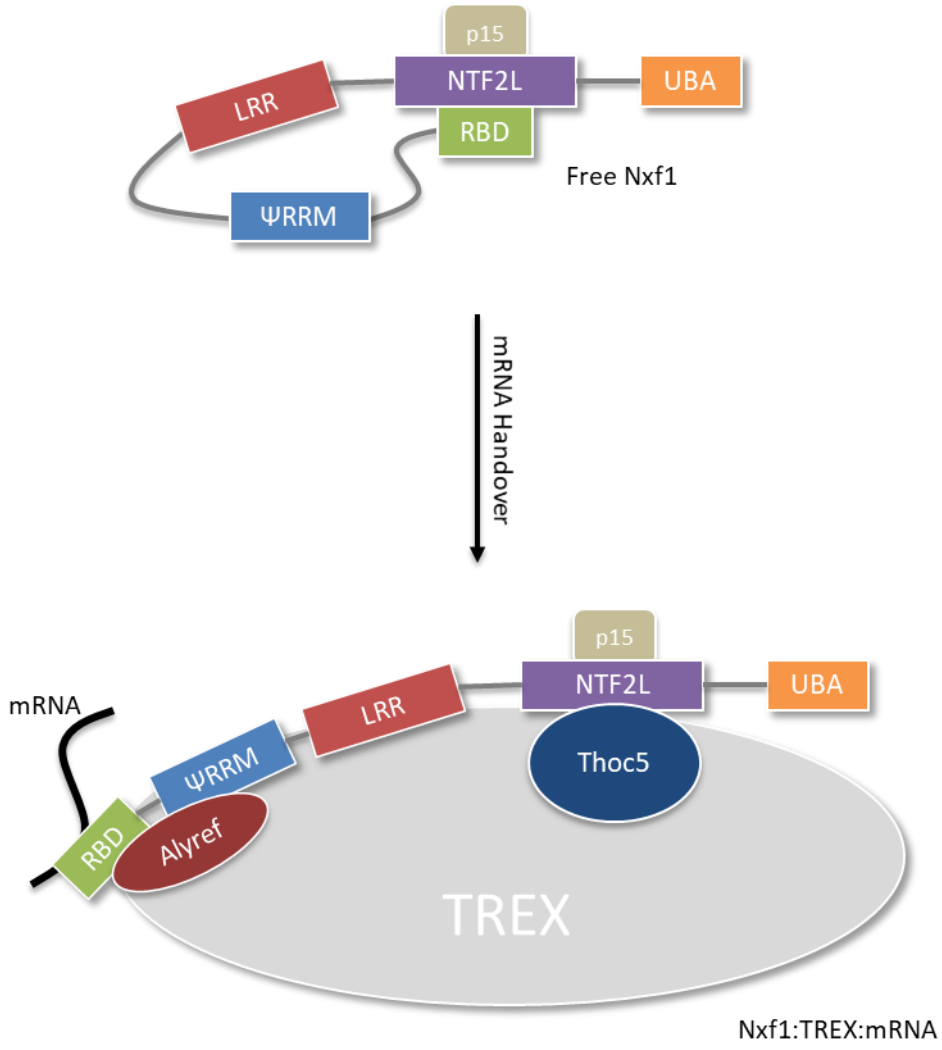

Figure 1.5 The mechanism of the Nxf1 mRNA handover. Nxf1 sequesters its own RNA binding ability via intramolecular interactions between the RBD and NTF2L domains. Binding of adapters to the RBD and ΨRRM along with Co-adapter binding NTF2L induce a conformational change resulting in an increased RNA binding affinity.

1.4 m^{6}A: The 5th Nucleotide

DNA, RNA and proteins can all undergo post synthesis modifications allowing for close regulation and diverse function. Currently 100 distinct chemical modifications have been mapped on eukaryotic RNA that occur post transcriptionally (Horkawicz *et al.*, 2006). The most abundant chemical modification present within eukaryotic mRNA is *N*^{6}-methyladenosine (m^{6}A) (Desrosiers *et al.*, 1974). However, it was difficult to resolve and decode the epitranscriptomic code of m^{6}A until advances in antibody based high throughput sequencing technologies became available (Dominissini *et al.*, 2012; Meyer *et al.*, 2012). The transcriptome wide mapping of human m^{6}A revealed widespread modification covering one third of the transcriptome confined to the consensus sequence of RRACU (Meyer *et al.*, 2012). Initially, m^{6}A was identified at the 3' terminus of a transcript with enrichment in the 3' untranslated regions (UTR) (Dominissini *et al.*, 2012; Meyer *et al.*, 2012; Ke *et al.*, 2015). Up to 30% of m^{6}A can lie within the coding region of a transcript, it must be noted there have been varying reports between ~30-50% m^{6}A on the CDS (Meyer *et al.*, 2012; Zhao *et al.*, 2014). Further studies identified a sharp peak of m^{6}A in the 5' UTR. (Schwartz *et al.*, 2014; Zhao *et al.*, 2014). Therefore the current methylation landscape, on average per methylated transcript, contains a distinct 5' UTR m^{6}A peak and a 3' CDS and UTR with cluster of m^{6}A.

The addition of m^{6}A upon select transcripts appears to decrease their stability, leading to a shorter half-life (Ke *et al.*, 2017). The modification imparts influence on a number of steps within an mRNA life cycle. Nuclear processing, export and translation all appear altered with the addition of m^{6}A (Zhao *et al.*, 2016). The coupling of the m^{6}A modification, methyltransferase complex and mRNA processing pathways leads to a system regulating specific mRNAs. The key players within the m^{6}A pathway have been identified (illustrated in Figure 1.6) and can be separated into three classes. Writers are responsible for the addition of the modification, these include Wilms' tumour 1-associating protein (Wtap), Kiaa1429, Rbm15 and a Methyltransferase-like protein 3/14 (Mettl3, Mettl14)

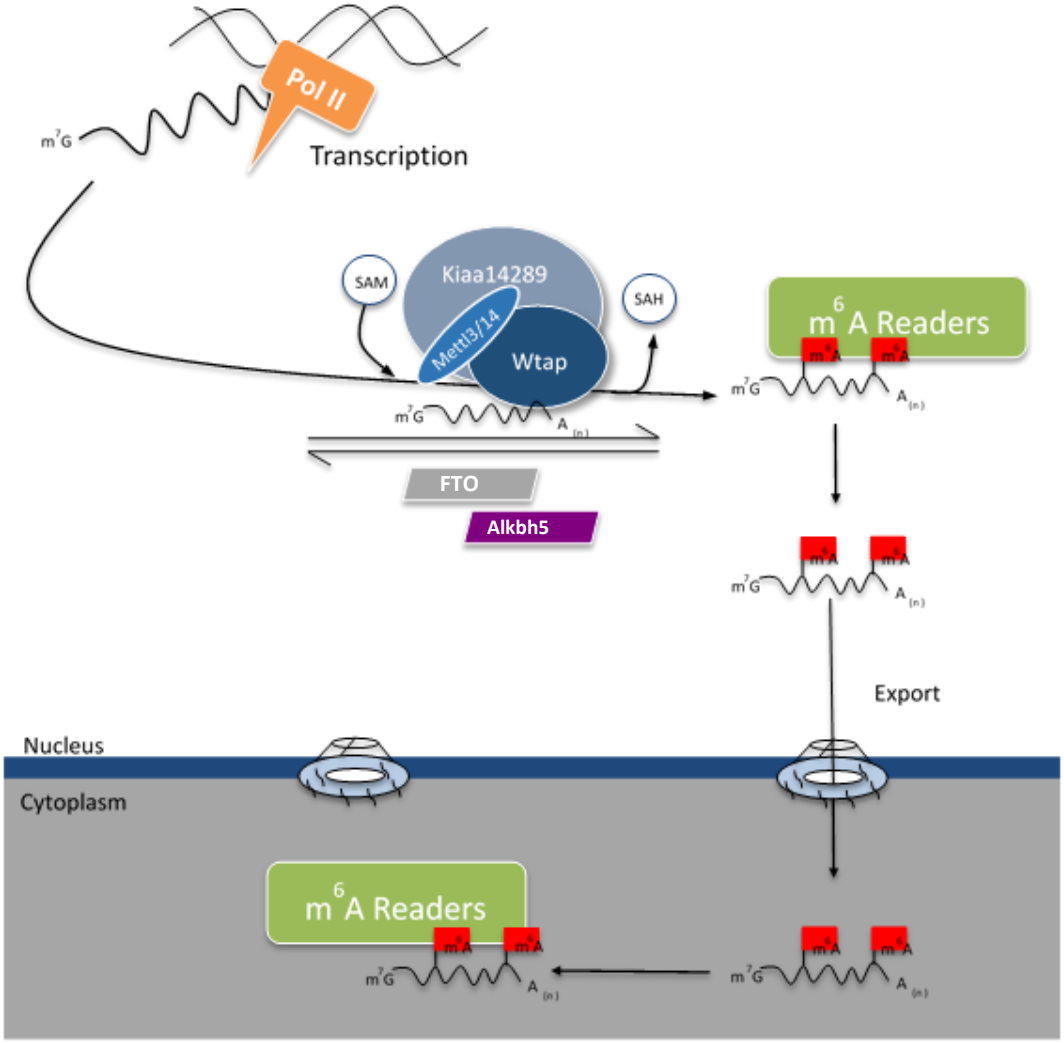

Figure 1.6 The methyladenosine pathway. The adenosine methylation of mRNA is coordinated by nuclear writers (Wtap, Kiaa1429, Mettl3 and Mettl14). Demethylase enzymes, also known as Erasers, can remove the modification (Alkbh5 and FTO).

heterodimer. The writers are nuclear localised. Erasers reverse the modification via catalytic oxidation, there are currently two m^6A specific demethylase enzymes FTO (nuclear/cytoplasmic distributed) and Alkbh5 (nuclear). The modification is decoded by reader proteins. This diverse set of proteins carry's out a plethora of functions that tie the m^6A modification into mRNA maturation/metabolic pathways. Six reader proteins have been identified, Ythdf1, Ythdf2, Ythdf3 are cytoplasmic readers whilst HnrnpC, HnrnpA2B1 and Ythdc1 are nuclear readers (Reviewed Zhao et al. 2016).

1.4.1 m^6A: Writers

The addition of the m^6A modification upon target mRNAs is conducted in the nuclear speckles via the writers. Initially a 200 kDa nuclear complex was identified as being responsible for the catalytic addition of methylation (Liu *et al.*, 2014). Further studies have dissected the complex constituents and defined roles for each member. The regulatory members of the methyltransferase complex are initially recruited via Rbm15. The Rbm15 binding sites were identified adjacent to the point of m^6A deposition (Patil *et al.*, 2016).

At the core of the writer complex sits Wtap. Wtap is a ubiquitously expressed protein identified in a yeast–two hybrid screen associating with splicing factors and was subsequently linked to mammalian cell cycle progression from G2 to M (Little *et al.*, 2000; Horiuchi *et al.*, 2006). Further studies conducting mass spectrometry on Wtap revealed multiple methyltransferase complex members such as Rbm15,Kiaa1429 and Mettl3/Mettl14 (Horiuchi *et al.*, 2013). The role of Wtap in the adenosine methylation pathway was not identified until 2014. Wtap was solidified as a Mettl3/Mettl14 binding partner and responsible for their recruitment to mRNA to undergo methylation. Although Wtap does not appear to harbour a catalytic domain, its knockdown resulted in a 6.25-fold decrease in m^6A throughout the transcriptome, indicating its role in Mettl3/14 recruitment. The interaction with Mettl3/14 is coordinated by the N-terminus of Wtap (Ping *et al.*,

2014; Schwartz *et al.*, 2014). Photoactivatable-ribonucleoside-enhanced crosslinking and immunoprecipitation (PAR-CLIP) illustrated Wtap binds multiple RNA species but overwhelmingly bound mRNA (92.08%). It's mRNA binding sites are distributed throughout the 3'UTR, CDS and 5'UTR (17.74%, 43.16% and 35.17% respectively). Further analysis revealed Wtap binding sites are static across a wide range of eukaryotic systems (Schwartz *et al.*, 2014). PAR-CLIP data of Mettl3 and Wtap illustrated a tight asymmetric heterodimeric complex allowing regulation of alternative splicing events within RNA processing and transcription related genes (Ping *et al.*, 2014).

The catalytic transfer of a methyl group to nitrogen of an adenosine is carried out by a tight heterodimeric complex consisting of Mettl3 and Mettl14. The methylation donor was identified as S-Adenosyl-methionine (SAM) (Liu *et al.*, 2014). Mettl3/Mettl14 preferentially methylate at a GGACU consensus. Mechanistic details of methylation by the heterodimer were divulged from crystallographic studies (Wang *et al.*, 2016; Wang *et al.*, 2016). Surprisingly Mettl14 appears to harbour no catalytic activity, instead acting as a RNA binding scaffold to facilitate Mettl3 (Wang *et al.*, 2016). The binding of an RNA substrate is coordinated by two gate loop structures of Mettl3. Upon binding, gate loop 1 flips open whilst gate loop 2 undergoes substantial conformation changes culminating in the closure of the active site region (Wang *et al.*, 2016) . The knockdown of either Mettl3 or 14 does not yield a dramatic reduction in transcriptomal m^6A (compared with Wtap) indicating possible redundancy and only low levels of the Mettl enzymes are required for methylation to occur (Schwartz *et al.*, 2014). Further evidence indicated Mettl3 may act independently of Wtap within certain pathways, for example the addition of m^6A to pri-miRNAs marking them for processing (Alarcón *et al.*, 2015).

Proteomic analysis of Wtap revealed the final member of the methyltransferase complex, Kiaa1429 (Schwartz *et al.*, 2014). The knockdown of Kiaa1429 results in a fourfold decrease in m^6A levels. Greater evidence of Kiaa1429s association within the m^6A pathway was produced upon studying the

Drosophila homologue Virilizer. Data produced from two independent groups identified Virilizer in an m^6A dependent regulation of sex determination via alternative splicing (Haussmann *et al.*, 2016; Lence *et al.*, 2016).

1.4.2 m^6A: Erasers

As well as writers the m^6A pathway contains erasers, demethylase enzymes that can remove the modification. Currently two methyladenosine specific demethylase enzymes, FTO and Alkbh5, have been identified. Both are members of the same Alkb subfamily superfamily Fe(II)/2-oxoglutarate dioxygenase. Alkbh5, a nuclear localised demethylase, employs one-step oxidative demethylation catalysed through a histidine-iron core. Mutations nullifying the iron binding histidine of Alkbh5 render it devoid of any activity (Zheng *et al.*, 2013). Crystallographic data revealed a structural binding specificity to single stranded methylated RNA facilitated by the iron bound histidine sandwich. A loop formation between amino acids 229-243 induced a steric clash with double stranded ribonucleic substrates (Xu *et al.*, 2014). This loop is not present in other family members. Immunostaining of Mettl3 and Alkbh5 identified an RNA-dependent co localisation within the nuclear speckles, more detailed interactions between the writers and erasers has yet to be studied (Zheng *et al.*,2013).

Throughout the literature FTO is described as the second demethylase. Whilst ALkbh5 acts upon multiple m^6A locations, FTO was shown to have a 5' bias (Zhao *et al.*, 2014; Huang *et al.*, 2015). FTO catalyses the removal of a methyl group via oxidation. However, recent work by Mauer et al has identified the preferential target of FTO is the $N^6$2'-O-dimethyladenosine (m^6A_m) modification not m^6A. m^6A_m is located adjacent to the mRNA m^7G cap and it was noted transcripts with this modification displayed an overall greater stability. The increase in stability appears to be imparted upon select m^6A_m transcripts by a resistance to mRNA-decapping enzymes (Mauer *et al.*, 2017).

1.4.3 m^{6}A: Readers Heterogeneous nuclear ribonucleoproteins (HNRNP)

The cellular functions denoted by the m^{6}A modification are conducted by the reader proteins. A wide array of reader proteins have been discovered and can be categorised into broad groups of direct and indirect. As the name suggests, direct readers bind to the m^{6}A modification directly and indirect readers act in a cis manner to alter local mRNA. Each reader carries out a specific predetermined function once bound to its target RNA. These functions range from degradation, translation initiation and alternative splicing.

Heterogeneous nuclear ribonucleoproteins (HNRNP) are a family of ubiquitously expressed RNA-binding proteins acting within diverse and complex RNA maturation pathways. Although they share similar characteristics, they comprise a wide array of different domains (Han *et al.,* 2010). Recently HnrnpA2B1 has been identified as a direct nuclear reader of m^{6}A and involved in the control and processing of a sub set of pre-miRNAs (Alarcón *et al.*, 2015). Discovery occurred when an HnrnpA2B1 knockdown phenocopied the global alternative splicing changes and reduction in miRNA expression observed in a Mettl3 knockdown. The m^{6}A miRNA processing pathway begins with Mettl3 methylation at the RGm^{6}AC consensus on the pre-miRNA. Post methylation HnrnpA2B1 binds to the methylated adenosine and bridges the initial interaction between pre-miRNA and the microprocessor complex, specifically Dgcr8 (Berulava *et al.*, 2015; Alarcón *et al.*, 2015).

RNA structural switches requiring m^{6}A have also been identified. The addition of m^{6}A within a stem loop structure causes a change in its thermostability, disrupting the secondary structure allowing protein-RNA interactions to occur. An example of an m^{6}A-dependent RNA switch can be found with indirect nuclear reader HnrnpC. This switch only occurs on a subset of HnrnpC target RNAs, pre-mRNAs and lncRNAs. PAR-CLIP analysis of HnrnpC revealed a reduced global RNA binding in stem loop regions in a background devoid of m^{6}A (Mettl3/Mettl14 knockdown) (Liu *et al.*, 2015). The results also identified 2798 switches with 87% of them occurring on introns, alluding to a possible role in splice site selection.

Gene ontology analysis of HnrnpC switches revealed an influence towards cell proliferation transcripts (Liu *et al.*, 2015).

1.4.4 m^{6}A Readers: YTH domain-containing family proteins

Ythdf1/2/3 are cytoplasmic readers that recognise the m^{6}A via an aromatic cage consisting of two conserved tryptophan residues, located in the YTH domain (Zhang *et al.*, 2010; Li *et al.*, 2014; Xu *et al.*, 2014, 2015b). Although all identified cytoplasmic readers contain a YTH-m^{6}A RNA binding domain they differ in further domain composition allowing for an array of functions (Yue *et al.*, 2015).

Ythdf1 is responsible for ribosomal loading onto methylated transcripts and subsequently their expression. This function is apparent as the interactome of Ythdf1 is heavily populated with translation initiation factors, notably eIF3. Although Ythdf1 has no preference to methyladenosine consensus sequence (Xu *et al.* 2015) this mechanism only occurs on a subset of m^{6}A transcripts (4951 transcripts revealed via PAR-CLIP), specifically those with binding sites clustered around the stop codon (Wang *et al.*, 2015).

Conversely Ythdf2 destabilises its m^{6}A-mRNA targets in the cytoplasm by directly recruiting them to the CCR4-NOT deadenylase complex (Du *et al.*, 2016). The methyladensoine-Ythdf2 complex can be located in the 3' UTR or ORF and alters the lifetime of transcripts. This degradation mechanism is orchestrated by the N-terminus of Ythdf2 whilst it's C-terminus YTH domain binds m^{6}A (Lee *et al.*, 2014; Zhou *et al.*, 2015). This leads to the formation of a multidimensional mechanism for select transcript expression via the m^{6}A modification, as Ythdf1 promotes protein expression and Ythdf2 can induce transcript degradation. Cross talk between these proteins is evident as they share 50% of their targets (Wang *et al.*, 2015). Ythdf2 carries out an alternative role in the heat shock response pathway. Upon heat shock induced stress an increase in 5' m^{6}A modification occurs coupled with a fourfold increase in Ythdf2 protein levels and subsequent translocation into the nucleus. Within the nucleus Ythdf2 binds the 5' m^{6}A

preventing FTO access, protecting the modification. Ythdf2 remains bound during nuclear pore translocation and promotes cap-independent translation in the cytoplasm (Zhou *et al.*, 2015). A third member of the cytoplasmic Yth-domain subfamily, Ythdf3, has been identified in both translation and degradation (Shi *et al.*, 2017). The current literature paints a methylation dependent regulatory pathway orchestrated by the cytoplasmic Yth containing proteins.

Viral replication mechanisms can employ Ythdf proteins. The Zika virus a member of the Flaviviridae family of positive single stranded RNA viruses has its genome methylated by the host m^6A machinery at twelve separate locations, and subsequently bound by Ythdf proteins. The Ythdf proteins appear to keep viral replication to a minimum as depletion of the readers causes an increase in viral protein production (Lichinchi *et al.*, 2016). An opposite affect was observed in HIV-1 infection; Ythdf proteins bind the 3' UTR m^6A sites enhancing viral protein production. It was also shown that over expression of the Ythdf enhances viral replication up to six fold. Further evidence was generated demonstrating CD4+ cells only express Ythdf2 and its knockdown within these cells results in reduced viral replication upon infection(Kennedy *et al.*, 2016).

Ythdc1 (YT521-B) is a nuclear YTH domain containing protein initially thought to be a splicing associated factor (Hartmann *et al.*, 1999). Early work identified nuclear YT domains consisting of Ythdc1 and Sam63, a nuclear transcriptomal scaffold protein. YT domains form at the beginning of S-phase and disperse during mitosis (Nayler *et al.*, 2000). The YT domains surround nuclear speckles and are focal points of transcription, shown by their dispersal upon Actinomycin D treatment (Nayler *et al.*, 2000). The formation of YT bodies is controlled via tyrosine phosphorylation of Ythdc1, phosphorylating Ythdc1 blocks its interaction with Sam63 resulting in sequestration at an insoluble site (Rafalska *et al.*, 2004).

A recent crystal structure of Ythdc1 revealed details of its m^6A binding activity. Firstly unlike the other Ythdf proteins Ythdc1 preferentially bound a

GGm^{6}A motif (Xu *et al.*, 2015a), but still recognised the modification via two tryptophan residues within an aromatic cage (Xu *et al.*, 2014). PAR CLIP analysis identified Ythdc1 bound to transcripts at stop codons (30%), and the coding sequence (34%). Interestingly 21% of all Ythdc1 bound transcripts are shared with Ythdf2 and 13% of all bound targets having a role in transcriptional regulation (Xu *et al.*, 2014). Further studies have unravelled the details of Ythdc1 and its role in m^{6}A dependent splicing regulation. Ythdc1 promotes exon inclusion working cooperatively with splicing factor Srsf3. Conversely Srsf10 can bind close to the m^{6}A site blocking Ythdc1 mRNA association therefore resulting in exon skipping (Roundtree and He, 2016; Xiao *et al.*, 2016). The current competition model of Ythdc1, Srsf3 and Srsf10 provides mechanistic reasoning for previous results showing exon inclusion is Ythdc1 dosage dependent (Nayler *et al.*, 2000; Rafalska *et al.*, 2004) Move evidence for multiple roles conducted by Ythdc1 was presented by Patil et al. 2016, indicating Ythdc1 in transcriptional silencing by XIST in a methylation dependent mechanism.

1.4.5 Cellular processes and Epitranscriptomics

Above we have discussed the key players and mechanistic details of the m^{6}A pathway. Working in concert these factors conduct cellular functions and if perturbed can result in tissue specific phenotypes. An example was demonstrated in Alkbh5-deficient mice. Removing Alkbh5 results in a significant increase of m^{6}A in mRNA, this leads to the apoptosis of spermatocytes and therefore defective fertility in these mice (Zheng *et al.*, 2013). It was not explored, but one may suspect this is a result of Ythdf2 dependent mRNA degradation. The cells circadian rhythm also appears to be regulated by m^{6}A and its protein interactome. Knockdown of Mettl3 results in a prolonged circadian period due to the reduced nuclear kinetics of two clock genes, Per2 and Arntl. They displayed a nuclear accumulation and are therefore decreased translation, causing a delay in the circadian clock (Fustin *et al.*, 2013).

The distribution of m^6A within the human and mouse embryonic stem cell (ESC) transcriptome has revealed a unique methylation dependent regulatory mechanism. Core factors required for pluripotency were identified as Mettl3 targets and therefore methylated (Batista *et al.*, 2014). Removal of Mettl3 resulted in impaired differentiation. Overall the m^6A mark is required for ESCs to differentiate into specific lineages. The m^6A modification is thought to reduce the stability of specific mRNAs required for ESCs to move from a naïve to a primed state (Geula *et al.*, 2015) . Therefore with low m^6A levels in ESC-related transcripts pluripotency can persist. Mechanistic details of ESC reprogramming via m^6A have recently been revealed. Chromatin associated zinc finger protein 217, Zfp217, is responsible for the regulation of core stem cells genes, and was found to associate with Mettl3. High Zfp217 levels in ESCs result in the sequestering of Mettl3 and therefore a reduction in methylation upon target mRNAs. Upon differentiation, Zfp217 levels decrease resulting in the release of Mettl3 and its subsequent complexing with Mett14. The Mettl3/Mettl14 complex acts upon key target *Nanog*, *Sox2* and *Kif4.* The methylation of these transcripts results in their degradation and ultimately differentiation of the ESC (Aguilo *et al.*, 2015).

Furthermore although demethylase enzymes have been identified the modification appears to be static in nature. Upon co-transcriptional addition of m^6A, the mark persists from chromatin associated to cytoplasmic mRNA. It was also revealed that m^6A has no influence on the splicing reaction for modified mRNAs (Ke *et al.*, 2017).

Cellular response mechanisms upon stress have been found to contain epitranscriptomic traits. The previously mentioned heat shock induced nuclear translocation of Ythdf2 resulting in protection of specific mRNA targets is one example (Zhou *et al.*, 2015). A more recent study identified m^6A as a key regulator in ultraviolet-induced DNA damage response (Xiang *et al.*, 2017). The DNA damage response is a cellular DNA repair mechanism that detects damage and halts cell division until the repairs have been carried out. Observations noted that at sites of DNA damage rapid localised deposition of m^6A upon select PolyA+ transcripts

occurred. The consequence of localised m^{6}A deposition at these sites appears to be for DNA repair enzyme DNA Pol *k* localisation (Xiang *et al.*, 2017).

1.5 m^{6}A and TREX

The epitranscriptomic literature is littered with evidence linking the m^{6}A machinery and the TREX complex, a quick reference guide is displayed in Figure 1.7. Historic work observed a nuclear export and processing defected of SV40 mRNA during infection when subject to a methionine inhibitor. It was noted a reduced level of methylation deposition within SV40 mRNA reduced cytoplasmic levels but nuclear abundance remained unchanged, indicating an export defect (Finkel and Groner, 1983).Recent work focusing on key members of the machinery has revealed further details on m6A and mRNA export. Wtap mass spectrometry revealed Alyref and Uap56 as binding partners (Horiuchi *et al.*, 2013). Knockdown of Mettl3 resulted in a delay of nascent transcript export (Fustin *et al.*, 2013). Furthermore Alkbh5 knockdown culminated in an increased PolyA+ RNA signal within the cytoplasm (Zheng *et al.*, 2013). Historic work on Alyref also revealed an interaction with Kiaa1429 via mass spectrometry (Masuda *et al.*, 2005). With the current evidence in mind we set out to identify and dissect a possible interplay between the m^{6}A machinery and the nuclear export of mRNAs via TREX.

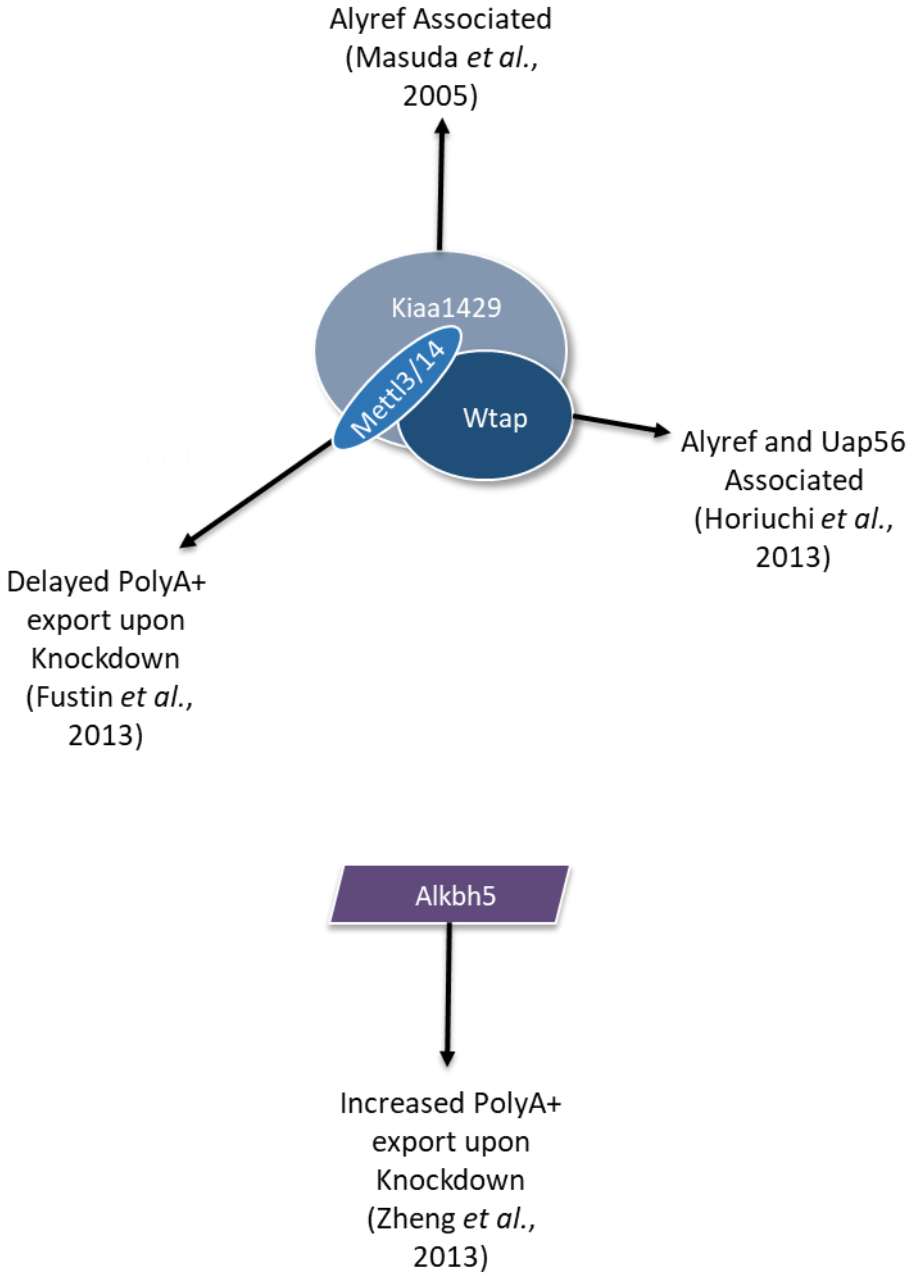

Figure 1.7 Methyltransferase pathway and TREX overlap. Throughout the literature members of the m^{6}A pathway have revealed possible links to the TREX complex. Each member is shown with its export phenotype or TREX association and reference.

1.6 Aims of Study

The links between the m^6A pathway and TREX above provided a base for us to begin our investigation of a functional overlap between the two pathways. We set out to identify any methylation response upon perturbation of mRNA export. Following this we aimed to refine and build on current interaction data between TREX members and methyltransferase machinery. This will allow us to construct a detailed map of protein-protein interactions shared between the complexes.

Following these binding studies we aim to identify the functional relationship imparted by the interactions. We will first use global techniques to measure any mRNA export phenotype upon knockdown of methyltransferase members. However we predict we will have to be more specific as the modification only affects a small proportion of the transcriptome. Therefore we will look at the export of specific methylated transcripts that have already been identified within the literature.

Finally we plan on investigating the nuclear reader Ythdc1. Again we will conduct interactions studies with TREX members and global mRNA export assays. We will construct inducible RNAi stable cell lines allowing for a variety of export assays to occur. The export of specific Ythdc1 bound transcripts will be assayed with the RNAi stable cell line. Finally we will look at the interplay between the methylation writers and readers as this has yet to be discussed within the literature. We will conduct mRNA localisation studies and binding studies in a variety of knockdown backgrounds. The culmination of this work will dissect the interactions between two pathways and give details on how they work in unison for a specific subset of mRNA transcripts.

Chapter 2 Materials and Methods

2.1 Materials

2.1.1 Bacterial Strains and Media

All *Escherichia coli* strains were purchased from Invitrogen

Strain	Genotype
DH5α	F– Φ80*lac*ZΔM15 Δ(*lac*ZYA-*arg*F) U169 *rec*A1 *end*A1 *hsd*R17 (rK–, mK+) *pho*A *sup*E44 λ– *thi*-1 *gyr*A96 *rel*A1
BL21 CodonPlus RP	B F^- *omp*T

Growth Media

Sterilised via autoclaving 15lb/in2 for 15 minutes. Stored at room temperature.

Luria Bertani (LB): 10 g/L Tryptone, 10 g/L NaCl, 5 g/L Yeast extract.

LB Agar: As above with addition 1.5g/100 mL Agar.

Terrific Broth: 12 g/L Tryptone, 24 g/L Yeast extract, 4mL/L Glycerol, 2.31 g/L KH_2PO_4, 15.54 g/L K_2HPO_4.

Super Optimal broth with Catabolite repression (S.O.C): Purchased from Invitrogen life science. 20 g/L Tryptone, 5 g/L Yeast extract, 4.8 g/L $MgSO_4$, 3.603 g/L Dextrose, 0.5g/L NaCl, 0.186 g/L KCl.

Antibiotics

Used as selective agents for identification of successful *E.coli* plasmid transformations.

Antibiotic	Concentration
Spectinomycin	50 µg/mL
Ampicillin	100 µg/mL
Chloramphenicol	12.5 µg/mL
Kanamycin	50 µg/mL (30 µg/mL for Agar)

2.1.2 Plasmids

Plasmids	Manufacture	Resistance Gene	Tag
pGEX6p1	Amersham	Ampicillin	GST
pET24b	Novagen	Kanamycin	6xHis
p3XFlag-myc-CMV-26	Sigma	Ampicillin	Flag/myc
pcDNA5-FRT	Invitrogen	Ampicillin	N/A
pCl-neo-MS2	Promega	Ampicillin	Myc
pcDNA6.2-mIR	Invitrogen	Spectinomycin	N/A

2.1.3 Tissue Culture

Growth Media

Cells propagated in Dulbeccos Modified Eagle Media (DMEM) (purchased form Sigma). DMEM was supplemented with 10% fetal calf serum (FCS), 1% penicillin-streptomycin and 2mM glutamine (purchased form Life Technologies).

Cell Lines

All cell lines were purchased form ATCC or Invitrogen.

HEK-293T – Human embryonic kidney.

FlpIn HEK-293T – Human embryonic kidney. Contains a single integrated FRT site at a transcriptionally active genome locus.

HeLa – Cervical cancer cells.

2.1.4 Buffers and Solutions

DNA and RNA

6x DNA Loading Buffer: 0.25% Xylene cyanol, 0.25% Bromophenol blue, 30% Glycerol

5x Tris-borate (TBE) Buffer: 54 g Tris base, 27.5 g Boric acid, 20 mL 0.5M EDTA (pH8.0), brought up to a final volume of 1000 mL with distilled water.

Protein Purification Buffers

Cobalt Binding Buffer: 50 mM Tris Hcl (pH 8), 1 M NaCl, 0.5% Tirton X, 5 mM Imidazole, 5% Glycerol.

Cobalt Wash Buffer: 50 mM Tris Hcl (pH 8), 1 M NaCl, 0.5% Tirton X, 10 mM Imidazole, 5% Glycerol.

Cobalt Elution Buffer: 50 mM Tris Hcl (pH 8). 500 mM NaCl, 200 mM Imidazole, 10% Glycerol.

GSH Elution Buffer: 50 mM Tris Hcl (pH 7.5), 100 mM NaCl, 40 mM reduced Glutathione. Stored 4˚C

SDS-PAGE/Western Blot Buffers

4x SDS-PAGE Loading Buffer: 200mM Tris HCl (pH 6.8), 1%Bromophenol blue, 50% Glycerol, 10% Sodium dodecyl sulphate (SDS).

4 x SDS-PAGE Stacking Gel Buffer: 0.5 M Tris HCl (pH6.8), 0.15% SDS.

4x SDS-PAGE Resolving Gel Buffer: 1.5 M Tris-HCl, (pH 8.8), 0.15% SDS.

SDS-PAGE Running Buffer: 25 mM Tris, 250 mM Glycine, 0.1% SDS

Coomassie Brilliant Blue Stain: 0.1% Coomassie Brilliant Blue R-250, 40% Methanol, 10% Acetic Acid.

Destain Solution: 40% Methanol, 10% Acetic Acid.

Transfer Buffer: 39 mM Glycine, 48 mM Tris, 0.037% SDS, 20% Methanol

BioRad TurboBlot Transfer Buffer: 200 ml 5x Commercial Stock combined with 200 ml Ethanol, 600 ml $H20_{mq}$.

5% Blocking Solution: 2.5 g Powdered Milk, 5 ml 10 x TBS, and 0.2% Tween-20

PolyA+ RNA Purification Buffers

PolyA+ Binding Buffer: 20 mM Tris-HCL pH 7.5, 1 M LiCl, 2 mM EDTA pH 8.

PolyA+ Wash Buffer B: 10 mM Tris-HCL pH 7.5, 150 mM LiCl, 1 mM EDTA pH 8.

PolyA+ Elution buffer: 10 mM Tris-HCL pH 7.5.

mRNP Capture Buffers

2 x Binding Buffer: 20 mM HEPES-K-NaOH pH 7.5, 1 M NaCl, 1 % SDS, 0.2 mM EDTA pH 8.

mRNP Lysis Buffer: 50 mM HEPES-K-NaOH pH 7.5, 100 mM NaCl, 1 mM DTT, 1 mM EDTA pH 8.0, 0.5 % Igepal Ca-630/NP-40, 0.5 % Na-deoxycholate, 10 % glycerol.

1 x Binding Buffer: 1:1 Mixture of 2 x binding buffer and mRNP lysis buffer.

mRNP Elution Buffer: 10 mM Tris pH 7.5, 1 mM EDTA pH 8.

Protein Immunoprecipitation Buffers

IP Lysis Buffer: 50 mM HEPES-NaOH pH 7.5, 100 mM NaCl, 1 mM EDTA pH 8.0, 0.125 % Triton X-100, 10% Glycerol, 1 mM DTT.

High Salt IP Lysis Buffer: 50 mM HEPES-NaOH pH 7.5, 1 M NaCl, 1 mM EDTA pH 8.0, 0.125 % Triton X-100, 10% Glycerol, 1 mM DTT.

Arginine Elution Buffer: 1 M Arginine-HCl pH 3.5

MS2-tethered Assay Buffers

Luciferase Assay Buffer: 25 mM Gly-Gly pH7.8, 15 mM KH_2PO_4 pH 7.8, 15 mM $MgSO_4$, 4 mM EDTA pH 8, 1 mM DTT, 2 mM ATP (added fresh before use).

ß-galactosidase Detection Kit: Purchased from Clonetec Bioscience.

MTT Assay Buffers

MTT Solution: 5 mg/ml MTT dissolved in PBS.

MTT Solvent: 4 mM HCl, 0.1% NP40 dissolved in isopropanol.

Microscopy Technique Buffers

Fix Solution: 4% paraformaldehyde, 0.18% Triton-X made up in 1 x PBS with a final pH 7.4.

Hybridisation buffer: 20 % Formaldehyde, 2 % SSC, 10 % dextran sulphate, 1% BSA.

RNA Nuclear/Cytoplasmic Extraction Buffer

N/C Lysis Buffer: 320 mM Sucrose, 3 mM CaCl2, 2 mM MgCl2, 0.1 mM EDTA pH 8, 10 mM Tris-HCl pH8.0

Buffer A: 10 mM HEPES pH 7.5, 10 mM KCl, 10% glycerol, 4 mM MgCl2, 1 mM DTT, 1 x Protease Inhibitors.

NRB: 20 mM HEPES pH 7.5, 75 mM NaCl, 1 mM DTT, 50% Glycerol, 1 x Protease Inhibitors.

NUN: 20 mM HEPES pH 7.5, 300 mM NaCl, 1 mM DTT, 10 mM MgCl2, 1 M Urea, 1 % NP-40

RNA Immunoprecipitation Buffers

RIP Lysis Buffer: 50 mM HEPES-HCl pH 7.5, 150 mM NaCl, 10 % glycerol 1% NP-40, 0.1% SDS, and 0.5 % sodium deoxycholate.

RIP High Salt Wash Buffer: 50 mM HEPES-HCl pH 7.5, 1 M NaCl, 10 % glycerol 1% NP-40, 0.1% SDS, 0.5 % sodium deoxycholate.

2 x Reverse Crosslinking Buffer: 100 mM Hepes pH 7.5, 200 mM, NaCl, 2 % SDS, 10 mM EDTA pH 8, 20 mM DTT

Miscellaneous Buffers

1x PBS (Phosphate buffered saline): 137mM NaCl, 2.7 mM KCL, 4.3 mM NaH_2PO_4, 1.47 mM KH2PO4. HCL used to bring to pH 7.4

1x PBS-Tween: 1x PBS containing 0.1% Tween-20.

1x TBS (Tris Buffered Saline): 50 mM Tris HCl (pH7.5), 150 mM NaCl.

1x TBS-Tween: 1x TBS containing 2% Tween-20.

ECL Solution #1: 100 mM Tris HCl (pH 8.5), 10 mM EDTA (pH 8.0), 1M NaCl.

ECL Solution #2: 100 mM Tris HCl (pH 8.5), 5.3 mM Hydrogen Peroxide.

2.1.5 Molecular Biology Kits

Small scale plasmid DNA extraction and purification: Qiagen Mini Spin Preparation kit.

Medium scale plasmid DNA extraction and purification: Qiagen Midi Spin Preparation kit.

DNA extraction from agarose gels: Qaigen Gel Extraction kit.

RNAi Hairpin design and Construct creation: Invirtogen Block-It RNAi

2.2 Methods

2.2.1 Molecular Biology

Polymerase Chain Reaction (PCR)

PCR reactions were set up with a final volume of 50 µl containing 50 ng of template DNA, 10 µM forward and reverse primers, 1x reaction buffer, 200 µM dNTPs, 2.5-5 U of DNA Polymerase (dependent on manufactures requirements). Routine PCR reactions underwent 35 cycles with an annealing temperature of 59-62˚C (primer dependent) and an extension temperature of 72˚C, time of extension dependent on target size and polymerase.

Reverse Transcriptase Polymerase Chain Reaction (RT-PCR)

All RT-PCR reactions were carried out using the BioScript Kit form Bioline. RT-PCR reactions were carried out in two steps. Step one the total RNA template (500 ng-5 µg), 200 µM of dNTPs and Qiagen Random Hexamer mix (2 µM) were mixed in a 200 µl PCR tube and made to a final volume of 10 µl. The mixture was heated to 70˚C for 5 minutes then immediately placed on ice for at least 1 minute.

Step two consisted of preparing a reaction mix by adding 5 x RT buffer, 200 U Ribosafe RNAse Inhibitor (Bioline) and 200 U Bioscript Reverse Transcriptase. Then made up to a final volume of 10 µl. The reaction mix is then added to the step 1 RNA mix. The sample is homogenized by pipetting up and down gently.

Samples and then incubated at 25˚C for 10 minutes followed by 42˚C for 30 minutes. Termination of the reaction is achieved by heating to 85˚C for 5 minutes. The resulting cDNA is either used directly for qPCR or stored at -20˚C

Quantitative PCR (qPCR)

cDNA from RT-PCR was diluted 2-5 fold with RNase-free H_2O. qPCR reactions were set up on ice. Each reaction consisted of 2 µl diluted cDNA, 1 µl primer mix (100 ng/µl), 5 µl 2 x Sensimix (Bioline) and 2 µl RNase-free H_2O. Reaction were cycled as follows; 10 minutes 95˚C then 45 cycles of 10 seconds 95˚C, 15 seconds 59˚C and 25 seconds 72˚C. All qPCR was carried out in a Qaigen Roto-gene Q.

DNA Restriction Digest

Restriction digest reactions were carried out in optimal buffer that is designated by the manufacture. Reactions were incubated 37˚C for 1-2 hours per microgram. If fast digest enzymes were used reaction was carried out for 10 minutes at 37˚C per microgram.

Agarose Gel Electrophoresis of DNA

The required amount of agarose was dissolved in 1x TBE and heated in 800w microwave at 80% power for 3-4 minutes. The mixture was allowed to cool before the addition of ethidium bromide (Bio-Rad) to a final concentration of 10 µg/mL. The agarose mixture was poured into an appropriate mould and a well comb inserted. Left to set a room temperature.

Agarose Concentration (%)	**Effective Range of DNA Molecule Separation (kb)**
0.5	1-20
0.8	0.8-10
1.0	0.5-7
1.5	0.2-3
2.0	0.1-2

The set gel was loaded into an electrophoresis tank (Bio-Rad) and filled with 1x TBE until the gel was covered. DNA samples were loaded with corresponding commercial makers and run at a constant voltage, 90-110 volts depending on gel/tank size. Gels were run until loading dye was no longer present. Visualisation of DNA bands occurred upon exposure to a UV light source using a transilluminator.

Extraction of DNA from Agarose Gel

DNA fragments that had been resolved by gel electrophoresis and are required for downstream procedures are removed from the agarose gel with a sharp blade. Purification of this gel containing DNA fragment is done via Qiagen Gel Extraction kit according to manufactures instructions.

Phenol Chloroform-Isoamyl Alcohol DNA purification

The DNA sample is made up to 100 µl using H_2O_{mq}. Phenol chloroform-isoamyl alcohol is then added at a 1:1 ratio, therefore 100 µl. Mixture is vortex for 1 minute. Then centrifuged 3 minutes at 13 200 rpm, room temperature. Upper phase removed to a fresh tube containing 10 µl of 3 M Sodium acetate (pH 5.3) and 300 µl 100% ethanol. Mixed by inverting 10 times. Incubated at -20˚C for 30 minutes minimum. Then centrifuge for 30 minutes 13 200 rpm. Supernatant removed, 70% ice cold ethanol added. Spin 10 minutes 13,200 rpm. Supernatant removed and pellet air dried. Once dried pellet was resuspended in required volume of H_2O_{mq}.

Ligation of DNA

200 ng of digest and purified vector was incubated with respective DNA at ratios of either 1:1, 3:1 or 5:1 insert at room temperature for 1.5 hours. The reaction mixture was made up according to manufactures guidelines with a final volume of 10 µl and containing 1 U of T4 Ligase.

Transformation of Chemically Competent Escherichia coli

Competent cells were thawed on ice. 100 µl of competent cells was then added to 10 µl of the ligation reaction or 2.5 µl of an existing construct/plasmid. The reaction mixture was allowed to equilibrate on ice for 15 minutes. Heat shock was then preformed, 5 minutes at 37˚C. Post heat shock 1 ml of LB was then added and cells allowed to recover for 1 hour at 37˚C, shaking 200 rpm. Then cell are spun down 6800 rpm, 1 minute. Cell pellet then resuspended in 100 µl LB and spread onto pre-warmed antibiotic containing agar plate then incubated overnight at 37˚C

Plasmid DNA Isolation from E.coli

All plasmid DNA isolation was carried out using Qiagen purification kits. Cultures for midi-preps ranged from 50-200 ml and for mini 1-3 mL, of bacterial culture in LB. All cultures were incubated overnight at 37˚C and shaking at 200 rpm. Purification was subsequently conducted using manufactures specifications.

Molecular Cloning by Restriction Digest

Recipient plasmids underwent double restriction digests. 4 µg of plasmid was digested with 50 U of each enzyme for 3 hours at 37˚C. Upon completion of digest the plasmids samples undergo phosphatase treatment (CIAP, Calf Intestinal Alkaline Phosphatase), 1 U of enzyme for 30 minutes at 37˚C. The processed

plasmid then undergoes DNA phenol-chloroform extraction and ethanol precipitation, resuspend in required volume of H_2O_{mq}.

Insert fragments are generated via PCR. Primers are designed with the required restriction digest recognition sites and also a 6 nucleotide 5' flank sites. PCR products are run on appropriate agarose gels are gel extracted using the Qiagen kits. Gel extracted products where eluted into 50 µl H_2O_{mq} and double restriction digest performed overnight, 100 U of enzymes, 37˚C. Then DNA phenol-chloroform extraction and ethanol precipitation resuspend in required volume of H_2O_{mq}.

Concentration of DNA was determined 200 ng of linearized vector and corresponding insert (ratios of either 1:1, 3:1 or 5:1) went into the T4 ligase reaction. Ligation product was subsequently transformed into *E.coli* DH5α.

Molecular Cloning by Isothermal Assembly (ITC)

The Gibson Assembly Cloning Kit (New England Biolabs) was used for all ITC cloning. The following reaction was set up on ice; 0.02-0.5 pmols of linearized vector and PCR fragments, 10 µl 2 x Gibson Assembly Master Mix and made to a final volume of 20 µl using H_2O mq. Samples are then incubated for 15 minutes at 50˚C in a thermocycler and subsequently transferred to ice. 2 µl of the reaction is then used for transformation into NEB 5-alpha competent E.Coli (New England Biolabs). Cells are incubated with the reaction for 30 minutes on ice then undergo a 30 second 42˚C heat shock. Tubes are then incubated on ice for 2 minutes before adding 950 µl SOC media, proceeded by a 1 hour incubation at 37˚C and shaking 250 rpm. 100 µl of cell suspension is plated onto selective agar plates and incubated over night at 37˚C.

Cloning BLOCK-IT RNAi Vectors

The BLCOK-IT RNAi system is a commercially available cloning kit. It contains a pre-linearized pcDNA 6.2GW miR vector. RNAi hairpins are designed via the BLOCK-IT manufacturer's website (Invitrogen).

DNA Sequencing

All plasmid DNA sequencing was outsourced to Source Bioscience LifeSciences using stock primers provided by them.

2.2.2 Protein Biochemistry and Expression

Recombinant Protein Expression in E.coli

Plasmid constructs were transformed into *E.coli* BL21 codon plus RP for protein expression. Expression test were conducted with a single transformed colony that was cultured in 10 ml TB (with appropriate antibiotic), 37˚C, shaking 200 rpm. The culture was grown to 0.6 OD then induced for 2 hours with 1 mM IPTG, 37˚C and shaking 200 rpm. The culture was then pelleted, 6800 rpm resuspend in appropriate binding buffer for purification or stored at -20˚C.

Big batch protein expression was conducted in 2000 ml conical flask. An overnight starter culture (containing selection antibiotic and chloramphenicol) was used to inoculate 750 ml of TB (containing appropriate antibiotic) to 0.05OD. The culture was grown 37˚C, shaking 200 rpm until 0.6OD then induced with 1 mM IPTG. Induction occurred at 20˚C shaking at 200 rpm overnight. Cultures then spun down at 4000 rpm and resuspended in appropriate binding buffer for purification or stored -20˚C.

Purification of Affinity Tagged Recombinant Proteins from E.coli

All recombinant protein purification was done in the presence of 1x protease inhibitors (Sigma Protease cocktails) and RNAse A (if required). GSH beads where used for GST tagged constructs. For expression test 30 µl of bead slurry was washed with 1 ml 1x PBS, 0.1% Tween-20op. Bacterial pellets are resuspend in PBS-Tween,1 x protease inhibitor cocktail and lysed by sonication, 5 seconds on 25 seconds off, lysate was cleared by spinning at 16 100 xg at 4˚C. Lysate was added to washed GSH beads then placed on a wheel spinning 4˚C, 15 rpm for 1 hour to allow binding. GSH beads were then pelleted 400 xg and washed 3 x with 1 ml of PBS-Tween. After the third wash beads were dried and 60 µl of GSH Elution buffer added. Protein were eluted for 30 minutes, 4˚C and spinning at 15 rpm.

Hexa-His tagged recombinant proteins followed the same protocol for expression test as GST tagged constructs. Hexa-His tagged protein purification differed via use of 40 µl of Cobalt bead slurry and Cobalt binding buffer, 1 x protease inhibitor cocktail to resuspend cells and Cobalt binding buffer to wash bead slurry. Cobalt wash buffer to washed bead post binding incubation and Cobalt elution buffer for elution. When purifying larger quantities of recombinant proteins the above protocols were scaled up appropriately.

Pulldown Binding Assay using Recombinant Proteins

Protein pulldown assays were performed with either 30 µl GSH or 50 µl Cobalt bead slurry per condition. Bait proteins were purified as described above then allowed to bind to required beads 1 hour, spinning 15 rpm at 4˚C. Once bound beads were washed 3 times with appropriate buffers, upon final wash resuspend in 400 µl wash buffer. Prey proteins were lysed in identical buffer to bait bead wash buffer. Cleared lysate containing the prey protein was added to the bead bound bait at a molar ratio of 2:1 or higher if stated. Pulldowns occurred for 1 hour, spinning 15 rpm at 4˚C. Once complete beads were washed 3 times with required buffer then subsequently eluted into 60 µl elution buffer. 12 µl of elution was run on a 12 % SDS-PAGE gel.

In-Vitro expression systems

In-vitro expression of plasmid constructs was achieved via the Flexi Rabbit Reticulocyte Lysate System (Promega). The manufactures protocol was not followed, all reaction had a final volume of 10 µl. Extra precautions were taken to maintain RNase free plasticware. The reaction consisted of 8 µl rabbit reticulocyte lysate, 1.5 µl DNA (final weight of 250 ng) and 0.5 µl S35 Methionine. Reaction were incubated for 1.30 hours, 30˚C. 8 µl reticulocyte reaction was then added to pelleted beads (GSH or Cobalt) that had a suspected interaction partner already

bound (bait). The remaining 2 µl of Reticulocyte reaction was used as an input for SDS-PAGE. Washing and elution of protein complexes proceeded as described in the above section (Pulldown Binding Assay using Recombinant Proteins).

Protein Immunoprecipitation

Each condition requires 60 µl Protein-G beads blocked over night at 4˚C in 500 µl of IP lysis buffer containing 1 % BSA and 2-10 µg of antibody. Beads are then washed 3 times in 1 ml IP lysis buffer.

Cells are washed with PBS before being lysed in IP lysis buffer containing protease inhibitors, DNAse 1, RNAse A and DTT. Extracts are cleared via centrifugation at 13 200 rpm, 5 minutes at 4˚C. Equal amounts of extract (measured via Bradford assay) are loaded onto the beads and incubated for 2 hours at 4˚C rotating 18 rpm. 0.1-10 % of extract is kept on ice for the input.

Beads are then washed 3 times in 1 ml ice cold IP lysis buffer. Inverted 10 times and spun at 400 xg for 1 minute. After the final wash beads were dried using a gel loading tip and resuspend in 72 µl Arginine elution buffer. Beads were incubated for 2 minutes at room temperature and then spun for 1 minute at 400 xg. Eluate is then transferred to a fresh 1.5 ml tube and subsequently neutrilised with 3µl 1.5M Tris.HCl (pH 8.8). Eluates are resolved by SDS-PAGE and underwent subsequent Western blot analysis. It is worth noting two separate antibodies for Wtap Co-IP experiments have been employed. The antibody used will be disclosed within the accompanying figure descriptions. Antibodies from Abcam (Ref:ab195380) and Santa cruise (no longer available).

Flag Tagged Protein Immunoprecipitation

Flag tagged constructs were transfected 48-72 hours prior to immunoprecipitation. 50 µl of Flag-agarose beads (Sigma-Aldrich) are blocked for 2 hours in IP lysis buffer containing 1 % BSA. The Flag-agarose beads are then washed 3 times in 1 ml IP lysis buffer. Processing of cells and lysis is as above (see. Protein Immunoprecipitation).

Elution of Flag-tagged constructs is done via competition. Beads are dried and resuspended in 60 µl of Flag peptide and incubated for 1 hour rotating at 18 rpm 4˚C. Beads are then spun at 400 xg and eluate removed. Eluates are subsequently resolved by SDS-PAGE and analysed via Western blot.

High Salt Protein Immunoprecipitation

High salt Immunoprecipitation experiment were carried out as follows above (see. Protein Immunoprecipitation). With the addition of 3 times 1 ml washed in high salt lysis buffer (1 M NaCl) after the initial post incubation washes. A subsequent 3 time's 1 ml wash step occurs in IP lysis buffer, after the high salt treatment.

mRNP Capture Assay

mRNP capture assays were used to identify protein interactions with mRNA *in vivo* in varying conditions. 1 x 15 cm dish was used per condition and was incubated depending on RNAi needs or confluency. Prior to starting the assay the 2 x binding buffer was incubated at 37 ˚C. 1 x binding buffer was made by mixing 1:1 mRNP lysis buffer with 2 x binding buffer. Per condition a 100 µl of magnetic oligo dt beads (New England Bioscience) were used and washed 3 times in 1 x binding. Cells were crosslinked with 300 mJ/cm2 U.V on ice whilst covered in cold PBS. Whilst crosslinking was occurring control plates were processed (minus U.V).

Each 15 cm dish was lysed in 600 µl of mRNP lysis buffer supplemented with protease inhibitor cocktail and RNase inhibitors. One control dish was lysed lacking RNAse inhibitors and subject to RNAase A treatment - this will allow for conformation of a PolyA$^+$ pulldown of observed proteins. 1-10% of the cleared lysate is kept on ice and used as an input.

Post lyses samples were spun at 4 ˚C, 13 200 rpm for 10 minutes and subsequently transferred to a new pre cooled tube. Lysates were then quantified via a Bradford assay. Equal loading was calculated for addition to the oligo dt beads, each sample was denatured by adding 1:1 lysate and warm 2 x binding buffer at room temperature. Finally before addition to the beads volumes were equalled with 1 x binding buffer. Denatured lysates were added to the beads and incubated for 1 hour at 25 ˚C rotating at 18 rpm. Samples were washed 3 times in 1 x binding buffer at room temperature. Each wash consisted of 1 ml binding buffer, inverted 10 times and then resting on the magnetic rack for 2 minutes. Once washed, beads were dried using a gel loading tip and then resuspended in 60 µl of mRNP elution buffer supplemented with RNase A. Elution was carried out at 25 ˚C shaking at 800 rpm for 30 minutes. Beads were then incubated on the magnetic rack and eluates removed. Eluates and inputs are resolved by SDS-PAGE and analysed via Western blot.

Sodium Dodecyl Sulphate – Polyacrylamide Gel Electrophoresis

All SDS-PAGE gels were run at 30 mA for 1 hour in the Bio-rad Electrophoresis Chambers.

5% Stacking Gel

Component	**Volume**
H_2O_{mq}	6.3 ml
30% Acrylam/0.8% Bisacryl	1.2 ml
Tris pH 6.8	3.5 ml
10% APS	50 µl
TEMED	20 µl

12% Resolving Gel

Component	**Volume**
H_2O_{mq}	3.5 ml
30% Acrylam/0.8% Bisacryl	4 ml
Tris pH 7.8	2.5 ml
10% APS	50 µl
TEMED	20 µl

10% Resolving Gel

Component	**Volume**
H_2O_{mq}	4.1 ml
30% Acrylam/0.8% Bisacryl	3.33 ml
Tris pH 7.8	2.5 ml
10% APS	50 µl
TEMED	20 µl

Western Blotting

A semi dry western blot transfer system was used for all transfers. The transfer cassettes were constructed from 6 sheets of Whatman filter paper (10 cm by 6 cm) and a single sheet of Whatman membrane (10 cm by 6 cm) all pre-soaked in transfer buffer. Three sheets of filter paper followed by the membrane then the SDS-PAGE gel then the final three sheets of filter paper layered on top of the gel. Transfer occurs for 1 hour at 150 mA. The quality of protein transfer was then assed via Ponceau-S stain.

Blocking of the membrane was done via addition of 15 ml Blocking solution onto the membrane gently shaking for 1 hour. Blocking solution was removed and primary antibodies were added (in recommended dilutions) to 10 ml blocking solution, mixed and poured onto the membrane. Incubated gently shaking for 1 hour. After primary incubation the membrane was washed 3 x briefly with TBS-Tween followed by 3 x 15 minutes washed whilst shaking.

Secondary antibody was then incubated on the membrane, again at required dilution in 10 ml of blocking solution. Incubated 30 minutes on shaker. Post-secondary incubation the membrane was washed 3 x briefly with TBS-Tween followed by 3 x 15 minutes washed whilst shaking. Membranes were exposed via the addition of 1:1 volumes of ECL-1 and ECL-2 solution and being placed into the transilluminator. Exposure in the transilluminator occurred at position O, setting Chemi Hi Sensitivity starting at 0.05 with the iris completely open. Pictures for protein markers were taken post exposure using the EPI White setting and not moving the membrane allowing for direct comparison.

Loading was normalised via probing the membrane with anti-Tubulin or anti-Actin at a dilution of 1 in 10 000 and an anti-mouse secondary at a dilution of 1 in 10 000. Prior to probing for Tubulin/Actin the membranes were washed 3 x briefly with TBS-Tween followed by 3x 15 minutes washed whilst shaking. After probing the same exposure protocol as described above was followed.

Protein containing membranes were stored in 10 ml TBS-Tween containing 0.02% Azide at 4˚C. Prior to re-probing the membrane was washed extensively (20 ml x 3 15 minute incubations whilst shaking) with TBS-Tween to remove Azide.

2.2.3 Mammalian Cell Biology

Mammalian Tissue Culture

All cells grown as a monolayer in DMEM supplemented with 10% fetal calf serum (FCS), 1% penicillin-streptomycin and 2 mM glutamine and incubated at 37˚C with 5% CO_2. Cells are passaged twice a week, upon each passage cell were washed with 1x PBS then detached using 0.25% Trypsin/EDTA solution that had been pre warmed to 37˚C. Trypsin was deactivated by the addition of DMEM, then appropriate amounts distributed into flask and/or dishes.

Long Term Storage of Cells

All tissue culture cell lines are stored cryogenically until required. Cells are spun down at 1000 rpm and then the pellet was resuspend in cell freezing media, FCS and 10% DMSO, at a concentration of 3 x10^5 cells/ml. The resulting suspension was transferred into 2 ml cryovials (1 ml of cell suspension) frozen in a -80˚C freezer, when frozen transferred to liquid nitrogen storage.

Defrosting cells from cryogenic storage requires quick thawing at 37˚C then washing of the pellets in 10 ml pre-warmed DMEM. The pellet was finally resuspend in 5 ml DMEM and transferred to a culture flask .

Transient Transfection using TurboFect

Transient transfections were carried out using TurboFect transfection reagent (Thermo Scientific). For a 6 cm dish 6 µg of DNA and 1 ml of reduced serum media (Hyclone MEM-RS) were incubated at room temperature with 12 µl of TurboFect for 20 minutes. Following incubation, all of the media/DNA solution was gently added to the receiving cells. A 24 well plate followed the same experimental procedure, per well, but with a reduced volume and concentration of DNA, 200 µl reduced serum media, 700 ng of DNA and 1 µl of TurboFect.

Transient Transfection using Polyethylenimine (PEI)

A stock of 1 µg/ml PEI was made up in H_2O and stored at 4 ˚C short term and -20˚C long term. The transfection protocol followed that of TurboFect above but instead used 3.5 µg/µl final concentration of PEI. A typical PEI transfection for a 10 cm dish consisted of 15 µg of plasmid incubated in 1.8 ml reduced serum media for 20 minutes with 3.5 µg/µl PEI.

siRNA Transfections with Lipofectamine RNAiMAX Reagent.

siRNA transfections were carried out in either 24 well or 6 well plates. Cells were seeded to achieve 80 % confluence upon transfection (2 x 10^5 for a 24 well plate and 1 x 10^6 for a 6 well plate). RNAiMAX and the required siRNA concentration were diluted in Opti-MEM (Life Technologies) then homogenised and incubated at room temperature for 5 minutes. The siRNA-lipid complex was then added to the cells in a dropwise manner.

Generation of RNAi FlpIn-293t Stable Cell Lines

FlpIn-293 cells were split in DMEM contain Tet free-FCS and no antibiotics into a 6 cm dish with 1 x 10^5 of FlpIn-293 cell suspension per dish and incubated 37 ˚C. 24 hours after splitting the cells are transfected with DNA at a ratio of 6:4 w/w, 3.6 µg of FlpIn recombinase construct (pPGKFLPolpA) and 2.4 µg of FRT vector containing desired RNAi hairpin cassette.

24 hours post transfection the medium (DMEM contain Tet free-FCS and no antibiotics) is renewed. 48 hours post transfection cells are split into 2 x 10 cm dishes in DMEM contain Tet free-FCS and no antibiotics using 500 µl Trypsin. 6 hours after splitting into 10 cm dishes the media is changed to the selection medium, DMEM containing Tet free-FCS and two antibiotics, Blastomycin (15 µg/ml final) and Hygromycin (0.1 mg/ml final). Upon addition of the selection

media cells are left for 48 hours to die. Dead cells are then removed by renewing the selection media. Incubation for a further 5 days occurs before another selection media renewal. Cell growth in colonies is then monitored over a 1-2 week period. Upon colonies filling the 10x magnification of the light microscope objective colonies are subsequently isolated.

Isolating single selected colonies occurs as follows, selection media is removed and cells were washed with 6 ml of 1 x PBS. 3 mm cloning disks were soaked in Trypsin pre warmed to 37˚C and PBS from cells was removed. A single cloning disk was placed onto a single colony for 2 minutes. The disk was then gently scraped off the plate picking up the colony. The soaked disk covered in the selected cells was subsequently dipped into 500 µl of selection media present in a well of a 24 well plate. Several colonies are picked, 24 well plate were incubated until cells were confluent. When cell became confluent they were split into 4 wells for induction and testing.

Induction of incorporated constructs occured via the addition of Tetracycline at a final concentration of 1 µg/µl. Tetracycline was renewed every 48 hours. Efficiency of protein knock down was determined via a western blot.

Luciferase Assay

This assay was employed to measure the levels of luciferase protein in the cytoplasm in MS2-tethered experiments. A 24 well plate was used for transfection of the MS2 constructs and incubated for 48 hours. Cells were then washed in PBS, lysed in 80 µl of Reporter Gene lysis buffer supplemented with protease inhibitors. Cells lysates were transferred to pre cooled 1.5 ml tubes and cleared via centrifugation at 13 200 rpm, 10 minutes, 4 ˚C.

Luciferase activity of the cleared extracts was then measured using the Sirius Luminometer (Berthold Detection Systems). Typically 10 – 15 µl of cleared extract was added to a luminometer tube, mixed with 200 µl luciferase assay

buffer, incubated for 10 seconds then the luminescence was measured. Each condition was done in triplicate and averaged.

Chemi-luminescent ß-galactosidase Assay

This assay allowed for determination of the transfection efficiency for the MS2-tethered constructs used in the luciferase assay. As noted above (Luciferase Assay) cells were lysed in Reporter Gene lysis buffer and cleared via centrifugation.

Dilution of the cleared lysate was carried out, taking 5 µl of cleared extract and diluting 1 in 500 with Reporter Gene lysis buffer. From this dilution 10 µl of cleared extract was mixed with 50 µl ß-galactosidase Detection Kit (CloneTek) reaction mix. The reaction mixture was incubated for 1 hour at room temperature in a luminometer tube. ß-galactosidase activity was subsequently measured using the Sirius Luminometer (Berthold Detection Systems). Again each condition was carried out in triplicate and averaged.

MTT Assay

This was employed to measure cell growth in FlpIN RNAi cell lines. Yellow MTT is reduced in the mitochondria of living cells to purple formazan. Cells were initially plated and induced with Tetracycline in a 24 well plate. Upon day of measurement cells were incubated for 3.5 hours at 37 ˚C in 100 µl of MTT solution. The media is then removed and 750 µl of MTT solvent is added to each well. The plate is then covered in tinfoil and agitated for 15 minutes shaking at 150 rpm. Lysed cells are then transferred into 1 ml crevettes and spectrophotometrically measured at 590 nm. All condition were done in triplicate and averaged.

Fixing Cells

All cells were fixed in 24 well plates onto cover slips. Media is removed from each well and washed 3 times in 500 µl PBS. Next 150 µl of FIX solution is gently pipetted onto each cover slip and incubated for 15 minutes at room temperature. Fix solution is then removed and cells subsequently washed 3 times with 500 µl PBS.

Fluorescence In-Site Hybridisation (F.I.S.H)

Cells were fixed as outlined above. After the final PBS wash cover slips are transferred onto Whattman paper then covered with 150 µl of F.I.S.H hybridisation buffer supplemented with tRNA, ssDNA and Cy-3. Cover slips were then incubated for 2 hours at 37 ˚C. Post incubation cover slips are moved back into the 24 well plate and undergo 3 times 500 µl PBS wash. Once washed, cover slips are mounted onto slides using Vectashield mounting medium supplemented with DAPI. If slides are to be stored they were sealed with nail varnish.

Immuno-staining

All immuno-staining was carried out in 24 well plates containing cover slips. Upon confluency, cover slips were incubated for 1 hour with 500 µl PBS containing 1% BSA. The primary antibody was then added onto the cover slips in PBS containing 1% BSA and incubated for 1 hour. Post primary incubation the cover slips were washed in 1 mL PBS containing 1% BSA, 3 times with a 5 minute incubation per wash. Subsequently the secondary antibody was added to the over slips at a dilution of 1/800 in PBS + 1% BSA, incubated for 30 minutes. Finally the cover slips were washed a further 3 times (as previously conducted) then mounted onto slides with 2 µl Vectasheild mounting medium containing DAPI. Slides are then sealed and stored at 4˚C.

2.2.4 RNA Biology

Total RNA Extraction

Total RNA extraction from HEK293t cells was carried out using TRIzol reagent (ThermoFisher). 1 ml of TRIzol reagent was added to cells post PBS wash. Samples were homogenized via vigerous pipetting up and down. Samples were then incubated for 5 minutes at room temperature, followed by the addition of 200 µl Chloroform and further homogenization. A further 15 minutes room temperature incubation then takes place. Next centrifugation of samples at 12000 xg, 15 minutes and 4˚C. The aqueous phase was then transferred to a clean tube in which the RNA was precipitated with 1 µL glycogen and 500 µL isopropyl alcohol per 1000 µL TRIzol initially used.

RNA samples were incubated for 10-15 minutes at room temperature then centrifuged again 12000 xg for 5 minutes at 4˚C. The RNA pellet was subsequently washed with ice cold 75% Ethanol then centrifuged again at 7500 xg at 4˚C for 5 minutes. The RNAi pellet was then air dried to remove excess Ethanol before resuspension.

DNase I Treatment

All RNA extracted was subject to DNase treatment. RNA pellets were resuspended in 42 µL $H_2O_{RNase\ Free}$ and 5 µL 10x Buffer- Turbo DNase (NEB) via soaking 20 minutes on ice and shaking 1100 rpm for 20 minutes. 2 µL (10U) Turbo DNase and 1 µL of RNase Inhibitors (Bioline) were added to each sample then treated for 1 hour at 37 ˚C.

RNA Phenol Chloroform Precipitation.

Phenol-Chloroform precipitation was conducted to remove DNase from the samples. Each RNA sample was made to a final volume of 100 µL using $H_2O_{RNaseFree}$. Acidic phenol (pH 5.5) was mixed with each sample at a 1:1 ratio. Homogenisation was done via shaking followed by 5 minute room temperature incubation. 90 µL of the aqueous phase was then moved to a fresh tube with 1 µL glycogen, 10 µL NaAc (3M pH 5.8) and 250 µL Ethanol.

PolyA+ RNA Purification from Total RNA

All buffers are initially brought to room temperature. Per condition, 200 µL of magnetic oligo-dt Dynabeads are washed 3 times with 100 µL PolyA+ binding buffer, beads remain in final wash. Then 30-75 µg of Total RNA was adjusted to a total volume of 100 µL with $H_2O_{RNaseFree}$, subsequently mixed with 100 µL PolyA+ binding buffer (1:1 ratio if Total RNA volume exceeds 100 µL). The Total RNA mix was then denatured for 2 minutes at 65˚C followed by immediately placing it ice. The denatured RNA was then mixed with the Dynabeads and incubated for 5 minutes, room temperature rotating at 27 rpm. Post incubation the beads were washed twice with 200 µL PolyA+ wash buffer B. Elution was carried out using 20 µL ice cold PolyA+ elution buffer and heating to 80˚C for 2 minutes. Eluted PolyA+RNA was transferred to a fresh pre cooled RNase free tube.

m^6A -Dot Blot Assay

Purified PolyA+ RNA samples (50-200 ng) were made up to 10 µL with $H_2O_{RNaseFree}$. Samples were blotted onto Hybond membrane with an area of 1 cm^2 per sample. Blotting was done in a drop wise fashion whilst under 200 mbar of pressure, provided via a vacuum pump. The membrane was allowed to dry before

U.V crosslinking with 70 mJ/cm^2. Next the membrane was blocked for 1 hour, 25˚C in 5% nonfat dry milk in PBS-Tween (0.1%). Anti- m^6A (Synaptic Systems No. 202 003) was incubated for 1 hour, with the membrane at a dilution of 1 in 2000 in PBS-Tween (0.1%). Subsequently the membrane was washed 3 times for 15 minutes in 20 mL 0.1% PBST. The secondary antibody (anti-Rabbit, 1 in 5000) was incubated on the membrane in 5 % nonfat dry milk PBS-Tween (0.1%) for 1 hour. A further 3 times, 15 minutes in 20 mL 0.1% PBST washing before exposing the membrane. The membrane was exposed using ECL solution as previously described for the Western Blot technique. Equal loading of RNA was determined via incubating the membrane for 30 minutes in 0.02% Methylene Blue and 0.3 M Sodium Acetate. The stain was removed via 2 quick washes in H_2O, RNA blots were stained blue and the membrane returned white.

Formaldehyde RNA Immuno-Precipitation

Formaldehyde crosslinking was carried out on a 6 cm dish (2 dishes per condition). First the media was removed and cells washed with 3 mL of PBS. Next, incubated for 10 minutes in 3 ml of the fix solution (PBS -Formaldehyde (0.1%)) at room temperature. The fixing reaction was sequestered with the addition of Glycine (0.125 M final concentration per dish), dishes were rotated for 5 minutes at 10 rpm. The fixed cells underwent 3 ice cold PBS washes in 15 mL Falcon tubes, cells were spun at 500 xg for 3 minutes after every wash. The resulting pellet was stored at -80°C if not proceeding immediately.

Each sample required 100 µL Protein-G Dynabeads. The beads were prepared by initial washing in 900 µL RIP lysis buffer before being blocked for 1-24 hours in 300 µL, 1% BSA, RIP lysis buffer and relevant antibody (2-10 µg). The blocking of beads was done at 4°C rotating at 18 rpm. Once blocked, beads were washed 3 times in 900 µL RIP lysis buffer, before addition of lysate.

Fixed cell lysis and RNA shearing was achieved using sonication. The Bioruptor machine (Diagenode) was pre-cooled to 4°C. Each pellet was then lysed

in 400 µL RIP lysis buffer supplemented with protease inhibitors (Protease inhibitor cocktail, Sigma Aldrich), RNase inhibitors (Ribosafe, Bioline) and TurboDNAse (Ambion). The lysate was homogenised and transferred to pre cooled Bioruptor 1.5 mL tubes. Sonication occured at the high amplitude setting with 30 seconds on 30 seconds off, for 5 cycles. Sonicated samples were then transferred to a fresh 1.5 mL tube and spun 16 100 xg for 10 minutes at 4°C to remove cellular debris.

Immunoprecipitation was carried out with the cleared lysate. 300 µL of each sample was homogenised with the Dyna beads, 30 µL of lysate was kept as an input (10%). The beads and lysate were incubated at 4°C for 2 hours whilst rotating at 18 rpm. Post incubation the beads are washed twice in 900 µL RIP lysis buffer. Then washed twice more in 900 µL high-salt RIP lysis buffer, each wash was incubated on ice for 5 minutes. The beads then underwent 2 final wash steps in 900 µL RIP lysis buffer. Each wash step was carried out using a magnetic rack, once washed beads were allowed to separate from the buffer for 2 minutes on the rack.

Elution from the beads was done via incubation with Protease K to digest the antibody. The washed beads were suspended in 56 µL $H_2O_{RNaseFree}$ and 33 µL 3x reverse crosslinking buffer. The inputs were diluted with 26 µL $H_2O_{RNaseFree}$ and 33 µL 3x reverse crosslinking buffer. Each elution and input was incubated for 1 hour at 42°C shaking 1100 rpm for 2 hours with 10 µL Proteinase K (Roche, 19 mg/mL). Proteinase K was subsequently denatured via incubation at 55°C for an hour. Beads were then moved to the magnetic rack and eluate/input removed. The resulting eluates and inputs were made up to 250 µL using $H_2O_{RNaseFree}$ and subjected to TRIzol extraction (Detailed above).

The RNA is further subject to DNase treatment before undergoing reverse transcription. All RNA obtained from the immunoprecipitation and inputs was used for cDNA synthesis. Finally the cDNA undergoes qPCR analysis.

RNA extraction from 293T cells: Total or Nuclear/Chromatin/Cytoplasmic RNA

The starting material for each condition was two 10 cm dishes. All tubes and buffers were kept on ice throughout the procedure. Cells were washed with 10 mL PBS then removed from the dish via Trypsinization (0.25-0.5 mL trypsin/EDTA pre-warmed at 37°C) and inactivated with 4 mL of medium + 10 % FCS, decanted into a 10 mL round bottom tube. The cells were pelleted at 500 xg, 3 minutes and washed 3 times in 10 mL PBS.

Cell lysis was carried out in 400-1000 µL N/C lysis buffer supplemented with 0.5% Triton-X, protease inhibitors (Protease inhibitor cocktail, Sigma Aldrich), RNase inhibitors (Ribosafe, Bioline) and DTT. The N/C supplemented lysis buffer was added to the 10 mL round bottom tube. Hand rotation/rocking was employed to resuspend the pellet causing lyse. Once complete the lysate is transferred to a cool 2 mL tube and centrifuged for 5 min at 500 x g, 4°C. The resulting supernatant was the cytoplasmic fraction. The supernatant is removed then centrifuged again 1 min, 16100 x g, 4 °C, to clear any contaminates, and finally TRIzol treated to extract the cytoplasmic RNA. The pellet was the nuclei, it underwent a further 3 times wash in N/C lysis buffer. Each wash was followed by centrifugation 500 x g, 3 min, 4°C to pellet the nuclei. Post wash, the whole nuclei RNA extraction can be carried out by homogenization of the nuclear pellet with TRIzol.

If undergoing nucleoplasm and chromatin extraction the nuclei pellet was homogenised in 350 µL of NRB buffer via inversion. An equal volume of NUN buffer was added followed by incubation on ice for 5 minutes, with inversion mixing every minute. Samples were centrifuged 1200 x g for 5 minutes at 4°C. The resulting supernatant is the nucleoplasm, 250 µL was removed and subject to TRIzol LS extraction. The remaining supernatant was removed leaving the chromatin pellet. The chromatin was homogenized with 1 mL Buffer A, centrifuged 1200 x g for 5 minutes at 4°C. The supernatant was discarded and the resulting pellet subject to TRIzol extraction.

Western Blots were carried out to ensure accurate extraction of each phase. Histone 3 was used as a chromatin marker, Alyref or SSRP1 were used to identify a clean nuclear/nucleoplasm fraction and Tubulin was used as a cytoplasmic marker. Note that prior to western blot analysis chromatin fractions underwent a 30 minute Benzonase treatment to release the chromatin bound proteins.

All RNA extracted underwent DNase treatment after TRIzol extraction. Once DNase treated, and cleaned via phenol extraction, the RNA concentration was measure spectrophotomicaly. Equal amounts of RNA for each condition was used as a template in cDNA synthesis. The final step was analysis of transcripts via qPCR.

Chapter 3: The Relationship between m^{6}A machinery and the TREX complex.

The highly conserved Transcription Export (TREX) complex and heterodimeric export receptor, Nxf1-p15, are responsible for the bulk of mRNA export within a mammalian cell. Throughout the literature, data has been presented suggesting components of the TREX complex interact with members of the m^{6}A methyltransferase complex. Mass spectrometry studies have identified export adaptor Alyref associating with Kiaa1429 (Masuda *et al.*, 2005b), Wtap associating with Uap56 and Alyref (Small and Pickering, 2009). Phenotypic observations alluded to a possible mRNA export defect upon m^{6}A reduction (Fustin *et al.*, 2013) and increased mRNA export upon removal of the eraser, Alkbh5 (Zheng *et al.*, 2013). However there are no definitive experiments indicating a cooperative pathway involving TREX export and mRNA adenosine methylation.

The transcriptome wide m^{6}A landscape has been shown to change upon stress conditions, such as heat shock (Zhou *et al.*, 2015). With this information we set out to identify the epitranscriptomic response to an mRNA export block. To achieve an mRNA export block we targeted major components of the (TREX) complex and the export receptor Nxf1 via RNAi. Further investigation of the methyltransferase machinery and TREX produced interaction data indicating a possible functional overlap between pathways.

3.1 Perturbation of the TREX/Nxf1 pathway results in greater total m^{6}A.

The initial stages of this investigation set out to identify if the methylation complex and/or m^{6}A respond to an mRNA export block. This was measured via an RNA dot blot assay, probing with anti-m^{6}A. To ensure an effective export block central components of the TREX/Nxf1 export pathway were subject to RNAi. Total RNA was extracted from 48 hour induced Nxf1 RNAi and Thoc5/Alyref RNAi. A 48 hour induction of the RNAi provides an adequate protein knock down and ensures the cells have not begun to undergo apoptosis (Viphakone *et al.*, 2012) (Figure 3.1a). Total RNA was then subject to on bead PolyA+ purification, followed by blotting (100 ng per condition) and anti-m^{6}A probing. Specificity of the anti-m^{6}A antibody was demonstrated by Meyer et al in 2012, it does not recognise non methylated PolyA+ RNA or adenosine methylated at an alternative position. Loading of the PolyA+ RNA was controlled by 0.2% Methylene blue staining post blot exposure. The result indicated that upon a harsh export block there is an increase in m^{6}A within the total mRNA population (Figure 3.1b). However it must be noted that with this simple experiment we cannot determine if there is an increase in m^{6}A per transcript or an increase in expression of transcripts that are subject to methylation.

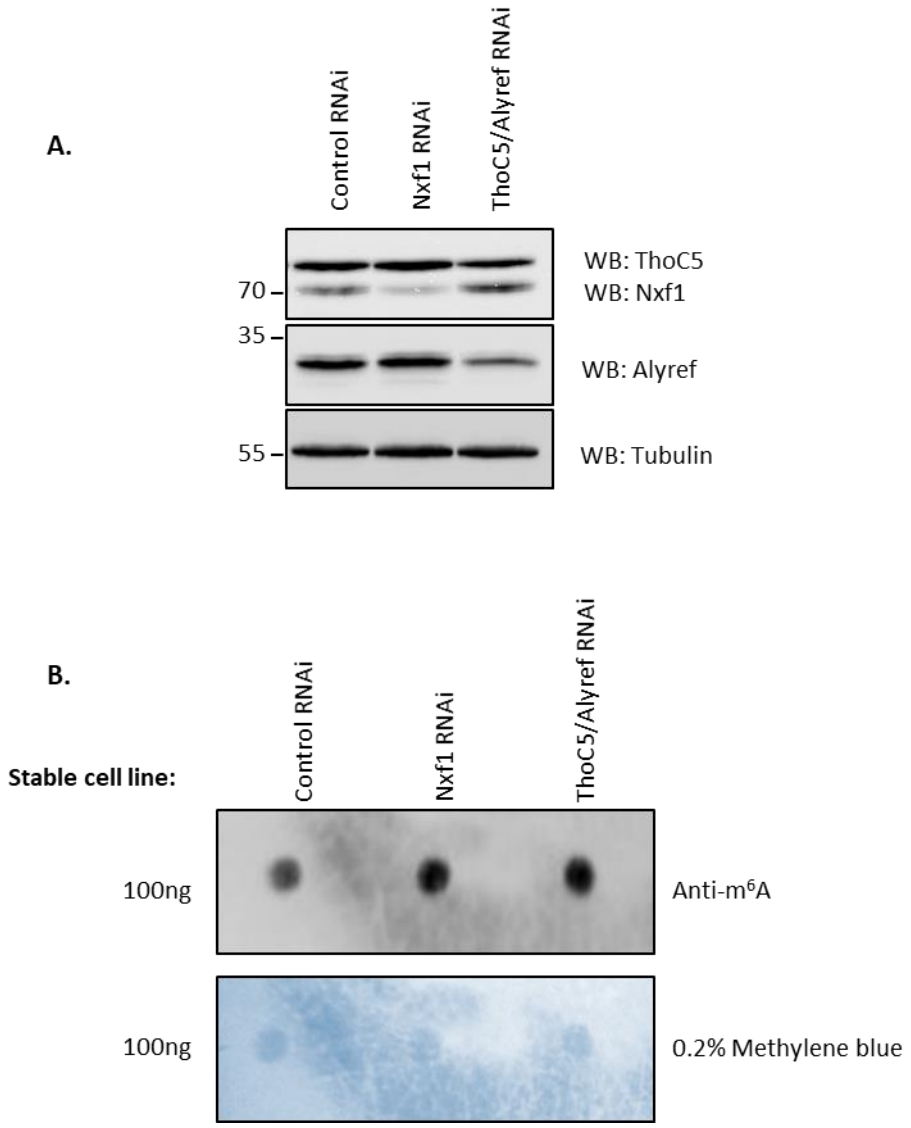

Figure 3.1 Dot blot illustrating m^6A response to the knockdown of Thoc5/Alyref and Nxf1. Total RNA was extracted from 48 hour RNAi of core TREX complex components and the export receptor Nxf1 (**A**) and subject to PolyA+ purification. **B.** 100ng of purified RNA was blotted and U.V crosslinked on Hybond N+. The results indicate a global increase in m^6A levels on PolA+ RNA.

3.2 Methylation writers and erasers respond to a TREX/Nxf1 knockdown.

The next stage of the study was to identify a possible mechanism responsible for the increased m^{6}A in the Thoc5/Alyref and Nxf1 RNAi conditions. Therefore cleared lysate from Thoc5/Alyref and Nxf1 RNAi, post 48 hours induction, and was subject to western blot analysis. This was to detect any change in protein levels of either the methyltransferase complex (Wtap, Mettl3) or the nuclear eraser Alkbh5 (Figure 3.2a). The resulting western blot indicated a possible basis for the increase in m^{6}A. Firstly, Wtap protein levels increased in the export block conditions. The anti-Wtap (Santa Cruz Biotechnology) blot also presents two separate bands, the ratio of these bands shifts within the export block conditions with a strong upper band present in Thoc5/Alyref RNAi compared with Control RNAi. The pattern observed in the ant-Wtap probe is indicative of the addition/removal of a post translational modification. It is interesting to note that the levels of Mettl3 do not increase along with Wtap in the export block conditions. The second writer enzyme Mettl14 was not probed as it has previously been published that its expression mimics that of Mettl3 (Ping *et al.*, 2014). The second observation from the western blot is the loss of the demethylase Alkbh5 in both export block RNAi condition. The reduction in Alkbh5 have previously been shown to increase global levels of m^{6}A (Zheng *et al.*, 2013).

Along with the protein analysis total RNA was extracted from each condition (Nxf1 and Thoc5/Alyref RNAi), and equal concentrations used as a cDNA template. The resulting cDNA was subject to qPCR analysis to assess the mRNA levels of the writers and the eraser. Figure 3.2b indicates that the *Wtap, Mettl3* and *Alkbh5* mRNA abundance in TREX/Nxf1 RNAi conditions does not significantly change, when compared to Control RNAi. The results of this experiment suggested change in m^{6}A protein machinery upon export perturbation.

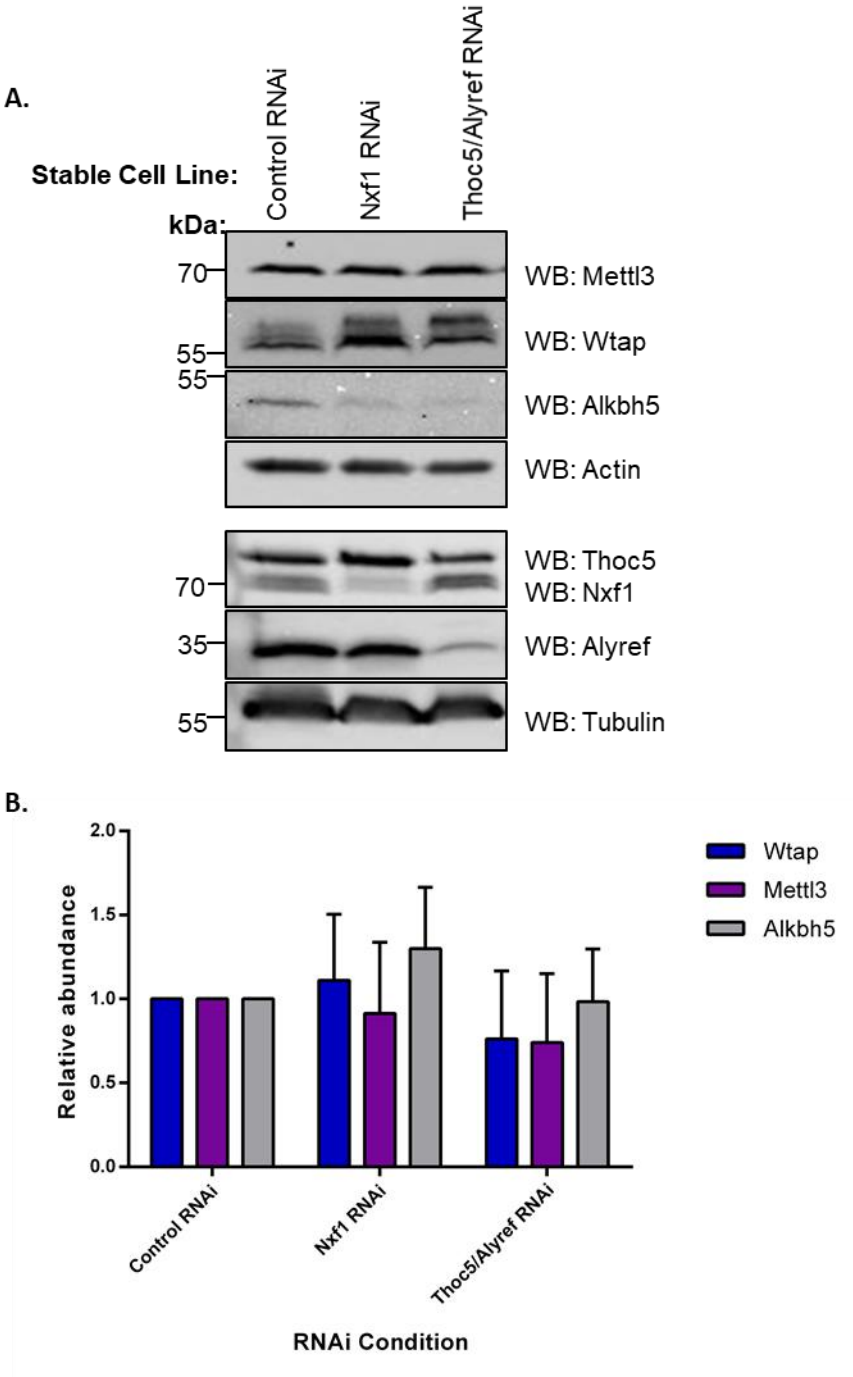

Figure 3.2 m^{6}A machinery protein and RNA response to a Thoc5/Alyref and Nxf1 knockdown. **A**. Western blot indicating Wtap levels appear increased in both knock down conditions. Alkbh5 protein levels decrease in each RNAi condition when compared to control RNAi. **B**. Total RNA extraction revealed no significant change in *Wtap, Mettl3* or *Alkbh5* mRNA.

3.3 *Alkbh5* and *Wtap* Transcript levels are reduced in the cytoplasm.

With the knowledge of Alkbh5 protein levels decreasing we aimed to determine if this was a targeted cellular response, or simply a nonspecific response to the mRNA export block. Nuclear and cytoplasmic RNA fractions from Thoc5/Alyref and Control RNAi were subject to cDNA synthesis and qPCR analysis. Sufficient fractionation of the nuclear and cytoplasmic RNA was assessed via western blot analysis and qPCR, Figure 3.3.1. Nuclear protein Ssrp1 and cytoplasmic protein Tubulin in Figure 3.3.1a show a clean separation of each fraction, further confirmation is presented in Figure 3.3.1b indicating no detectable unspliced HnrnpA2B1 in the cytoplasmic fraction.

Figure 3.3.2 confirms an export block in the Thoc5/Alyref RNAi condition, indicated by the positive nuclear cytoplasmic ratio (3.3.2a). The nuclear levels of *Alkbh5* and *Wtap* do not significantly increase (3.3.2b), this may be due to degradation of the mRNA when locked in the nucleus. As expected in a strong export block condition the levels of *Alkbh5* and *Wtap* significantly decrease within the cytoplasmic fractions (Alkbh5 p-value 0.0018 and Wtap p-value 0.0173), presented in Figure 3.3.2c. Interestingly a 76% reduction in *Alkbh5* abundance was observed compared with the 33% decrease of *Wtap*. This indicated a short half-life of the *Alkbh5* mRNA.

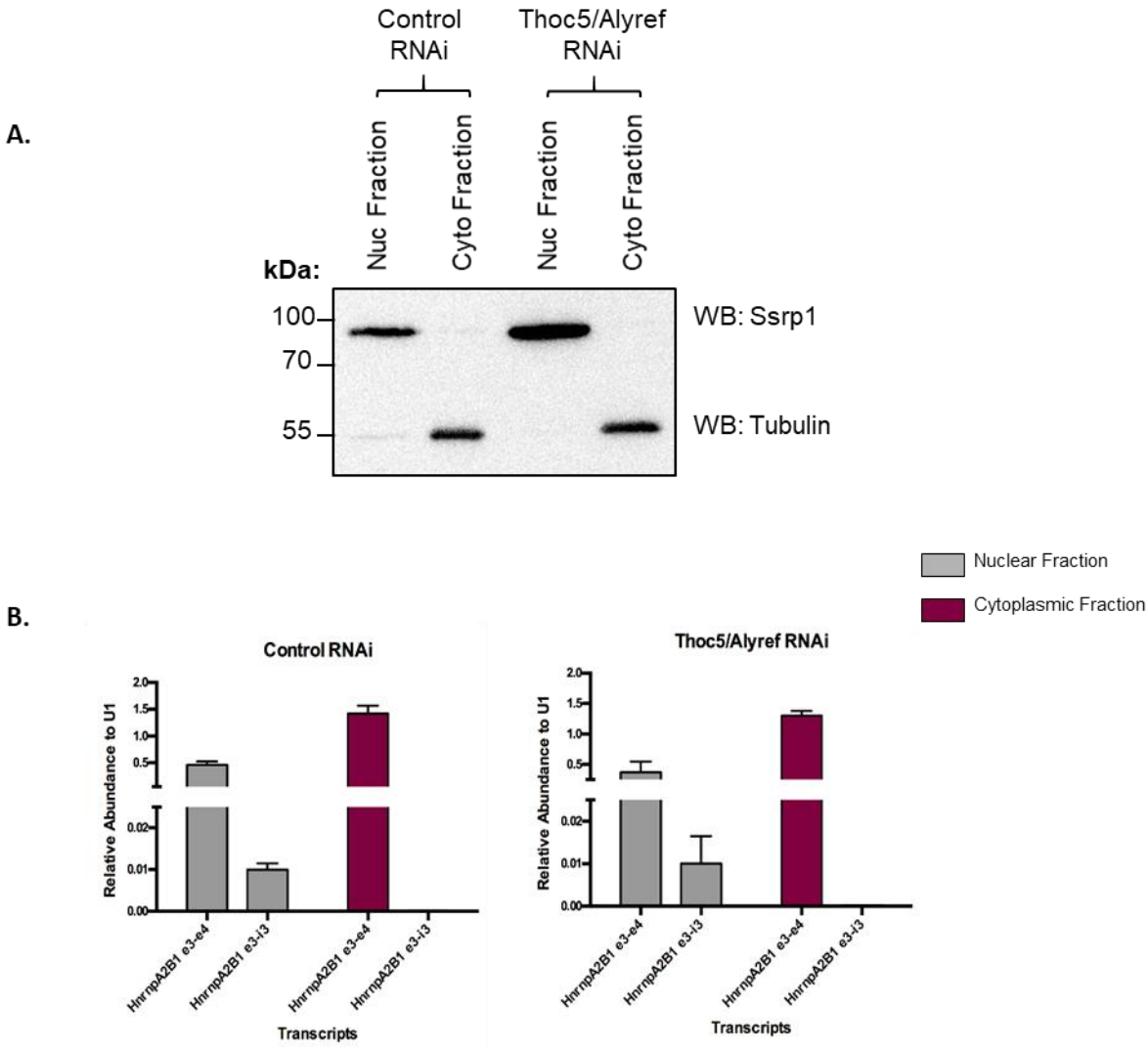

Figure 3.3.1 Validation of fractionation of RNA in Thoc5/Alyref RNAi for nuclear /cytoplasmic analysis. **A.** Western blot showing nuclear protein Ssrp1 and cytoplasmic protein Tubulin have not leaked between fractions. **B.** qPCR on each fraction for HnrnpA2B1 e3-e4, e3-i3. Confirms no pre-mRNA is present in the cytoplasm.

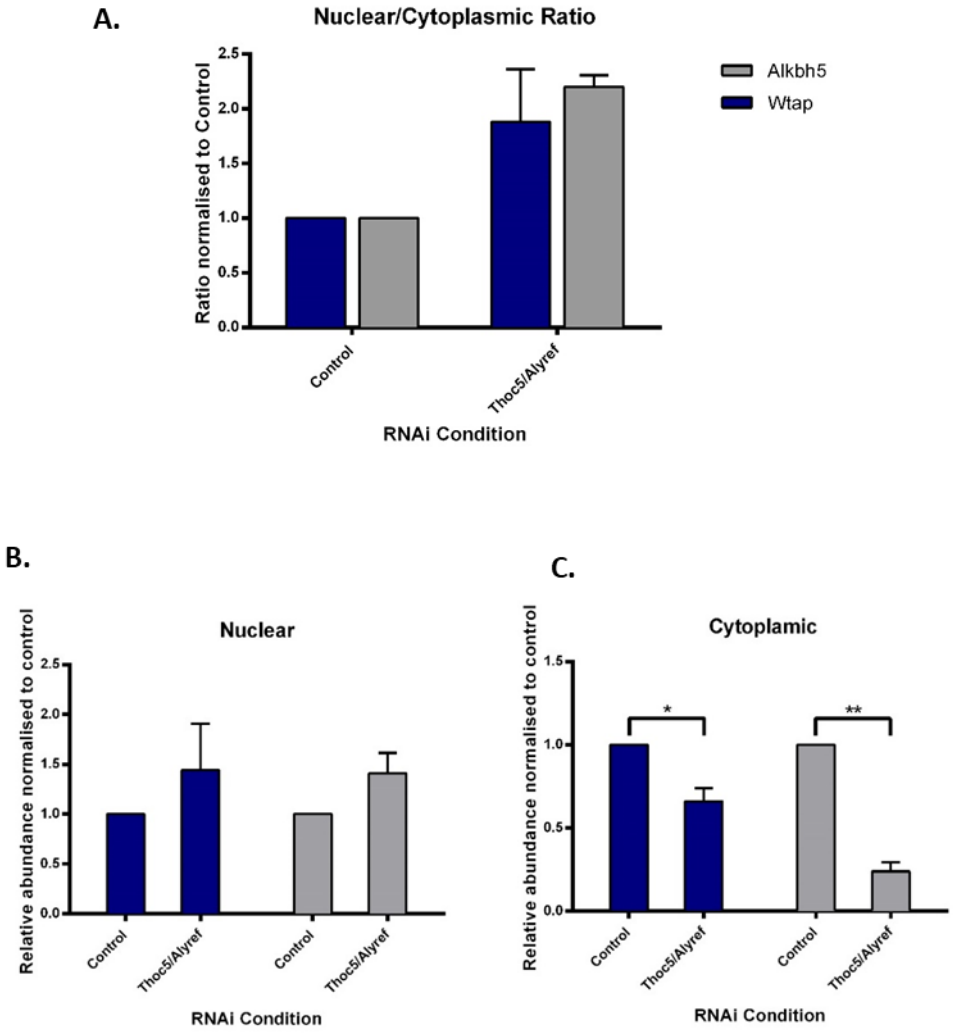

Figure 3.3.2 *Wtap* and *Alkbh5 transcripts* significantly decrease in the cytoplasm upon Thoc5/Alyref RNAi. A. qPCR Nuclear/cytoplasmic ratio of *Wtap* and *Alkbh5*, the positive ratio indicates an export block **B.** Nuclear levels of *Wtap* and *Alkbh5* do not significantly change **C.** Cytoplasmic levels of *Wtap* and *Alkbh5* significantly decrease compared to control. *Alkbh5* p-value 0.0018 and *Wtap* p-value 0.0173.

3.4 Alkbh5 has a shorter half-life that Wtap.

Previous observations identifying Alkbh5 sensitivity upon ThoC5/Alyref RNAi could be one of the reasons for its decreased protein levels. Therefore we set out to identify the half-life for Alkbh5 compared to the methyltransferase writer complex components. Cycloheximide was employed to inhibit translation within cells during the half-life time course, cycloheximide was renewed in the media after 8 hours. Alkbh5 has a shorter half-life compared to Wtap (Figure 3.4). After 12 hours Alkbh5 levels within a HEK293T cell were reduced to ~ 50%. A similar reduction was observed with Alyref. On the other hand Wtap presented a longer half-life whilst Mettl3 does not change up to 14 hours.

With the observed Alkbh5 half-life and its mRNAs sensitivity to an export block we could hypothesise the increase in methylation upon a Thoc5/Alyref and Nxf1 RNAi is an indirect affect resulting from the loss of Alkbh5. Our conclusion of increased m^6A resulting from reduced Alkbh5 is consistent with the current literature, knockdown of Alkbh5 significantly increases m^6A levels. (Zheng *et al.*, 2013).

3.5 TREX/Nxf1 RNAi does not affect the methyltransferase complex.

To identify any further response by the methyltransferase complex in an export block condition a Wtap-Flag co-immunoprecipitation (Co-IP) experiment was conducted in Thoc5/Alyref and Nxf1 RNAi background. Experimental conditions were co-transfection of Flag-Wtap and induction of RNAi cell lines followed by 48 hour incubation. All pulldowns were carried out in the presence of DNase and RNase. Figure 3.5a depicts no change in the methyltransferase complex formation in an export block background, compared with control. Specificity of the pulldown was confirmed by an HnrnpA1 probe producing no binding.

Observing a small increase in Wtap levels upon Thoc5/Alyref and Nxf1 RNAi (Figure 3.2) lead to the possibility of an increased deposition of Wtap upon mRNA,

alluding to further explanation for the increased methylation. To detect a global increase in deposition of Wtap on the mRNA we employed an mRNP capture assay, which detects proteins directly bound to poly A+ RNA *in vivo*. The mRNP capture assay was controlled with non-UV crosslinked capture and a UV crosslinked RNase supplemented condition. The RNAse condition illustrates the polyA+ specific pulldown. The resulting mRNP capture blot indicated no change in Wtap deposition onto the mRNA (Figure 3.5b). The input western blot also depicts a less pronounced difference in Wtap protein levels between RNAi conditions; therefore the observed pattern in Figure 3.2 may be an experimental artefact. However the Wtap western blot still produces a blurred band indicating a protein modification. Another interesting observation is the increase deposition of Alyref and Uap56 within Nxf1 knockdown.

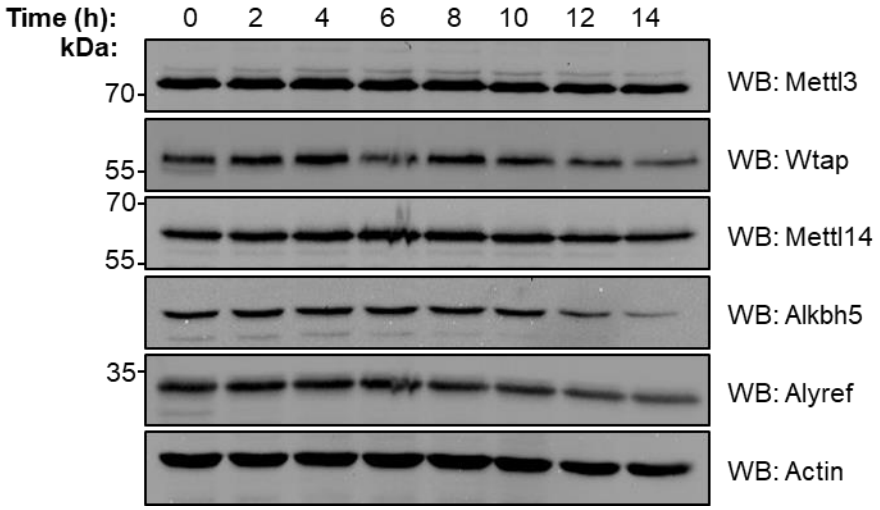

Figure 3.4 Protein half life of the methyltransferase machinery. 20uM Cycloheximide treated Hek293t cells were harvested at two hour intervals for 14 hours. Mettl3/Mettl14 levels did not change, Wtap levels reduced at 14 hours whilst Alkbh5 showed the shorted half life at 12 hours with minimal protein present at 14 hours.

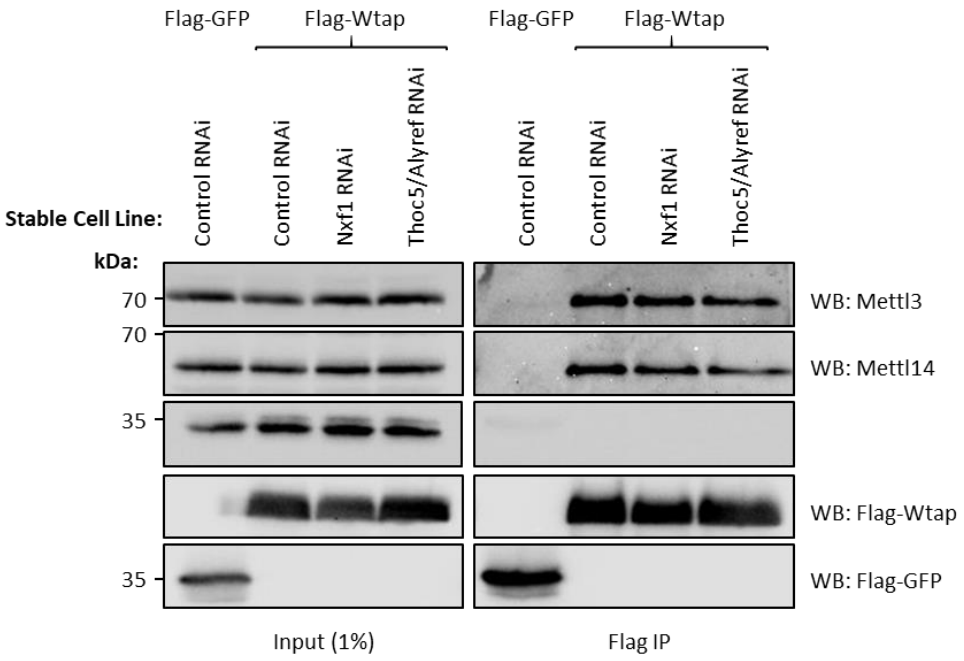

Figure 3.5a Thoc5/Alyref and Nxf1 Knockdown do not affect the m6A writer complex formation. CO-IP of Wtap-Flag transfected into Thoc5/Alyref and Nxf1 RNAi. No change in Mettl3/Mettl14 pulldown with Flag-Wtap compared to control RNAi.

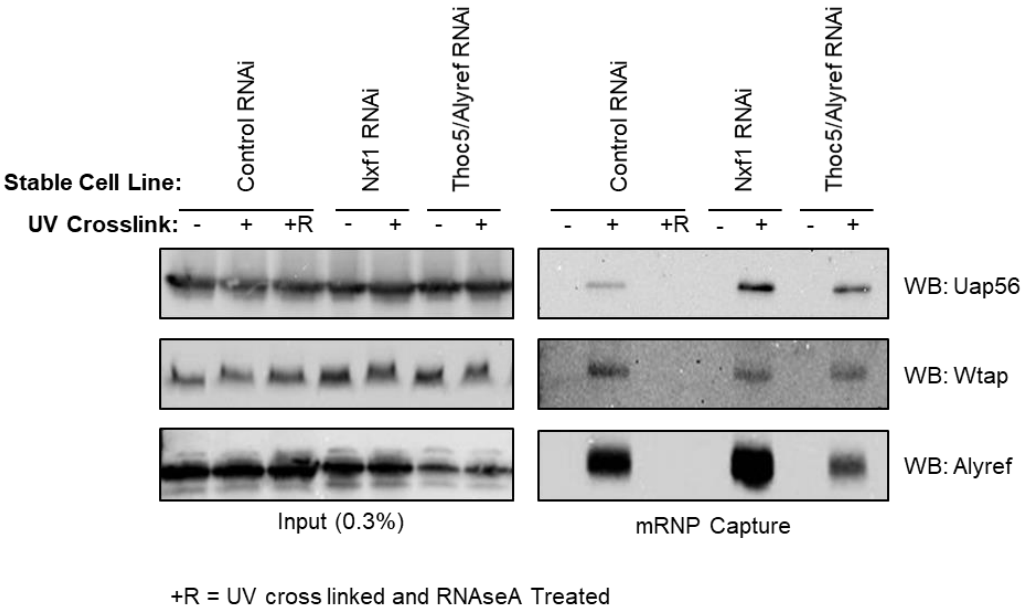

Figure 3.5b Thoc5/Alyref and Nxf1 RNAi does not affect Wtap loading onto the mRNA. mRNP capture with 48 hour RNAi. Wtap levels upon the mRNA did not change. Uap56 and Alyref deposition was increased upon Nxf1 RNAi.

3.6 m^{6}A Writers and the TREX complex associate.

Throughout the current epitranscriptomic literature are small links between the methyltransferase machinery and the TREX complex (Masuda *et al.*, 2005b; Small and Pickering, 2009; Fustin *et al.*, 2013; Zheng *et al.*, 2013). Therefore we aimed to identify any interactions using Co-IP experiments. All pulldowns were carried out in the presence of DNase and RNase. Figure 3.6a Co-IP of endogenous Wtap and Kiaa1429 from HEK293T lysate. The results confirm the TREX components can exist in a complex with the regulatory elements of the m^{6}A machinery. Thoc5, Uap56 and Alyref all pulled with both Kiaa1429 and Wtap, however the Wtap IP has a greater fold enrichment. This confirms Alyref mass spectroscopy studies identifying Kiaa1429 as an interacting partner (Masuda *et al.*, 2005b). Export receptor Nxf1 was also observed co-immunoprecipitating (Co-IP) with Wtap but not Kiaa1429. The nuclear reader Ythdc1 was also identified to associate with Wtap but surprisingly not Kiaa1429. The Co-IP was controlled using an antibody to detect HnrnpA1, a general mRNP binding protein. It's absence in the CO-IPs for WTAP and KIAA1429 indicate the interactions with the TREX complex are specific. . Mettl3 was included as a positive control and gave an increased enrichment compared with the input, indicating a strong association.

Further endogenous Co-IP experiments were conducted with the catalytic heterodimer Mettl3/Mett14, Figure 3.6b. Alyref, Uap56 and Thoc5 all Co-IP with each member of the heterodimer but were more enriched with Mettl14. Kiaa1429 only appeared to associate with Mettl14. Chtop pulldown with Mettl14 but not Mettl3, however it was not enriched over input levels suggesting a very weak association, this also indicated the specificity of the pulldown with other TREX members. The strong self-interaction of Mettl3/Mettl14 was observed and used as a positive control.

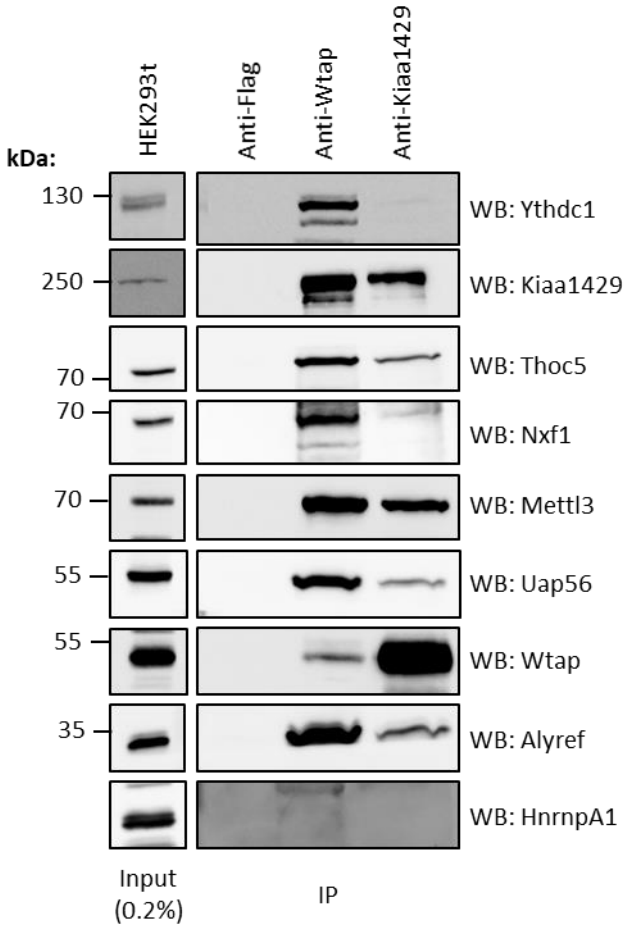

Figure 3.6a Wtap and Kiaa1429 are in complex with the TREX complex and Nxf1. An endogenous CO-IP of Wtap (Santa Cruz Biotechnology) and Kiaa1429 pulling down core TREX complex members Alyref, Thoc5 and Uap56. HnrnpA1 probe indicates the IP is specific.

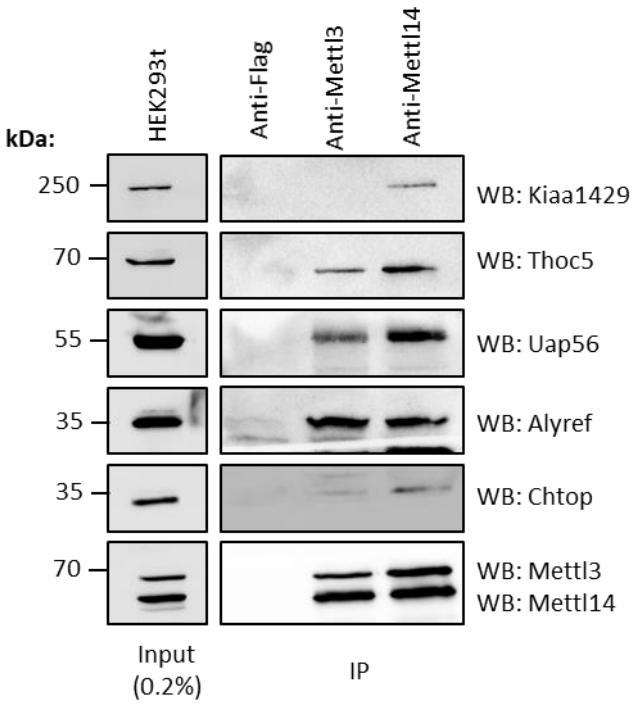

Figure 3.6b Mettl3 and Mettl14 are in complex with certain members of the TREX complex. An endogenous CO-IP of Mettl3/Mett14 with core TREX complex members Alyref, Thoc5 and Uap56. Chtop probe indicates the IP is specific to certain TREX members. Kiaa1429 is only associated with Mettl14.

3.7 Kiaa1429 acts as a scaffold for the methyltransferase complex and the TREX complex.

To further dissect the interaction between these two complexes we treated HEK293T cells with Kiaa1429 siRNA prior to an endogenous Wtap Co-IP. The hypothesis behind this experiment was Kiaa1429 may act as a bridge/scaffold between the methyltransferase complex and TREX due to Kiaa1429s large size (250 kDa) and previous binding data to Alyref (Masuda *et al.*, 2005b). The results after a 72 hour Kiaa1429 siRNA treatments and Wtap Co-IP are presented in Figure 3.7. Knock down of Kiaa1429 culminates in a reduced association of the TREX complex and Mettl3 with Wtap. This reduction is less apparent with ThoC5 compared to Alyref, Uap56 and Chtop. This result may explain the four-fold reduction in methylation observed upon Kiaa1429 siRNA (Schwartz *et al.*, 2014).

3.8 Kiaa1429 siRNA does not result in PolyA+ nuclear accumulation.

Using our Co-IP results we hypothesised that knockdown of Kiaa1429 may lead to an export block, as TREX has a reduced association with Wtap and may hinder mRNA maturation. Therefore fluorescence in situ hybridisation with oligo(dT) to detect poly A+ RNA (FISH) was conducted in Control and Kiaa1429 siRNA 72 hour treated HELA cells. The results displayed in Figure 3.8 indicate no accumulation of PolyA+ RNA within the nucleus upon Kiaa1429 knockdown. However, FISH detects global poly A+ RNA rather than methylated mRNAs and therefore this may account for the lack of phenotype.

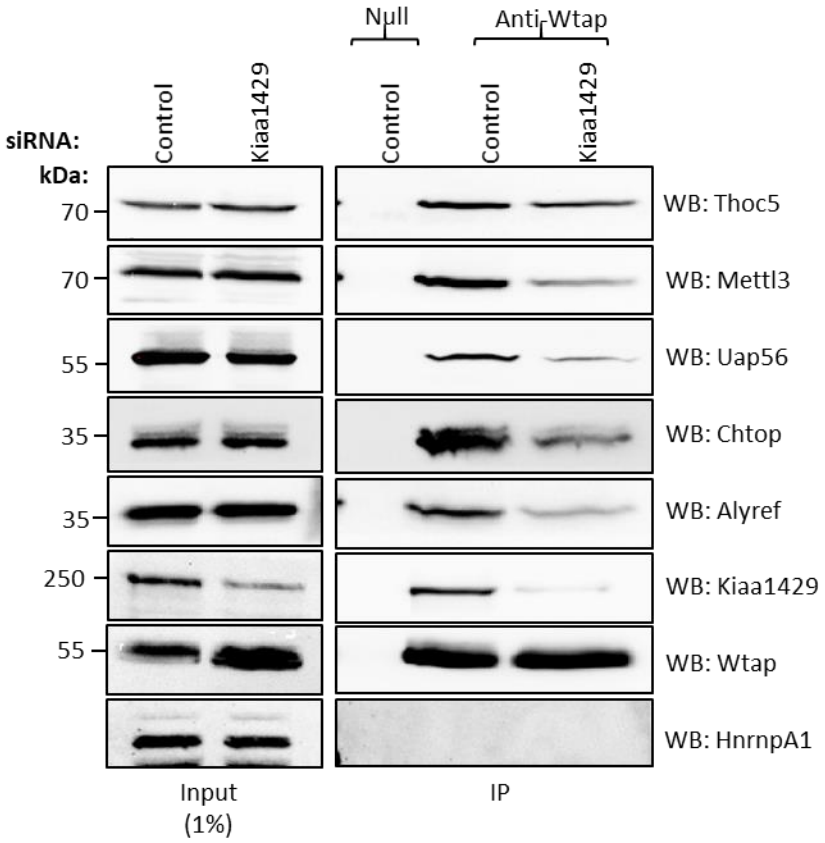

Figure 3.7 Kiaa1429 acts as a writer complex scaffold and TREX members only associates with a complete complex. An endogenous CO-IP of Wtap (Santa Cruz Biotechnology) in Kiaa1429 siRNA background. Core TREX complex members Alyref, Chtop, ThoC5 and Uap56 present in Control CO-IP. Reduced association of TREX members observed in Kiaa1429 siRNA CO-IP. Mettl3 CO-IP is decreased suggesting defective writer complex formation.

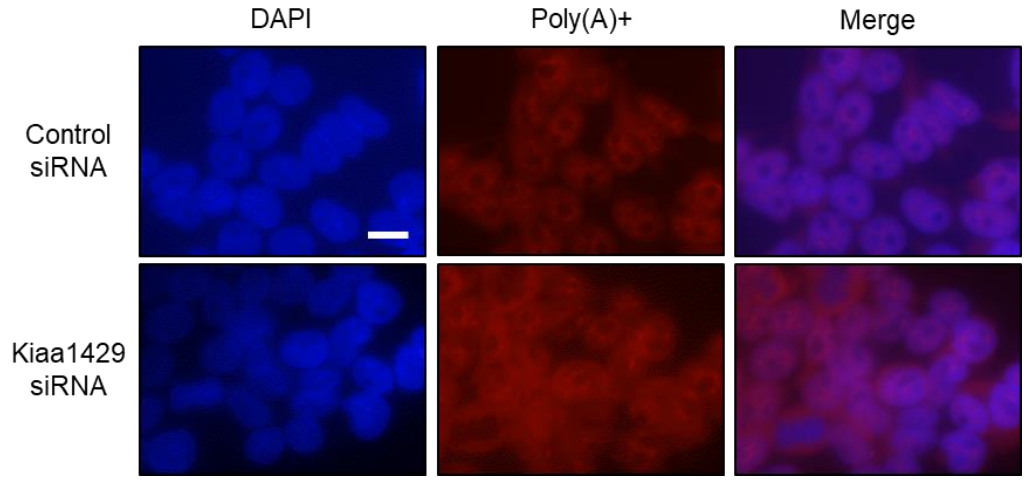

Figure 3.8 Kiaa1429 siRNA does not result in nuclear PolyA+ accumulation. Kiaa1429 siRNA was carried out for 72 hours prior to fixing and F.I.S.H. No PolyA+ nuclear accumulation was observed when compared to control siRNA.

3.9 Chapter 3: Summary

Initial work indicated an m^6A upregulation upon RNAi for Thoc5/Alyref and Nxf1. However upon further investigation we conclude that this is a non-specific response caused by the short half-life of Alkbh5 coupled with the sensitivity of *Alkbh5* mRNA. Furthermore Wtap western blot indicated the possibility of post translation modifications being present. Perturbing the export machinery does not change the deposition of Wtap upon mRNA nor does it alter the m^6A writer complex formation.

This chapter identifies the association between the methyltransferase machinery and the TREX complex. Core members of the TREX complex Uap56, Thoc5 and Alyref pulldown with the regulatory elements of the m^6A pathway Wtap and Kiaa1429 and also the heterodimeric catalytic complex Mettl3/Mettl14. This suggests TREX interacts with the complete m^6A writer complex. Further evidence for the requirement of a complex m^6A writer complex required for TREX interaction was demonstrated upon Kiaa1429 knockdown. Removal of Kiaa1429 results in reduced m^6A writer complex formation and TREX component association with Wtap. This also indicated Kiaa1429 is integral for the formation of the writer complex. However, although Kiaa1429 is required for complex formation and association with TREX its knockdown does not result in the accumulation of PolyA+ RNA within the nucleus. The interaction evidence presented in this chapter solidifies the methyltransferase machinery as an interacting partner of the TREX complex, the reason for this interaction is not yet clear.

Chapter 4: The C-terminus of Wtap is phosphorylated.

The western blot pattern observed for Wtap in Chapter 3 indicated the possibility of a post translation modification. This has not been reported within the literature, therefore we set out to investigate if Wtap is post translationally modified, where it is modified and what function these modifications may impart.

4.1. The C-terminus of Wtap is phosphorylated.

The observed Wtap western blot in Figure 3.2a and Figure 3.5b indicated post translational modifications. We began the investigation with an *in silico* analysis of Wtap primary amino acid sequence, Figure 4.1. The Bloomsbury Centre for Bioinformatics prediction of secondary structure (PSIPRED) was employed and results predicted an alpha helical rich N-terminus (positions 1-250) and a heavily phosphorylated C-terminus (position 250+), Figure 4.1a. Further *in silico* analysis revealed the potentially highly phosphorylated C-terminus is disordered (Figure 4.1b) and agreed with current literature indicating the N-terminus in protein binding (Ping *et al.*, 2014). However the *in silico* disorder profile did not predict a site of protein-protein interaction within the C terminal region.

Figure 4.1c confirms the *in silico* analysis, Wtap is phosphorylated. Protein extracts were collected form Control, Thoc5/Alyref and Nxf1 RNAi. Lysis buffer was either supplemented with Phosphatase inhibitors or Alkaline Phosphatase (AP). All lysates were incubated for 30 minutes at 37 ^{o}C. Furthermore Figure 4.1c confirms the increase in Wtap observed in figure 3.2a for Nxf1 RNAi However the shifting ratios of Wtap bands in Thoc5/Alyref and Nxf1 RNAi in figure 3.2a were not observed here, suggesting kinase activity in the lysate may have been the cause.

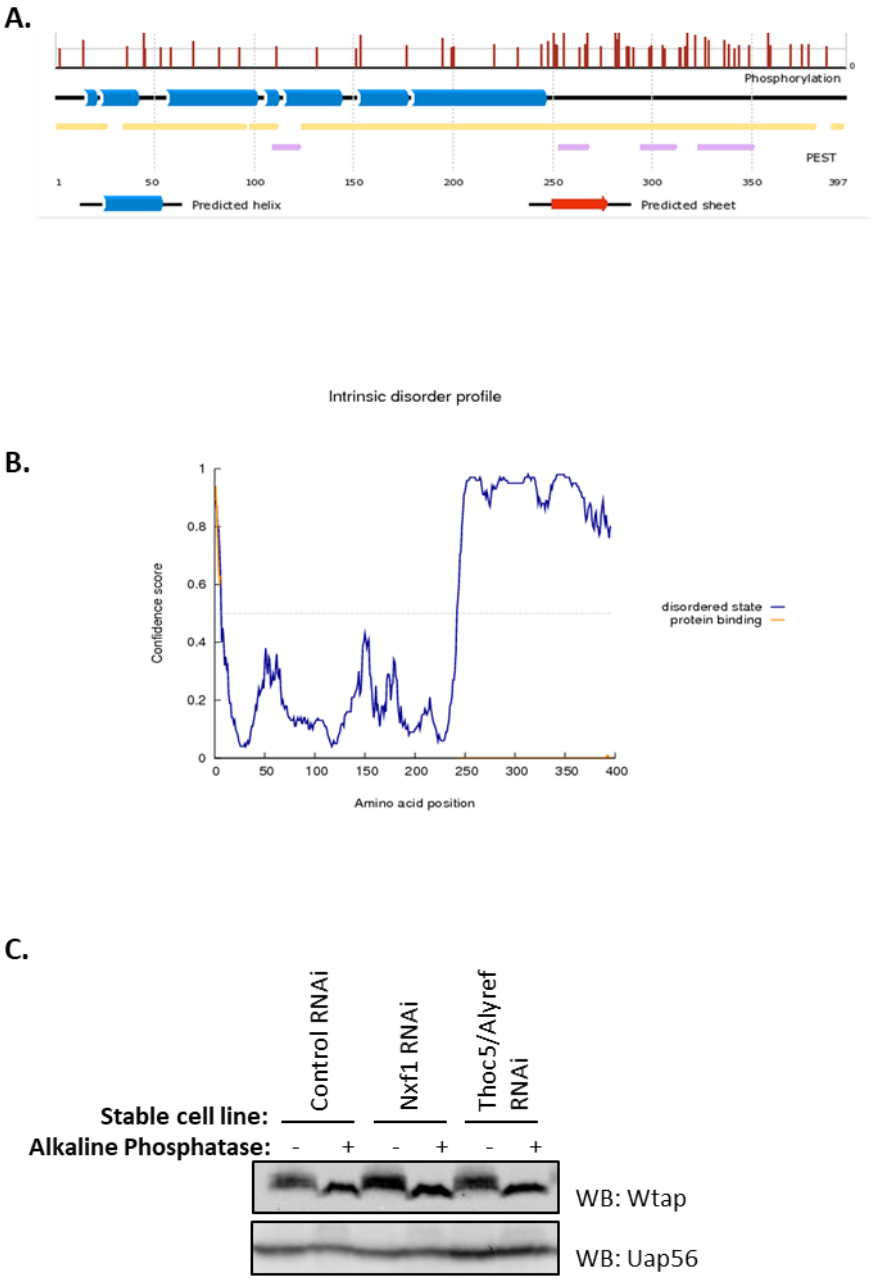

Figure 4.1 Wtap is phosphorylated. A. *In silico* analysis of Wtap secondary structure predicts a helical N-terminal and a heavily phosphorylated C-terminus. **B.** Disorder profile of Wtap indicating with high confidence an unstructured C-terminus (250aa+) and predicted its protein interaction site to be located in the N-terminus. **C.** Western blot of Wtap post Alkaline phosphatase treatment. Confirms Wtap is phosphorylated. More Wtap present in Nxf1 RNAi.

4.2 Wtap-Flag is phosphorylated.

To study the impact of phosphorylation on Wtap with our Flag-Wtap construct we verified its phosphorylation state and expression characteristics. Therefore 100 to 800 ng of Flag-Wtap was transfected into HEK293t cells. Post cell lysis the lysate was either supplemented with Phosphatase inhibitors or treated with AP in the manner mentioned above. Figure 4.2 demonstrates Flag-Wtap is phosphorylated. Bclaf1, a known heavily phosphorylated protein was used as a Phosphatase control. Actin was probed as a loading control. With these results in mind we concluded 400ng of Flag-Wtap per 6cm dish will be used for subsequent experiments.

4.3 Wtap phosphatase treatment results in a reduced binding affinity for Mettl3/Mettl14.

The initial question we sought to answer, “does the methylation state of Wtap change the composition of the methyltransferase complex?” This was accomplished via a Co-IP experiment using Flag-Wtap. Flag-Wtap cell lysate was either supplemented with Phosphatase inhibitors or subject to AP treatment. Phosphatase activity was confirmed using Bclaf1, as depicted in the inputs. The pull down indicated AP treated extracted had a reduced Mettl3/Mettl14 binding, compared to the Phosphatase inhibited extracts, Figure 4.3. The immune precipitation was controlled using Flag-GFP, confirming there was no non-specific binding to the Flag tag or beads. Further controls were demonstrated with Bclaf1 as it did not pull down with Flag-Wtap, indicating specificity of the pulldown. There are a number of limitations to this experiment that do not allow us to conclude that the phosphorylation of Wtap is responsible for reducing the Mettl3/14 pulldown. As we have treated whole cell extracts with AP, we have therefore subject all proteins to this treatment. As this is the case we cannot be certain of an altered phospho-state of another methyltransferase complex member inducing the loss of IP.

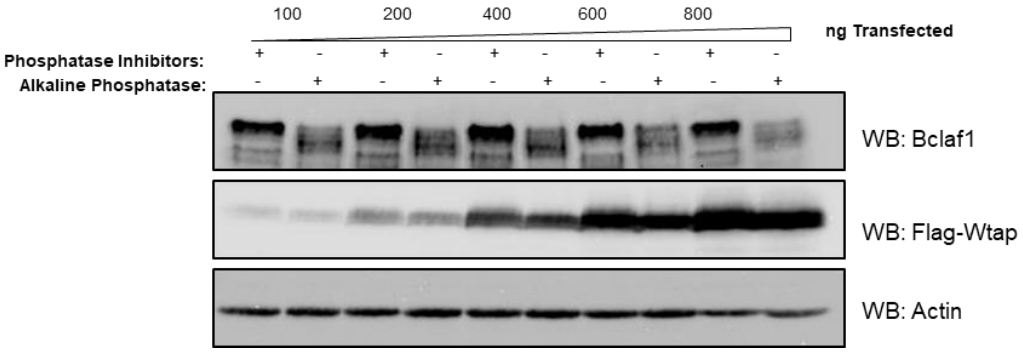

Figure 4.2 Flag-Wtap is phosphorylated. Western blot showing the expression levels and phosphorylation of Wtap following increasing ng transfected into HEK293t. Heavily phosphorylated Bclaf1 indicated successful AP treatment.

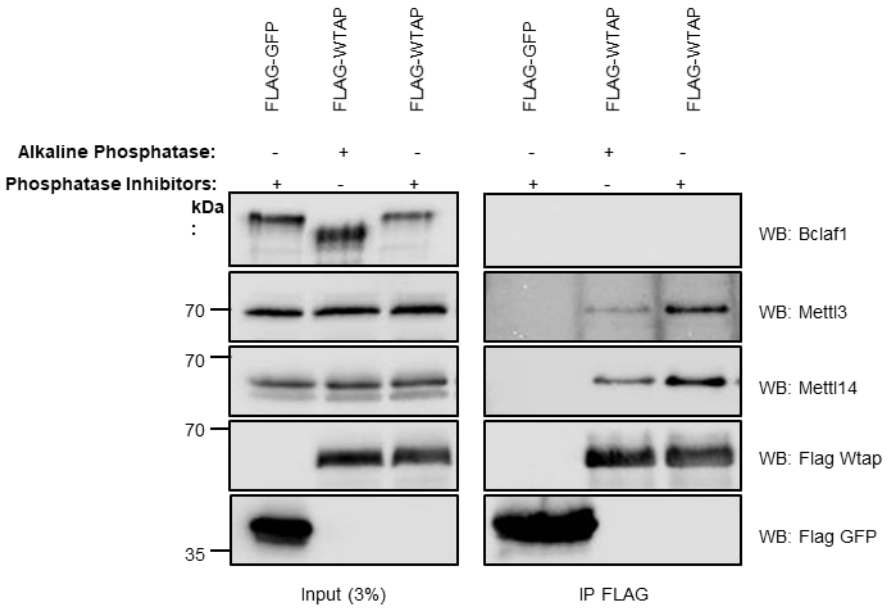

Figure 4.3 Flag-Wtap dephosphorylation results in decreased Mettl3/Mett14 binding. CO-IP of Flag-Wtap in AP or phospho-inhibitor background. AP treated background resulted in a decrease of Mettl3/Mettl14 CO-IP. Bcalf1 indicates the IP is specific.

4.4 Construction of Flag-WtapΔC mutant.

With the experimental limitations of Figure 4.3 we aimed to bolster the evidence for the phospho-dependent construction of the methyltransferase complex. Therefore a truncated form of Flag-Wtap was constructed. Taking into account the secondary structure predictions presented in Figure 4.1a we inserted a stop codon at amino acid position 250, resulting in a Flag-WtapΔC mutant. Flag-WtapΔC was expressed in HEK293T cells (Figure 4.4a) and also subject to AP treatment upon cell lysis (Figure 4.4b). Together the results indicate Flag-WtapΔC is not identifiably phosphorylated. However, it is possible that Flag-WtapΔC could still undergo phosphorylation in the N-terminus but to a small extent that the shift is no longer detectable via western blot analysis.

4.5 Flag-WtapΔC has a reduced methyltransferase complex formation.

The Co-IP experiment conducted in Figure 4.3 was repeated using Flag-WtapΔC. We hypothesised no change in the methyltransferase complex pull down would occur between the wild type (Phosphatase inhibitor) and WtapΔC, due to the previously reported result indicating the C-terminus is not required for Mettl3/14 binding (Ping *et al.*, 2014).

Equal amounts of wild type Flag-Wtap and Flag-WtapΔC construct were transfected into HEK293T, the lysates were treated with AP or supplemented with Phosphatase inhibitors. The resulting Co-IP experiment displayed in Figure 4.5 confirms the previous result (Figure 4.3). Interestingly the Flag-WtapΔC mutant did not pulldown Mettl3/14 to the same extent as the wildtype with inhibitors. The Mettl14 pulldown in the Delta C condition matches that of the Phosphatase treated wild type. However the Mettl3 decrease in pulldown is not as dramatic in the Delta C, when compared with the Phosphatase treated Wild type. As per Figure 4.3 Bclaf1 was employed as a Phosphatase control and a negative pulldown control. The results of this experiment indicate that the C-terminus of Wtap is required for complete and optimal formation of the methyltransferase complex.

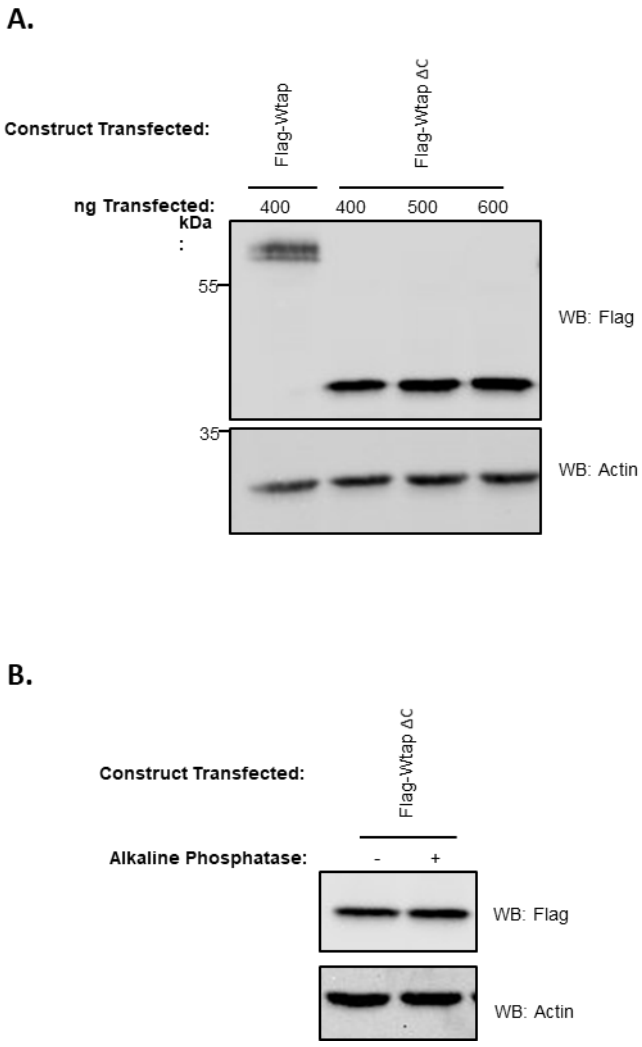

Figure 4.4 Majority of Flag-Wtap phosphorylation sites reside in its C-terminus. A. Western blot showing the expression of a Flag-WtapΔC compared to Flag-Wtap. **B.** Flag-WtapΔC western blot indicating no gel shift post AP treatment.

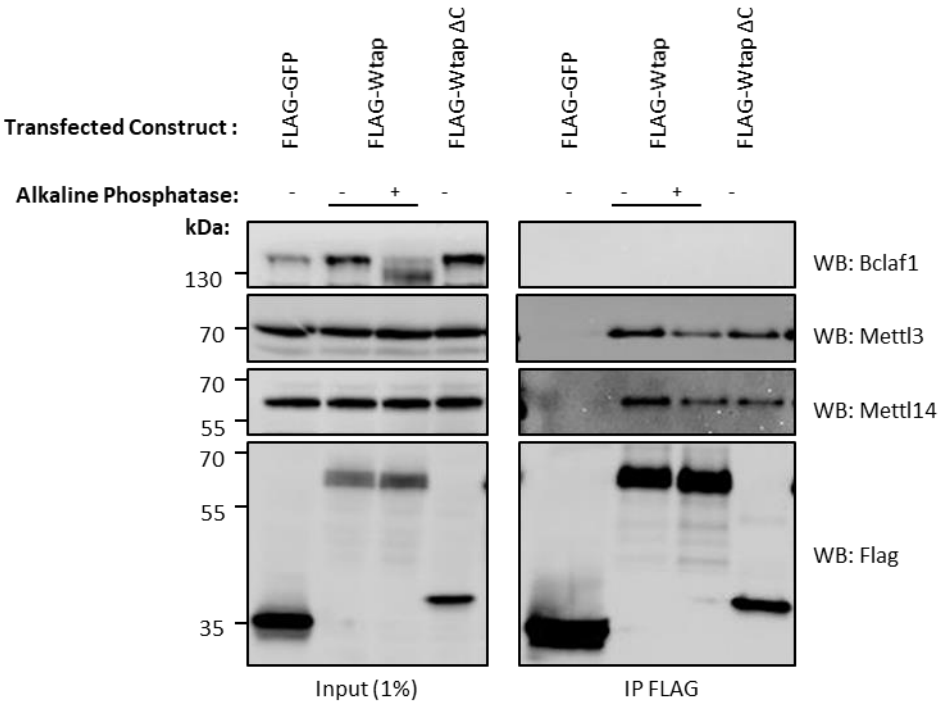

Figure 4.5 Flag-WtapΔC phenocopies AP treatment of Flag-Wtap. Flag-WtapΔC and Wtap-Flag CO-IP in AP background. Flag-WtapΔC results in the loss of Mettl14 to the same extent as Flag-Wtap AP. Mettl3 enrichment is reduced in Flag-WtapΔC but not to the extent as AP treated.

4.6 The Flag-WtapΔC localisation pattern does not change.

Further characterisation of Flag-WtapΔC was conducted using immune staining within HELA cells. This was to identify any abnormal localisation patterns presented by the mutant. Figure 4.6 depicts anti-Flag immune-stained HELA cells, equal amounts of each construct was transfected, and cells incubated for 48 hours. There was no obvious localisation difference between the Flag-Wtap and Flag-WtapΔC.

4.7 Flag-WtapΔC does not bind RNA.

We next asked if the Flag-WtapΔC still bound to RNA, more specifically methylated RNA. To answer this question we under took two RNA immune precipitation experiments. Firstly a Flag RNA immune precipitation (RIP) experiment followed by an m^6A dot blot. This allowed for the identification and comparison of methylated RNA levels bound to our mutant compared with the Wild Type Figure 4.7a. The experiment revealed a complete loss of m^6A binding in the Flag-WtapΔC, the signal observed on the dot blot is indifferent to the Flag-Gfp control precipitation. Whereas our Flag-Wtap RNA immune precipitation revealed an above background level of m^6A.

Our previous results indicate Mettl3/Mettl14 association is reduced for Flag-WtapΔC, therefore we may predict an impact on the amount of m^6A present. To confidently conclude that the Flag-WtapΔC is no longer associated with any PolyA+ RNA species an mRNP capture experiment was undertaken. The result, Figure 4.7b, confirmed our previous finding Flag-WtapΔC is not bound to the RNA, whereas Flag-Wtap is strongly RNA associated. The RNA binding protein Uap56 was probed to confirm similar levels of RNA pulldown in each condition. The Flag-Wtap +UV and RNase condition indicated the pulldown was polyA+ dependent.

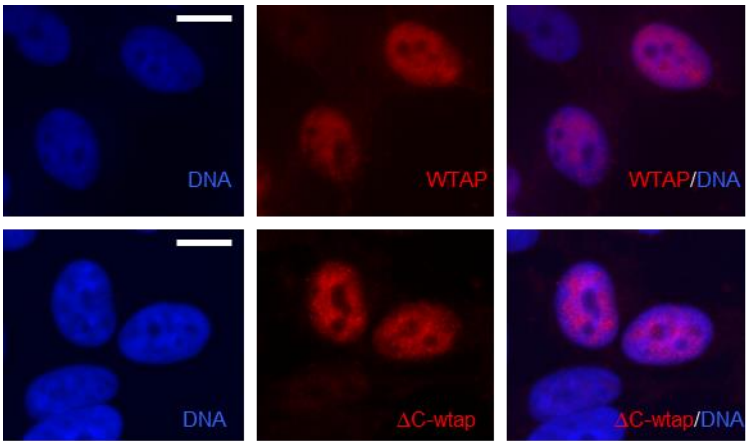

Figure 4.6 Flag-WtapΔC localisation does not differ from Flag-Wtap. Flag immunostaining in of transfected HELA cells. The distribution of Flag-WtapΔC does not differ to that of the wild type (red).

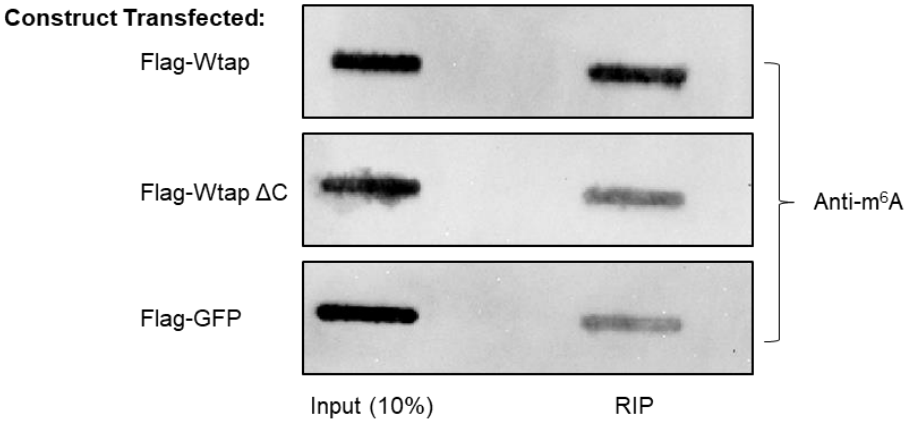

Figure 4.7a Flag-WtapΔC is not bound to m6A mRNA. Flag RNA immunoprecipitation experiment using transfected Flag-GFP, Flag-Wtap and Flag-WtapΔC. The dot blot indicates a reduced binding by Flag-WtapΔC as it's signal is consistent with Flag-GFP.

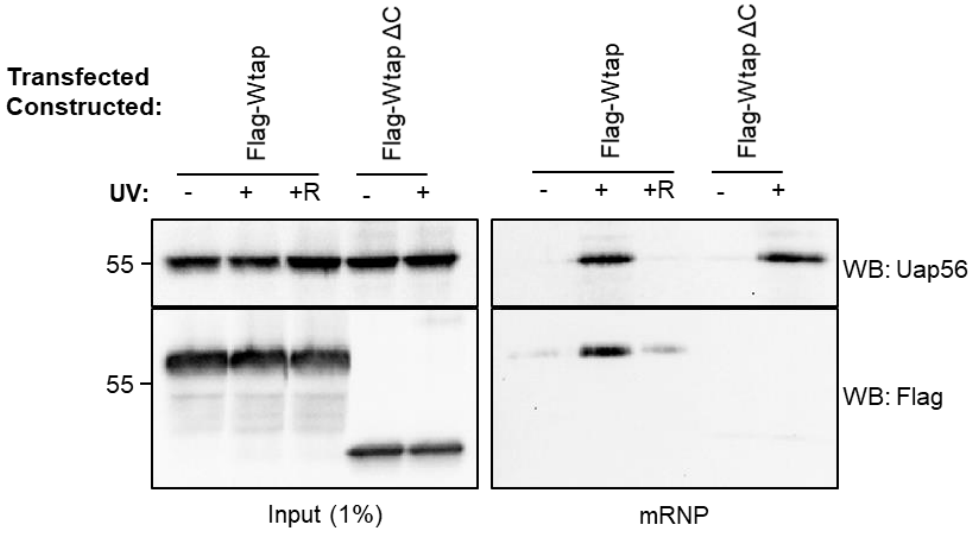

+R = UV cross linked and RNAseA Treated

Figure 4.7b Flag-WtapΔC is not bound to PolyA+ RNA. mRNP capture involving transferred constructs. Flag western blot of the resulting IP indicates no Flag-WtapΔC binding. Uap56 western blot confirms consistent PolyA+ RNA IP. The RNase A + U.V Flag-Wtap confirms the pulldown is RNA dependent.

4.8 Wtap has characteristics of an SR protein and can associate with Nxf1 in a hypophosphorylated state.

Members of the SR (serine- arginine) protein family can act as export adapters upon dephosphorylation aiding the mRNA handover to Nxf1 during the export pathway (Hautbergue et al., 2012; Muller-McNicoll et al., 2016). Wtap contains four SR doublets within its C-terminus, highlighted in Figure 4.8a. This observation allowed us to hypothesise that Wtap may interact with Nxf1 under different phospho-states. Figure 4.8b shows an endogenous Nxf1 Co-IP experiment in AP treated extract; non-treated extracts were supplemented with phosphatase inhibitors. Bclaf1 was employed as a negative IP control, Kiaa1429 was not present in the pulldown consistent with Figure 3.6a. The Wtap interaction with Nxf1 was greatly enriched upon AP treatment when compared to the inhibited lysate. To build on this foundation the reverse Co-IP, Wtap endogenous, was conducted in the same background conditions, Figure 4.8c. Again the Nxf1 pulldown was greatly enriched within the AP treated lane, compared with inhibitor. This time Kiaa1429 pulled down in the AP treated condition, this could be an indication of incomplete dephosphorylation. To build on these results and remove the possibility of another indirect interacting partner we conducted a Flag-Wtap and Flag-WtapΔC Co-IP in High salt post AP treatment. The high Salt IP wash removed interacting partners, specifically Nxf1, leaving hypo/phospho Wtap WT/ΔC on the beads. A fresh phosphatase inhibitor containing HEK293T lysate was subsequently incubated with the purified Flag constructs. (Figure 4.8d). This Co-IP reveals consistent results with Figure 4.8c, Nxf1 interaction is enriched when Wtap is in the hypophosphorylated state. The Flag-WtapΔC has minimal Nxf1 pulling down with the AP treated sample; this may indicate phosphorylated N-terminal positions are also involved with Nxf1 interaction.

MTNEEPLPKKVRLSETDFKVMARDELILRWKQYEAYVQALEGKYTDLNSNDVTGLRESEE
KLKQQQQESARRENILVMRLATKEQEMQECTTQIQYLKQVQQPSVAQLRSTMVDPAINLF
FLKMKGELEQTKDKLEQAQNELSAWKFTPDSQTGKKLMAKCRMLIQENQELGRQLSQGRI
AQLEAELALQKKYSEELKSSQDELNDFIIQLDEEVEGMQSTILVLQQQLKETRQQLAQYQ
QQQSQASAPSTSRTTASEPVEQSEATSKDCSRLTNGPSNGSSSRQRTSGSGFHREGNTTE
DDFPSSPGNGNKSSNSSEERTGRGGSGYVNQLSAGYESVDSPTGSENSLTHQSNDTDSSH
DPQEEKAVSGKGNRTVGSRHVQNGLDSSVNVQGSV

Figure 4.8a Wtap primary sequence with highlighted SR repeats. The C-terminus of Wtap highlighted in grey contains four SR repeats, highlighted in green.

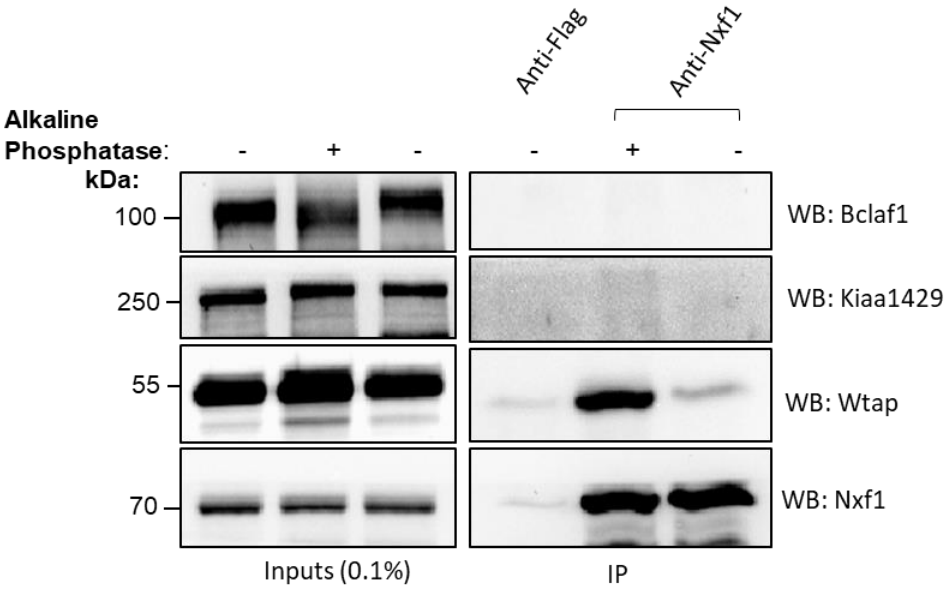

Figure 4.8b Nxf1 binds a dephosphorylated Wtap. CO-IP of endogenous Nxf1 in AP treated/ Inhibited background. Wtap enrichment increased in AP treated sample. Bclaf1 did not CO-IP indicating specificity. Kiaa1429 not present.

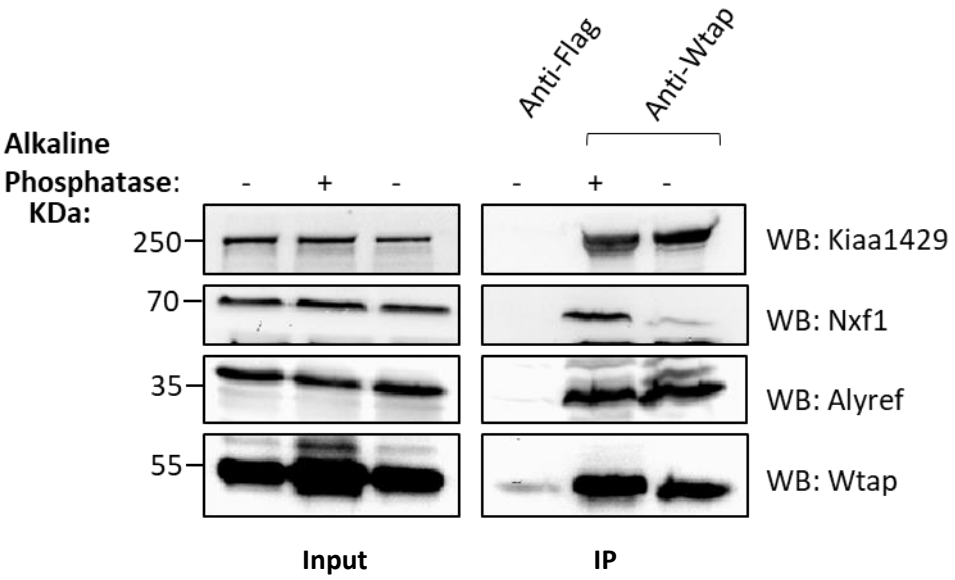

Figure 4.8c Nxf1 associates with a dephosphorylated Wtap. CO-IP of endogenous Wtap (Santa Cruz Biotechnology) in AP treated/ Inhibited background. Nxf1 enrichment increased in an AP treated background. Kiaa1429 present.

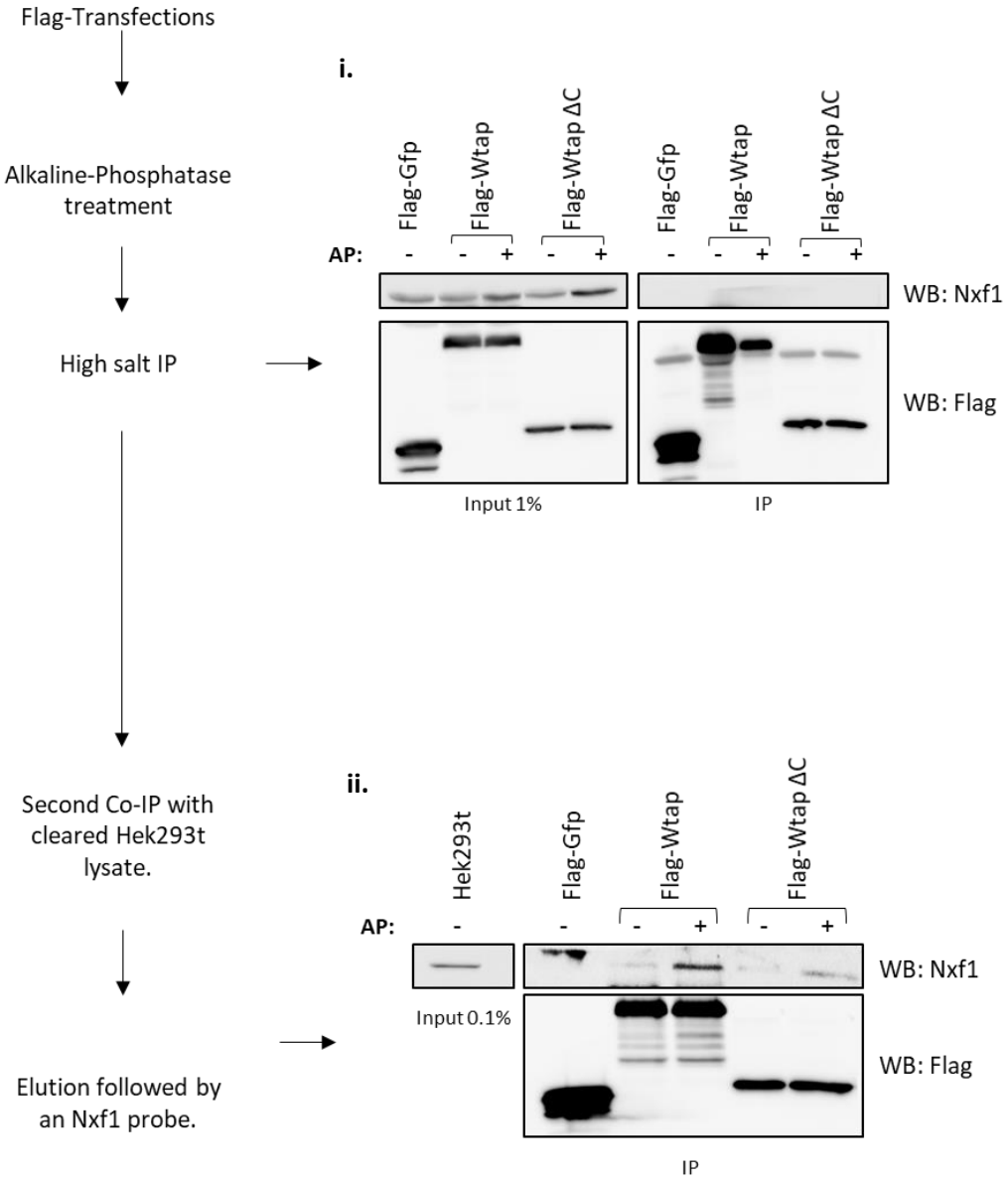

Figure 4.8d Wtap C-terminus is primarily responsible for Nxf1 binding in a hypophosphorylated form. Experimental work flow depicted on the left. **i.** High salt purification of Flag-Wtap constructs resulted in no Nxf1 pulldown. **ii.** High salt purified constructs incubated with fresh lysate. Indicates a direct interaction between Hypophosphorylated Wtap and Nxf1 that is primarily conducted by the C-terminus.

4.9 Chapter 4: Summary

The C-terminus of Wtap is heavily phosphorylated and disordered. The phosphorylation state of Wtap appears to play a role in Mettl3/Mettl14 association. The C-terminus of Wtap is not required for localisation but is required for mRNA binding. However with the evidence presented we cannot confirm Flag-WtapΔC RNA binding is directly hindered or it is simply a recruitment defect via loss of an interacting partner such as Rbm15 (Moindrot *et al.*, 2015).

Four SR repeats were identified within the C-terminus of Wtap. Upon dephosphorylation we predict, with the available data, these SR repeats allow for association of Wtap with nuclear export receptor Nxf1. Therefore we may hypothesise based on this evidence Wtap can act as an export adapter similar to Srsf3 and Srsf7 splicing factors (Muller *et al.,* 2016), though further experiments would be required to confirm this hypothesis.

Chapter 5: Perturbation of the writers results in nuclear accumulation of m^{6}A target transcripts

Throughout the later experiments of Chapter 3 we discovered an association between the methylation writer complex and the TREX complex. However, our initial experiments aiming to identify a global export block were unsuccessful. Due to the selective nature of the methylation mark , affecting ~30 % of the mRNA transcriptome (Dominissini *et al*, 2012)), our experimental techniques may not have been sensitive enough to pick up a subset of transcripts accumulating within the nucleus. Therefore, we aimed to approach the question with greater sensitivity.

We conducted nuclear/cytoplasmic fractionation assays in writer knockdown backgrounds and observed the behaviour of selected methylated transcripts. A transcriptome wide approach was taken to observe the global effect of perturbation the m^{6}A writers, indeed we saw nuclear accumulation of m^{6}A targeted transcripts. Finally, we aimed to understand the mechanisms behind the nuclear accumulation of these transcripts, it appears to be a lack of the TREX complex deposition upon certain m^{6}A transcripts upon knockdown of the writers.

5.1 Knockdown of the methyltransferase complex.

We began our investigation by knocking down each member of the methyltransferase writer complex via siRNA treatment. Kiaa1429, Mettl3, Wtap, Mettl3/Kiaa1429 and Wtap/Kiaa1429 knockdown condition were incubated for 72 hours post 10 nM siRNA transfection, a second 10 nM siRNA transfection was conducted 48 hours after the initial one. The resulting western blots are displayed

in Figure 5.1a-c and d. Each condition was compared to a 10nM Control siRNA transfection. Each western blot was also probed for Actin to ensure equal loading compared to the control siRNA condition.

Further confirmation of each knockdown was conducted at the mRNA level, Figure 5.1e depicts the resulting qPCR from total RNA extracted from siRNA transfected cells. On average the reduction of mRNA for each condition was ~70% compared to Control siRNA. Furthermore, we observed a two-fold increase in Wtap transcript levels upon Kiaa1429 siRNA, a similar protein response was observed in Figure 3.7.

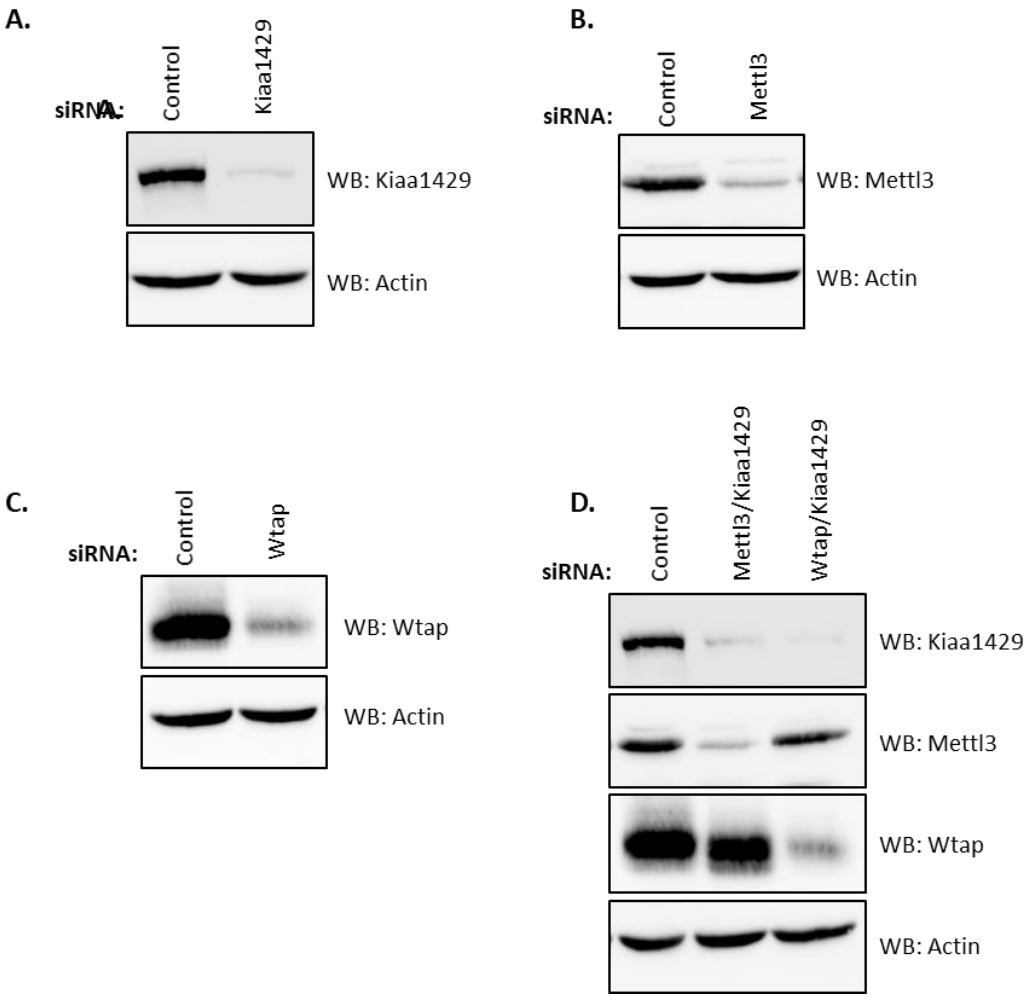

Figure 5.1 siRNA knockdown of the methylation writers. All transfections were carried with 10nM siRNA for 72 hours. Retransfection of siRNA occurred at 48 hours. Western blot of knockdown compared to control siRNA, **A**. Kiaa1429, **B.** Mettl3, **C.** Wtap, **D.** Kiaa1429/Mettl3 and Kiaa1429/Wtap.

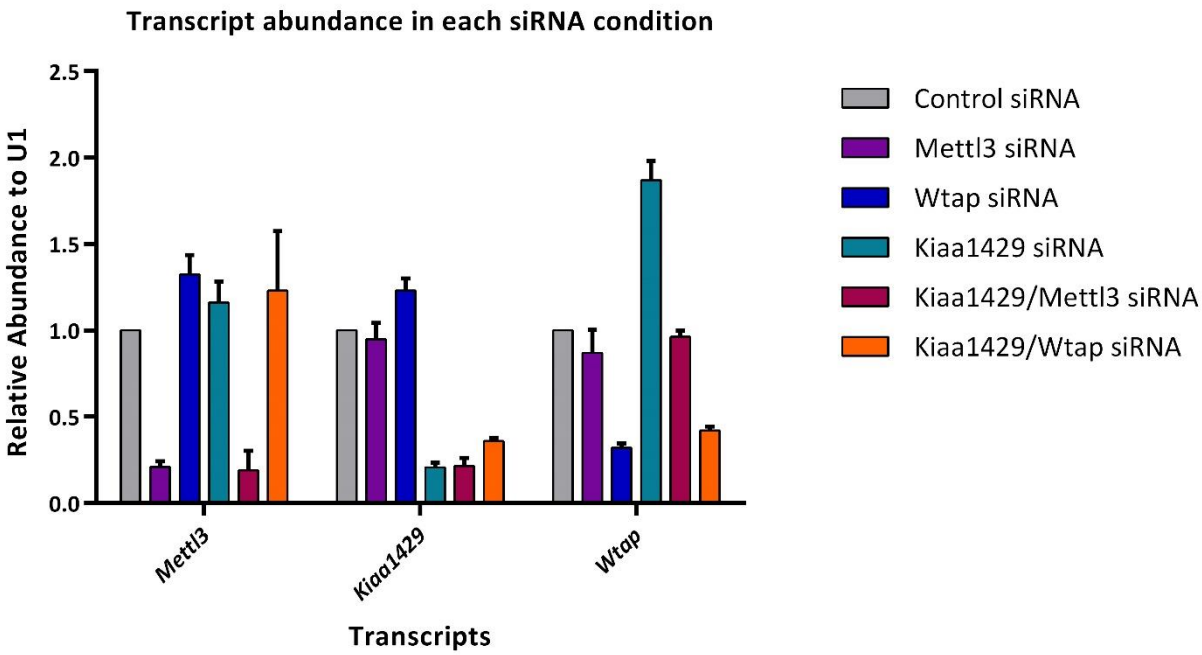

Figure 5.1e siRNA knockdown of the methylation writers, transcript levels. qPCR analysis from cDNA constructed from extracted total RNA.

5.2 Knockdown of individual m^{6}A writers did not result in nuclear accumulation of methylated transcripts.

With the identification of acceptable siRNA knockdown conditions for each writer we moved forward with a more targeted experimental approach, to identify any export block. Knockdown of single members Mettl3, Wtap and Kiaa1429 was conducted and nuclear/cytoplasmic RNA extracted. The resulting RNA was subject to DNase treatment and equal concentrations used for cDNA synthesis. Prior to qPCR analysis of the fractioned cDNA we constructed a list of high confidence m^{6}A containing transcripts. Transcripts were selected by cross referencing Wtap iCLIP (Ping *et al*, 2014), Ythdc1 PAR-CLIP (Xu *et al.*, 2014) and m^{6}A RIP sequencing (Ke *et al.*, 2015, 2017; Linder *et al.*, 2015). By comparing all three data sets we generated a high confidence set of methylated transcripts bound by both Wtap and Ythdc1. Taf7 was identified as a methylated intronless transcript, negating any splicing defect we may have observed. Ptpn12 and Dicer1 contain larger 3' exons with multiple methylation peaks, confirmed by previous work (Dominissini *et al.*, 2012) and recent studies (Ke *et al.*, 2017), illustrated in Figure 5.2a. We also identified the m^{6}A peaks in Ptpn12 and Dicer1 long 3' exon aligned with the Alyref, Chtop and Nxf1 iCLIP (unpublished), Figure 5.2b. We constructed primers spanning the observed methylation peak in Ptpn12 and Dicer1 (*Ptpn12 e13* and *Dicer1 e23* respectively), also 5' and 3' exon:exon boundary primers (*Ptpn12 e5-e8, Ptpn12 e14-e15, Dicer1 e3-e4* and *Dicer1 e24-e25*), diagrammatically depicted in Figure 5.2a. The final transcripts Gstp1 and Sympk did not appear in our filtered list, therefore we were confident they are not methylated.

With each fractionation HnrnpA2B1 pre-mRNA/mRNA distribution was initially tested to confirm a clean fractionation. Every set (n=3) from each condition was subject to this test prior to further analysis, if no pre-mRNA was found in the cytoplasm we proceeded with our specific set of primers. Figure 5.3a,b and c are the distribution of our selected transcripts within Mettl3, Kiaa1429 and Wtap siRNA compared to Control siRNA. qPCR was carried out using primers designed for *Taf7, Dicer1 e23, Ptpn12 e13, Gstp1* and *Sympk*.

A.

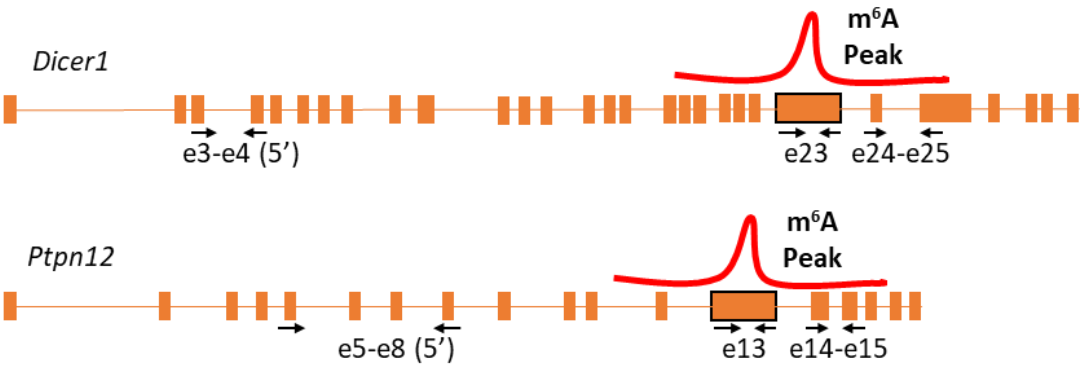

B.

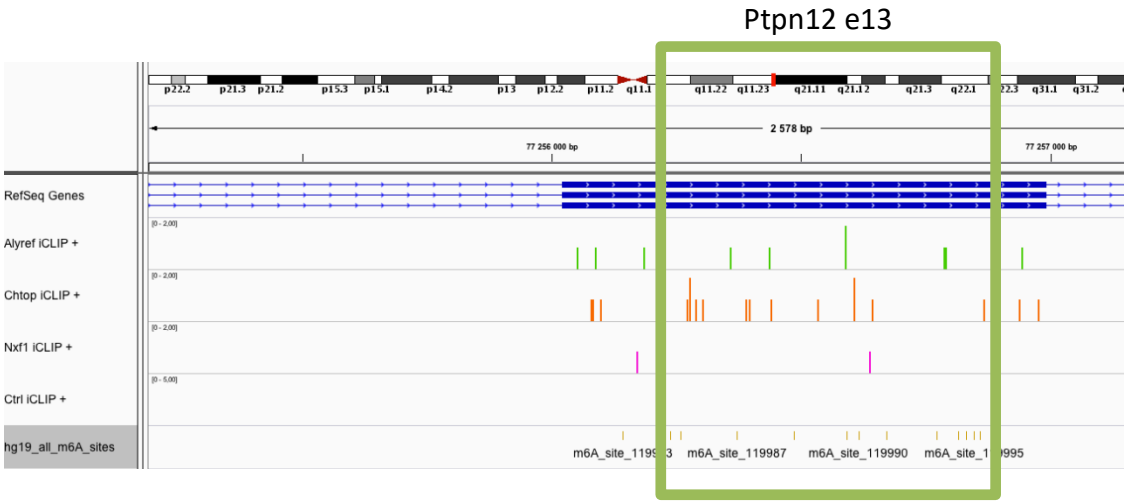

Figure 5.2 Primer design for nuclear/cytoplasmic and RIP experiments. A. Primer map for the m^{6}A containing long 3' exon of Ptpn12 and Dicer1. **B**. Alyref, Chtop and Nxf1 iCLIP indicating an overlap with Ptpn12 e13 m^{6}A site (Unpublished).

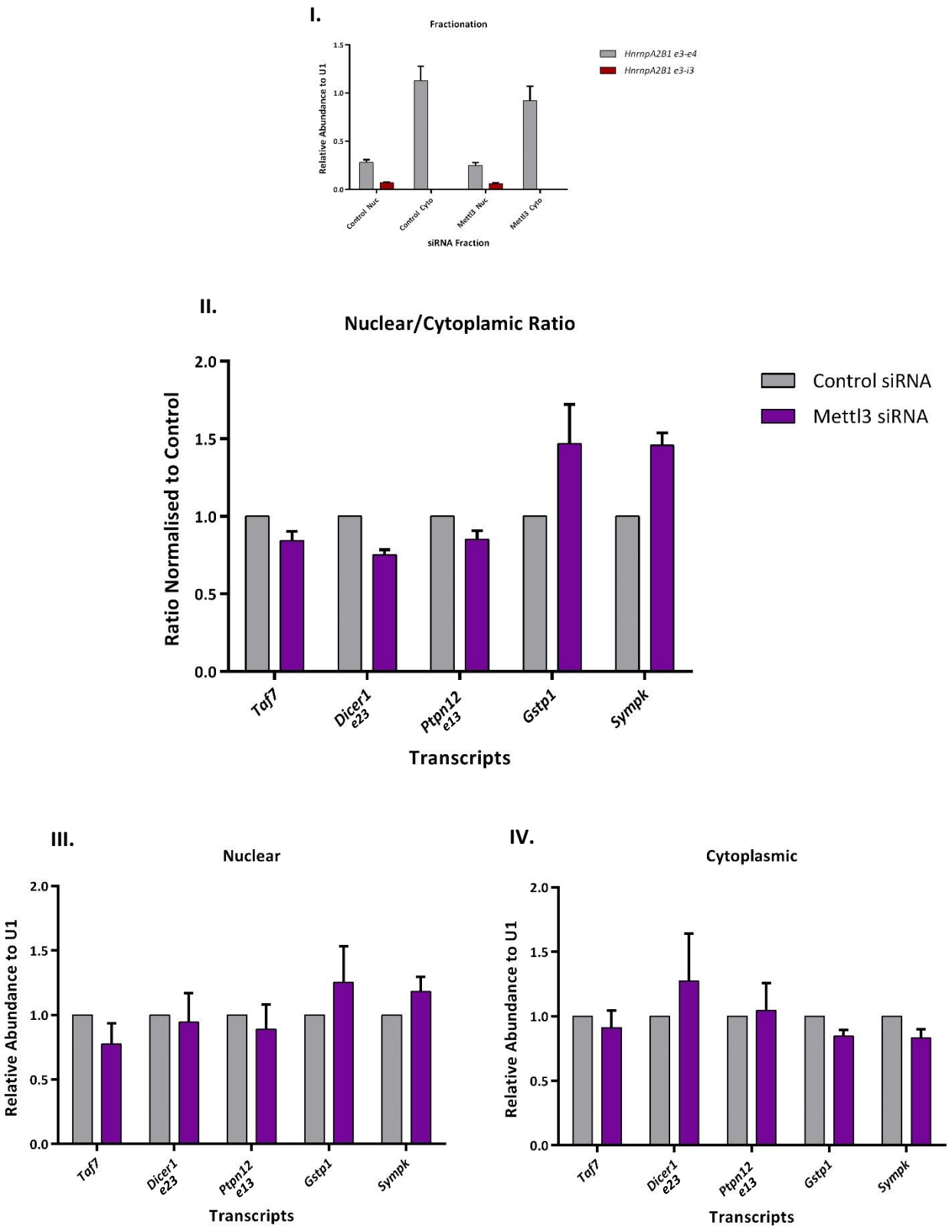

Figure 5.3a Nuclear/Cytoplasmic fractionation indicates a Mettl3 knockdown does not hinder mRNA export. **I.** *HnrnpA2B1 e3-i3* and *e3-e4* distribution between fractions. **II.** Nuclear/Cytoplasmic ratio of Mettl3 siRNA normalised to Control siRNA. **III.** Nuclear abundance of transcripts. **IV.** Cytoplasmic abundance of transcripts.

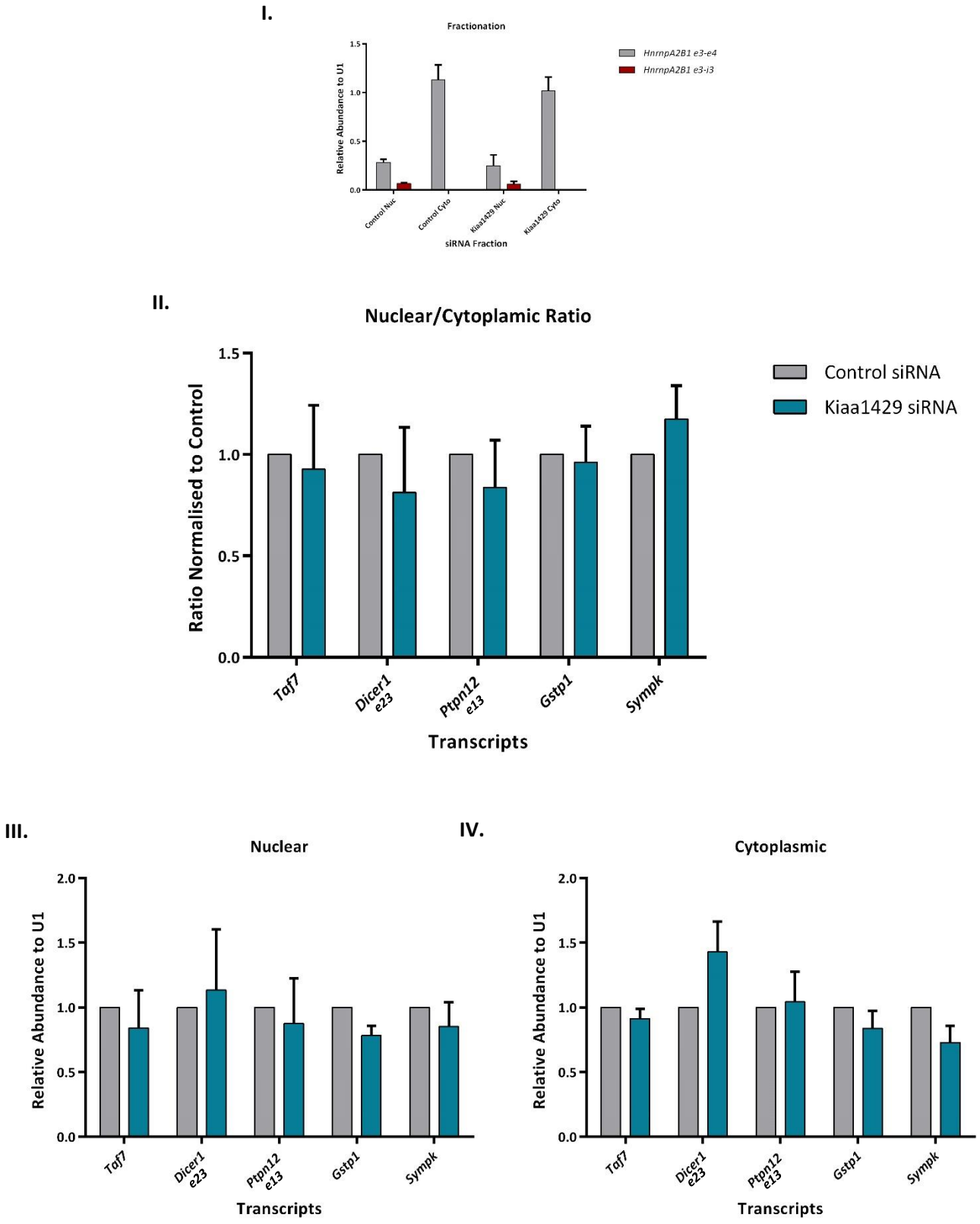

Figure 5.3b Nuclear/Cytoplasmic fractionation indicates a Kiaa1429 knockdown does not hinder mRNA export I. *HnrnpA2B1 e3-i3* and *e3-e4* distribution between fractions. **II.** Nuclear/Cytoplasmic ratio of Kiaa1429 siRNA normalised to Control siRNA. **III.** Nuclear abundance of transcripts. **IV.** Cytoplasmic abundance of transcripts.

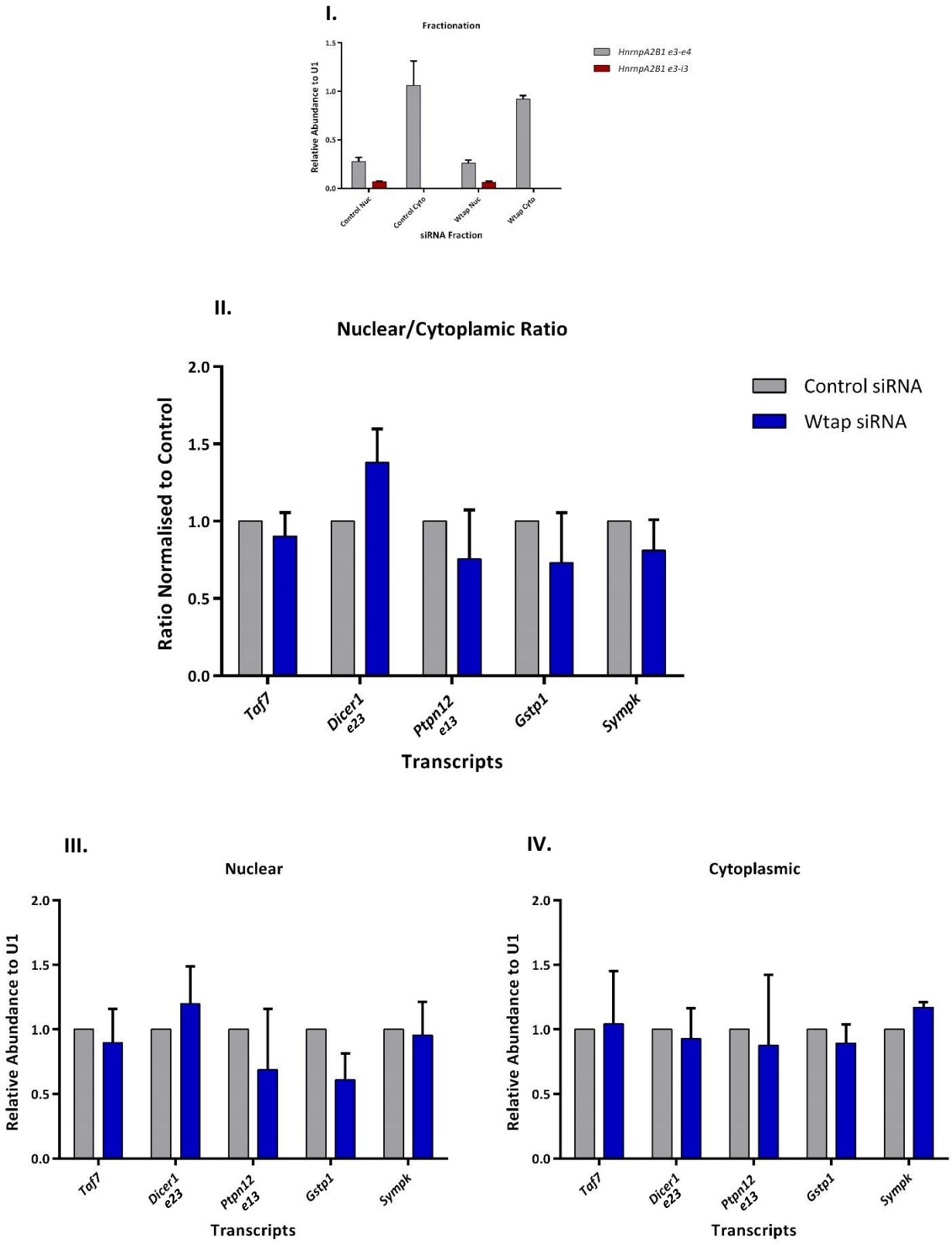

Figure 5.3c Nuclear/Cytoplasmic fractionation indicates a Wtap knockdown does not hinder mRNA export. **I.** *HnrnpA2B1 e3-i3* and *e3-e4* distribution between fractions. **II.** Nuclear/Cytoplasmic ratio of Wtap siRNA normalised to Control siRNA. **III.** Nuclear abundance of transcripts. **IV.** Cytoplasmic abundance of transcripts.

No significant difference was observed with the nuclear/cytoplasmic ratio for our suspected methylated transcripts, this was confirmed when analysing the nuclear and cytoplasmic levels individually. The Kiaa1429 nuclear/cytoplasmic result (Figure 5.3b) confirms our negative FISHH assay (Figure 3.8), no detectable change in the distribution of transcripts.

5.3 Knockdown of Mettl3/Kiaa1429 and Wtap/Kiaa1429 culminates in an export block for m^{6}A target transcripts.

With the negative results presented above we aimed to improve our chance of observing an export phenotype by knocking down two components of the methyltransferase complex at one time. The rationale behind this is due to the reported decrease of m^{6}A upon knock down of each writer was no greater than 70%, Mettl3 ~40%, Kiaa1429 ~60% and Wtap ~70% (Schwartz *et al*>, 2014). Our previous experiments also indicate redundancy within the m^{6}A machinery; Wtap protein and mRNA levels increase upon Kiaa1429 knockdown and we considered this compensatory activity might mask an mRNA export block. We hypothesised a double knockdown of Mettl3/Kiaa1429 and Wtap/Kiaa1429 would dramatically decrease the levels of m^{6}A, resulting in an observable phenotype. Figure 5.1d depicts the protein levels upon knockdown of the double 10 nM siRNA following a 72 hour incubation. We choose Kiaa1429 as a knockdown partner on the basis of Figure 3.7, as removing Kiaa1429 results in a decrease of writer complex formation, as well as TREX association with the writers. As with the knockdown of individual members, a double hit 72 hours siRNA transfection was undertaken prior to nuclear/cytoplasmic fractionation. Once the total RNA was extracted it was subject to DNase treatments and subsequent cDNA synthesis. qPCR was conducted on each sample (n=3) with HnrnpA2B1 pre-mRNA/mRNA as a control to control for clean fractionation. The resulting qPCR displayed in figures 5.4a and b of *Taf7, Dicer1 e23, Ptpn12 e13, Gstp1* and *Sympk* indicates transcripts with an identified m^{6}A modification are perturbed in export upon Mettl3/Kiaa1429 and

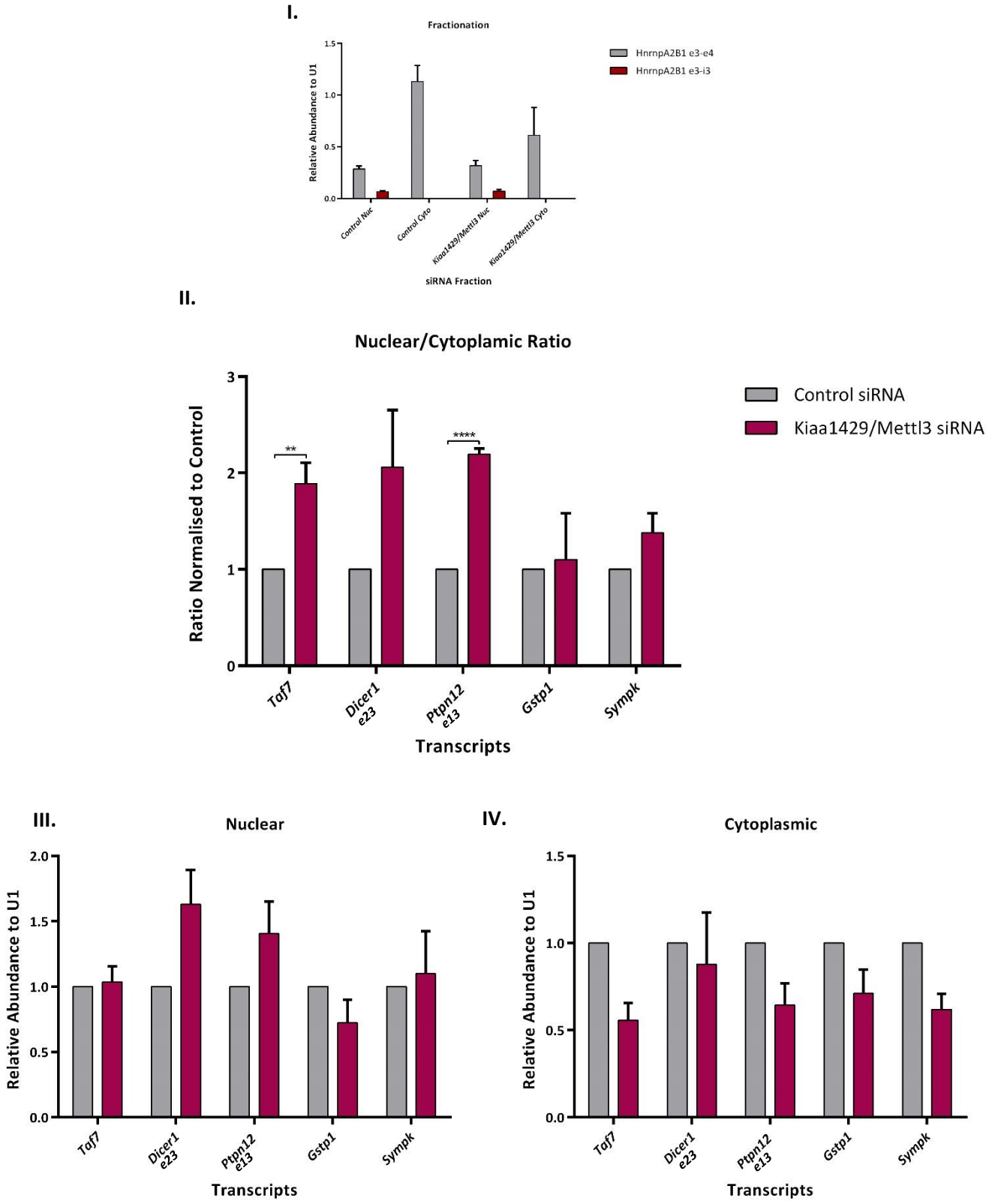

Figure 5.4a Nuclear/Cytoplasmic fractionation indicates a Kiaa1429/Mettl3 knockdown does hinder m^{6}A transcript export. **I.** *HnrnpA2B1 e3-i3* and *e3-e4* distribution between cell fractions. **II.** Nuclear/Cytoplasmic ratio of selected transcripts in Kiaa1429/Mettl3 siRNA treated cells normalised to Control siRNA. m^{6}A target transcripts *Taf7* and *Ptpn12* are significant (p=0.0045 and p=0.00001 respectively) . **III.** Nuclear abundance of transcripts. **IV.** Cytoplasmic abundance of transcripts.

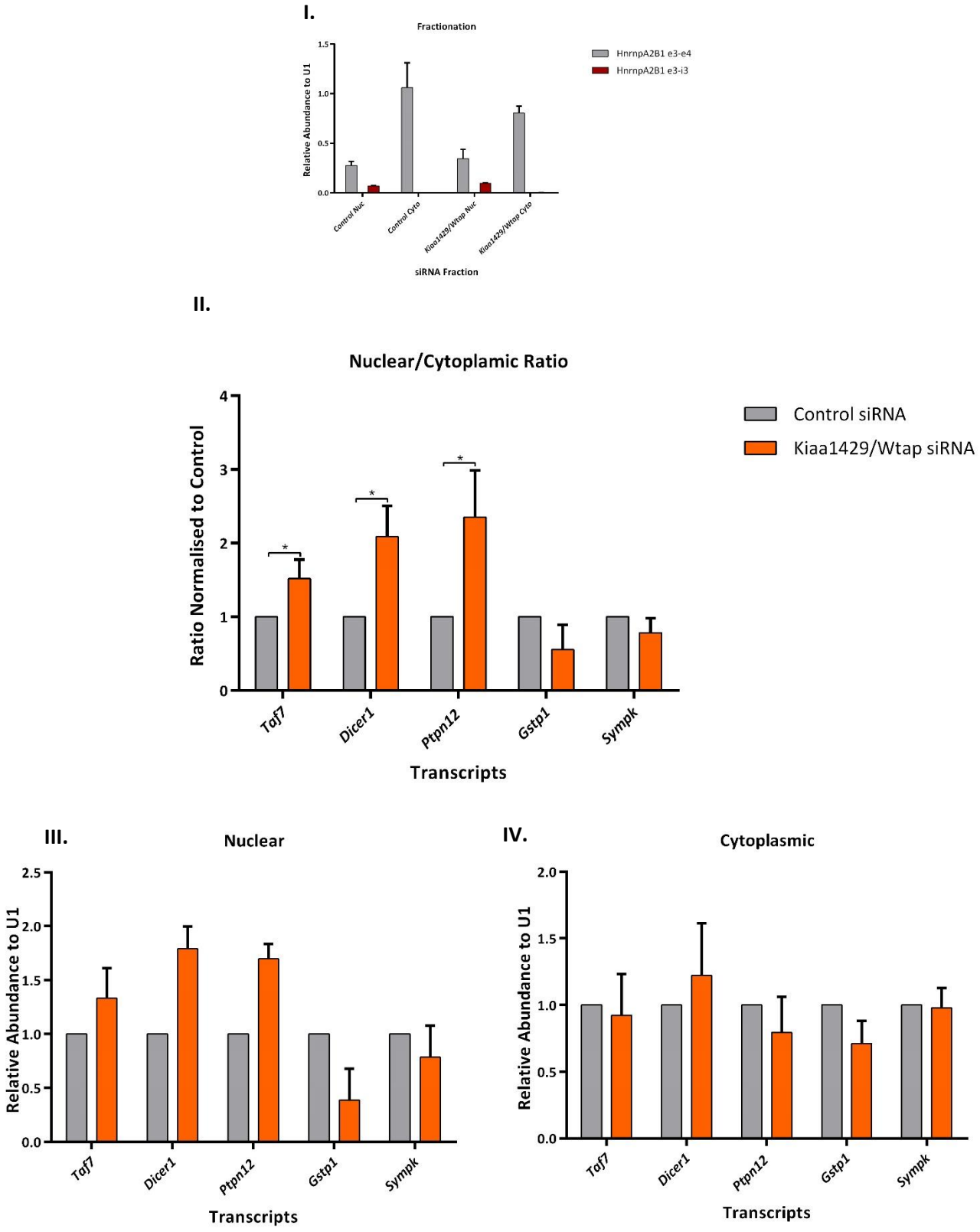

Figure 5.4b Nuclear/Cytoplasmic fractionation indicates a Kiaa1429/Wtap knockdown does hinder m^{6}A transcript export. **I.** *HnrnpA2B1 e3-i3* and *e3-e4* distribution between fractions. **II.** Nuclear/Cytoplasmic ratio of select transcripts in Kiaa1429/Wtap siRNA treated cells normalised to Control siRNA. m^{6}A target transcripts nuclear/cytoplasmic ratio significantly increases *Taf7 p=0.046, Dicer1 e23 p=0.020, Ptpn12 e13* p=*0.039*. **III.** Nuclear abundance of transcripts. **IV.** Cytoplasmic abundance of transcripts.

Wtap/Kiaa1429 knockdown. In Mettl3/Kiaa1429 siRNA *Taf*7 and *Ptpn12 e13* is significantly increased when compared to Control siRNA (p=0.00455 and p=0.00001 respectively). However, *Dicer1 e23* increased its ratio but was not significant (p= 0.065). Wtap/Kiaa1429 siRNA resulted in a significant increase in nuclear/cytoplasmic ratio for all methylated transcripts tested (*Taf7 p=0.046, Dicer1 e23 p=0.020, Ptpn12 e13* p=*0.039*) whilst non-methylated transcripts were not significantly different compared with Control siRNA (*Gstp1 p= 0.13* and *Sympk p= 0.19*). The results presented in figure 5.4a and b suggests the methyltransferase machinery may play a part in licensing selective transcripts for export.

To confirm the transcripts were also blocked within a TREX knockdown context a final nuclear/cytoplasmic experiment was conducted in a 72 hour Thoc5/Alyref RNAi background (Figure 5.4c). Effective fractionation of the Thoc5/Alyref RNAi can be seen in Figure 3.3.1. We observed a significant increase in the nuclear/cytoplasmic ratio for all methylated and non-methylated transcripts (*Taf7 p=0.047, Dicer1 e23 p=0.019, Ptpn12 e1 p=0.0012 3, Gstp1 p=0.009* and *Sympk p=0.015)*. Therefore, all transcripts selected require TREX for their nuclear export.

Finally, we looked at the splicing state at the 5' and 3' of *Ptpn12* and *Dicer1*. The primers used on the nuclear/cytoplasmic assay above would produce a product on pre-mRNA as well as spliced due to them targeting the middle of a long exon (*Dicer1 e23, Ptpn12 e13*). We designed primers spanning the exon:exon boundary and subjected the nuclear fraction of Wtap/Kiaa1429 and Mettl3/Kiaa1429 to qPCR. We observed the same increase in nuclear levels for the exon:exon primers as with the long 3' exon primers used within the nuclear/cytoplasmic assay. This suggests the transcripts may be spliced. However this is not definitive proof the whole transcripts have completed splicing.

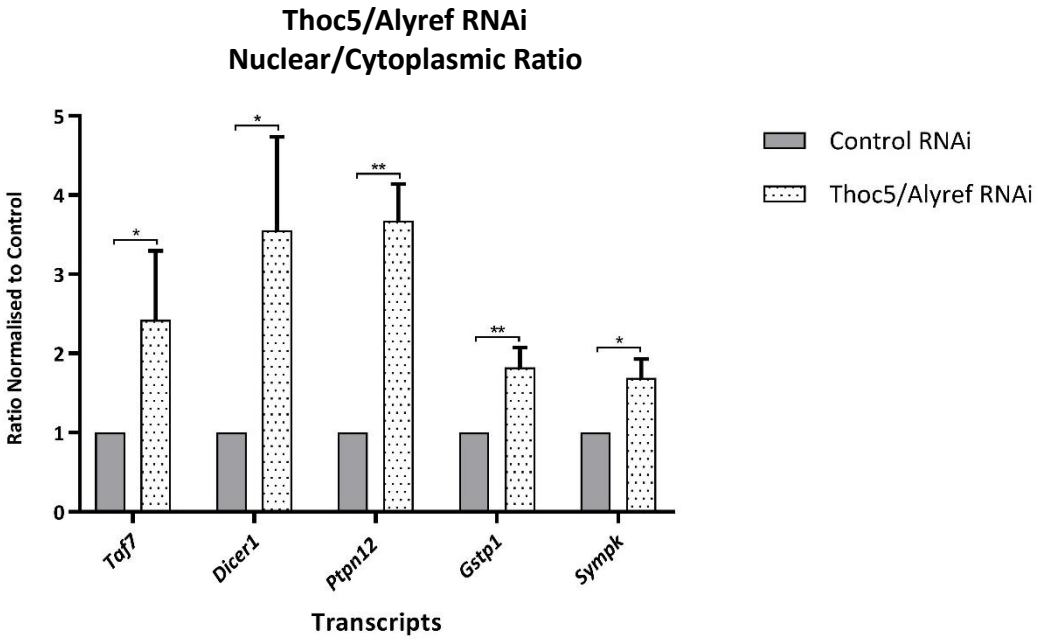

Figure 5.4c Nuclear/Cytoplasmic fractionation indicates all transcripts are dependent on Thoc5/Alyref for nuclear export. C. Thoc5/Alyref RNAi nuclear/cytoplasmic ration indicates all transcripts tested previously require TREX for export. *Taf7 p=0.047, Dicer1 e23 p=0.019, Ptpn12 e1 p=0.0012 3, Gstp1 p=0.009* and *Sympk p=0.015.*

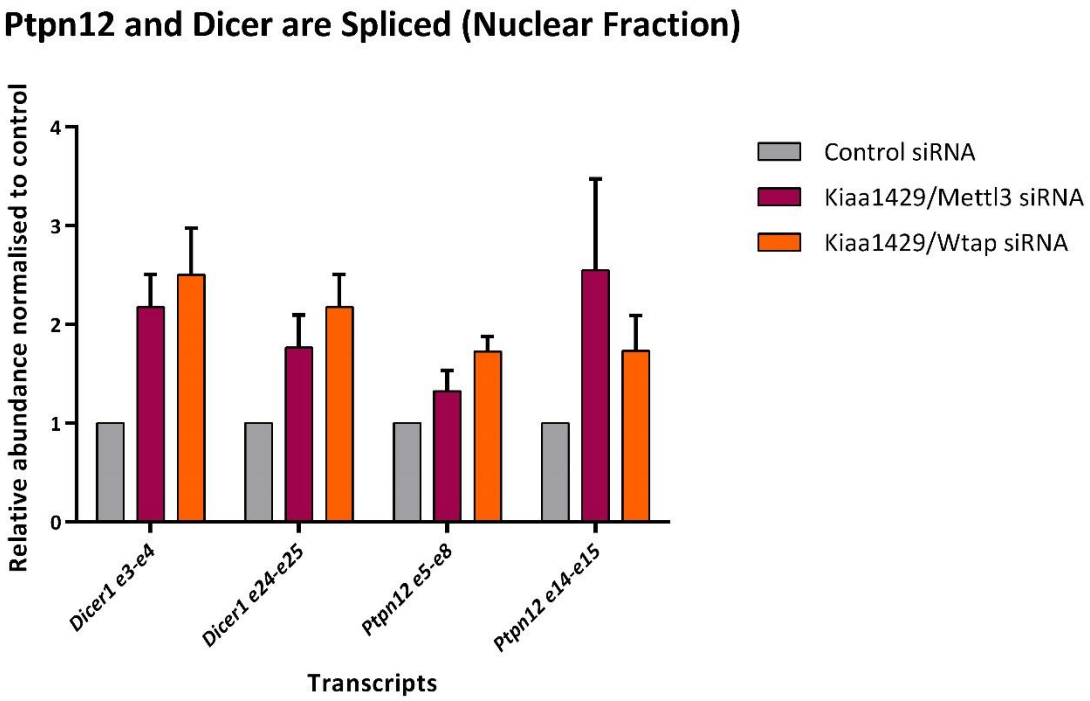

Figure 5.4d 5' and 3' exons of *Ptpn12* and *Dicer1* have undergone splicing. qPCR of the nuclear fraction from Control, Kiaa1429/Mettl3 and Kiaa1429/Wtap indicates primers spanning exon:exon boundaries result in similar accumulation to that of the long exon primers (*Ptpn12 e13 and Dicer1 e23*)

5.4 Transcriptomic wide response to Wtap/Kiaa1429 knockdown.

The next phase of our investigation required a global approach. It is difficult to construct conclusions from the limited number of methylated transcripts we have screened in our assays above. Therefore, we conducted whole transcriptome sequencing (mRNA seq) on Control and Wtap/Kiaa1429 siRNA nuclear and cytoplasmic fractions. Libraries were constructed using Lexogen mRNA sequencing kits from double hit 72 hour siRNA transfections. Bioinformatic analysis was conducted by Mathew Parker and Ian Sudbury, the graphs following (Figure 5.5-5.7) were constructed by them from our data sets. Strip plots in Figure 5.5a confirm a significant knockdown of Wtap/Kiaa1429 in all of our samples compared to control. For validation visualisation of nuclear/cytoplasmic distribution for *Dicer 1* is presented in Figure 5.5b. All of our m^6A containing transcripts from previous experiments followed a nuclear accumulation pattern upon Wtap/Kiaa1429 knockdown.

The sequencing revealed nuclear accumulation of transcripts upon Wtap/Kiaa1429 knockdown. To assess what proportion of these transcripts had previously been shown to contain m^6A we compared them to recent m^6A CLIP seq (Linder *et al.*, 2015). The Venn diagram in Figure 5.6a depicts the resulting analysis with 284 nuclear accumulated transcripts in total. Of the nuclear accumulated transcripts, 73% were identified as containing the m^6A modification. Gene ontology analysis (Panther Classification System) of the nuclear accumulated and methylated transcripts revealed an enrichment for transcripts involved in the cell cycle (fold enrichment 6.47), DNA repair (fold enrichment 3.74) and mRNA processing (fold enrichment 4.49), Figure 5.6b. We next looked at the number of m^6A sites identified on the nuclear accumulated and m^6A containing transcripts. Interestingly, Figure 5.6c shows that transcripts that are nuclear accumulated have a greater number of m^6A sites compared with the non-nuclear accumulated but methylated transcripts. The proportion of nuclear accumulated transcripts was higher, compared to non-accumulating but methylated, upon having greater than 7 m^6A site per transcript. Methylated transcripts that are non-nuclear

Figure 5.5a Strip plot illustrating the knockdown of Kiaa1429 and Wtap in the nuclear/cytoplasmic samples used for sequencing. 72 hour siRNA incubation with a renew of siRNA after 48 hours. Relative abundance (X Axis) of each transcript is displayed in the nucleus and cytoplasm. Control Cytoplasmic (CC), Control Nuclear (CN), Kiaa1429/Wtap siRNA Cytoplasmic (VWC) and Kiaa1429/Wtap siRNA Nuclear (VWN).

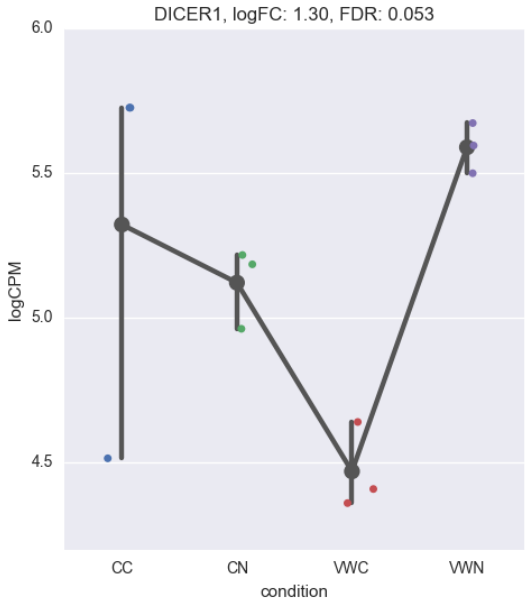

Figure 5.5b Strip plot visualisation of *Dicer1* in Wtap/Kiaa1429 knockdown. All of our m^6A containing transcripts from previous experiments followed a nuclear accumulation pattern upon Wtap/Kiaa1429 knockdown. Relative abundance (X Axis) of each transcript is displayed in the nucleus and cytoplasm Control Cytoplasmic (CC), Control Nuclear (CN), Kiaa1429/Wtap siRNA Cytoplasmic (VWC) and Kiaa1429/Wtap siRNA Nuclear (VWN).

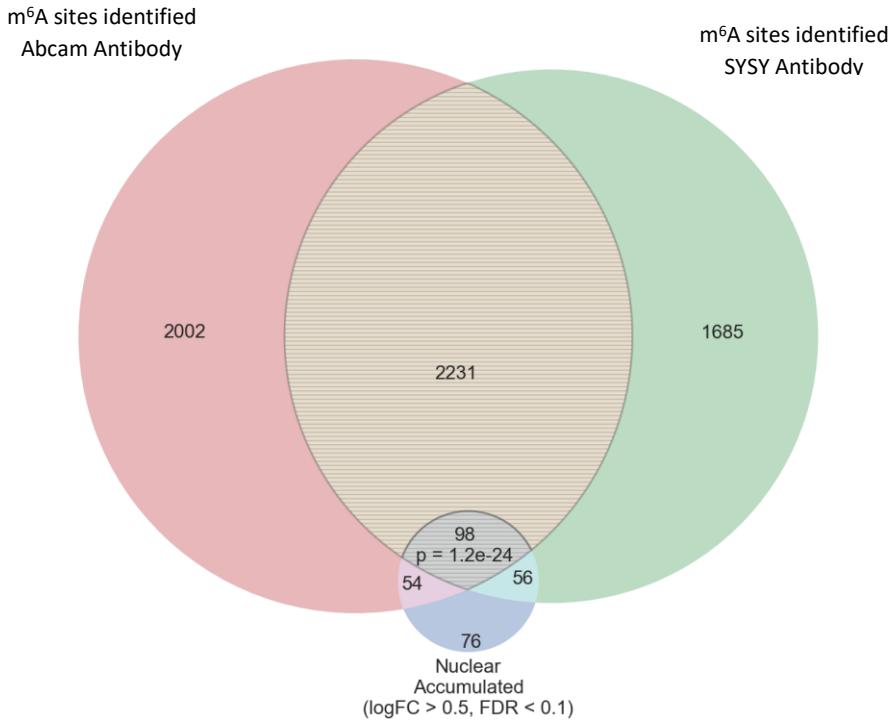

Figure 5.6a Venn diagram of nuclear accumulated transcripts upon Kiaa1429/Wtap knockdown compared with known m^{6}A containing transcripts. 73% of transcripts accumulating in the nucleus upon Wtap/Kiaa1429 knockdown were found to contain m^{6}A when compared with published m^{6}A CLIP seq using two separate antibody's (Linder *et al.,* 2015). FDR 0.1.

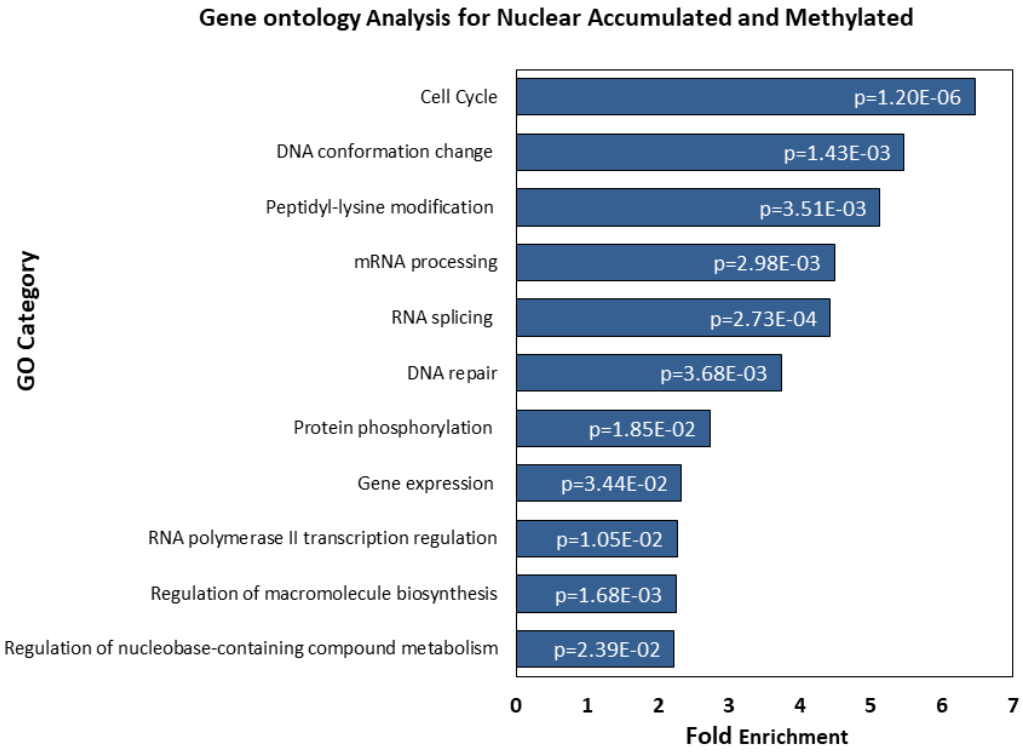

Figure 5.6b Gene ontology analysis of nuclear accumulated and methylated transcripts upon Wtap/Kiaa1429 knockdown. The most represented category was Cell cycle transcripts. Conducted with Panther Classification System

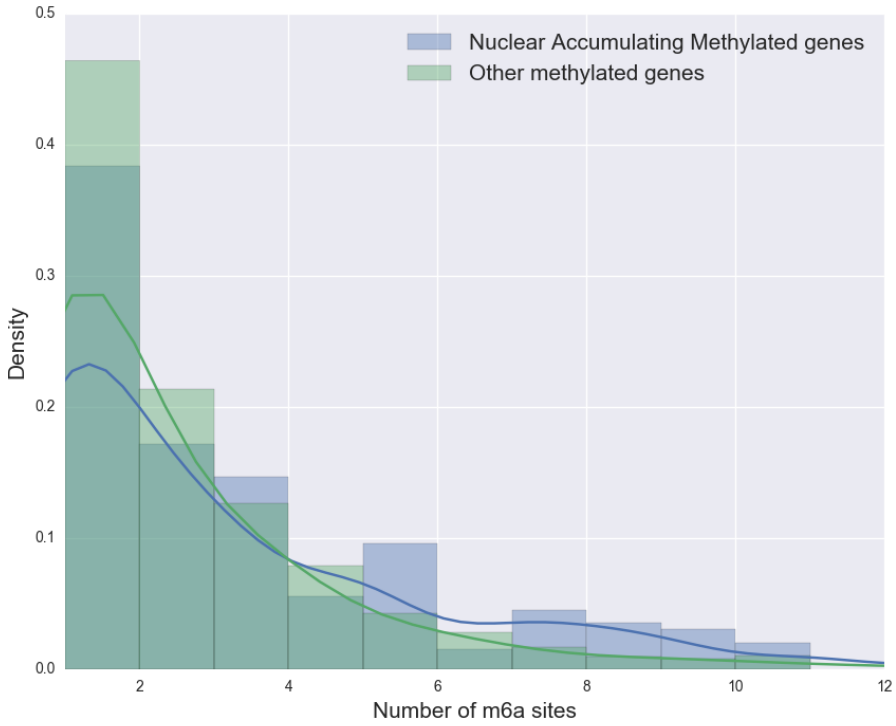

Figure 5.6c Nuclear accumulated transcripts have more m^{6}A sites compared to the m^{6}A average. Transcripts containing more than 5 m^{6}A sites accumulated in the nucleus, upon Wtap/Kiaa1429 knockdown, to a greater extent than other m^{6}A containing transcripts.

accumulated contained a lower density of m^6A sites, for example 37% of nuclear accumulated transcript contain between 1-2 m^6A sites whereas non-nuclear accumulated contain 46%. Our analysis also revealed nuclear accumulated and methylated transcripts contain longer exons when compared to non-nuclear accumulated genes, Figure 5.6d. A high proportion of m^6A containing nuclear accumulated transcripts contain an exon longer than 3500 base pairs. Furthermore, the final exon in the nuclear accumulated and methylated transcripts was on average of a greater length than non-nuclear accumulated transcripts, Figure 5.6e.

DaPars (Dynamitic analysis of alternative PolyAdenylation from RNA-seq) analysis was conducted to identify any alternative polyadenylation occurring upon Wtap/Kiaa1429 knockdown. It allowed us to identify a switch between distal or proximal usage in both our nuclear and cytoplasmic fractions. Figure 5.7a depicts the results in a Venn diagram. Indeed, we did observe PolyA site switching for 294 transcripts, 223 in the nucleus and 71 in the cytoplasm, compared to control. However the transcripts that had undergone the PolyA switch were different to our nuclear accumulated transcripts (Figure 5.7a), yet 58% of the transcripts experiencing a switch in PolyA site usage contained m^6A (Figure 5.7b). Therefore we have observed two phenotypes of m^6A containing transcripts upon knockdown of Wtap/Kiaa1429, nuclear accumulation and alternative polyadenylation. These phenotypes occur on two separate subsets of mRNA.

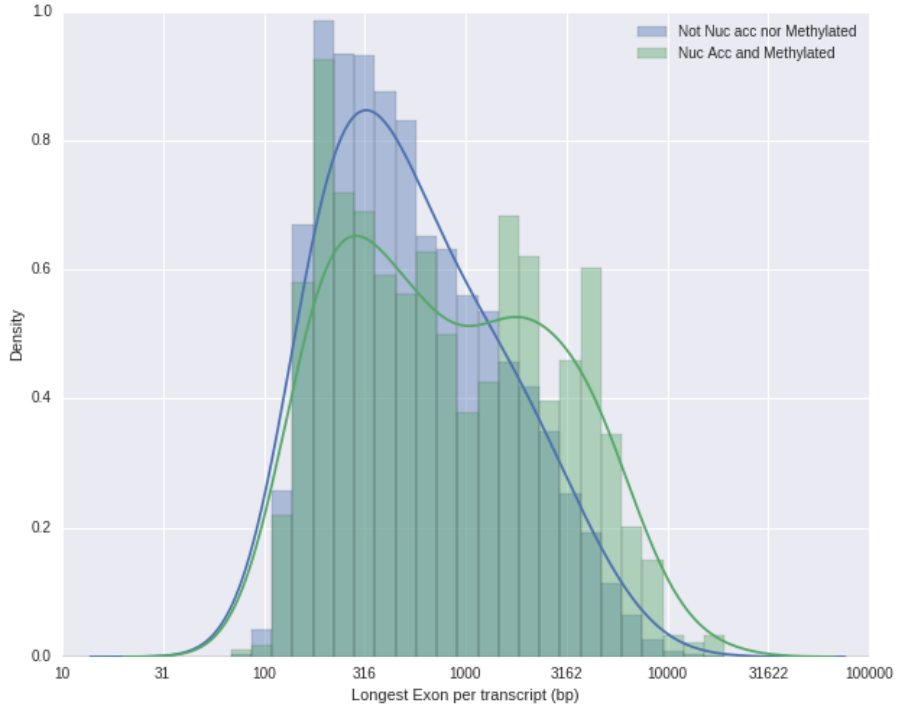

Figure 5.6d Wtap/Kiaa1429 knockdown nuclear accumulated and m^{6}A containing transcripts have longer exons. Transcripts containing a longer exon were over represented in the nuclear accumulated transcripts.

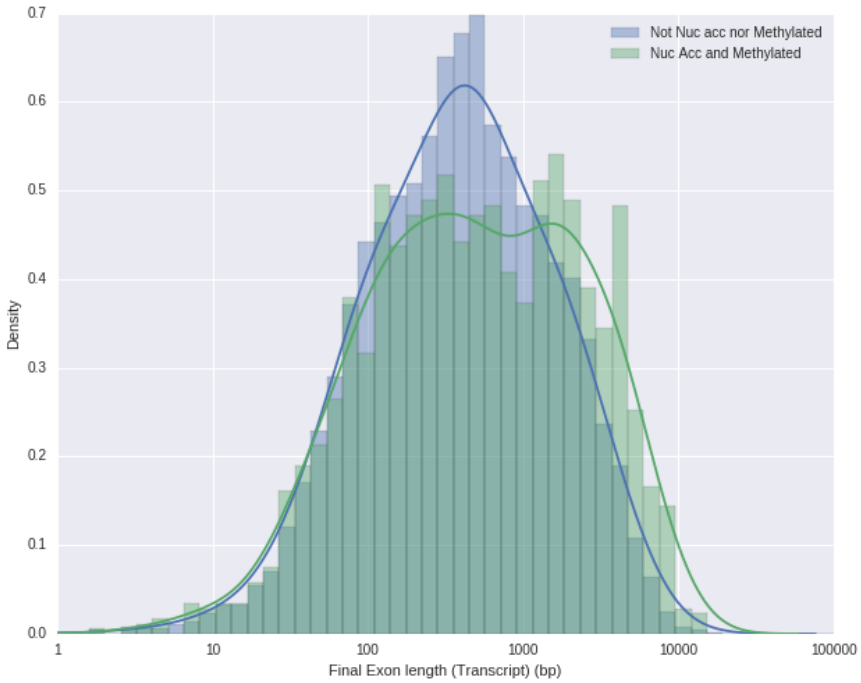

Figure 5.6e Wtap/Kiaa1429 knockdown nuclear accumulated and m^{6}A containing transcripts have longer final exons. Transcripts containing a longer final exons were over represented in the nuclear accumulated transcripts.

A.

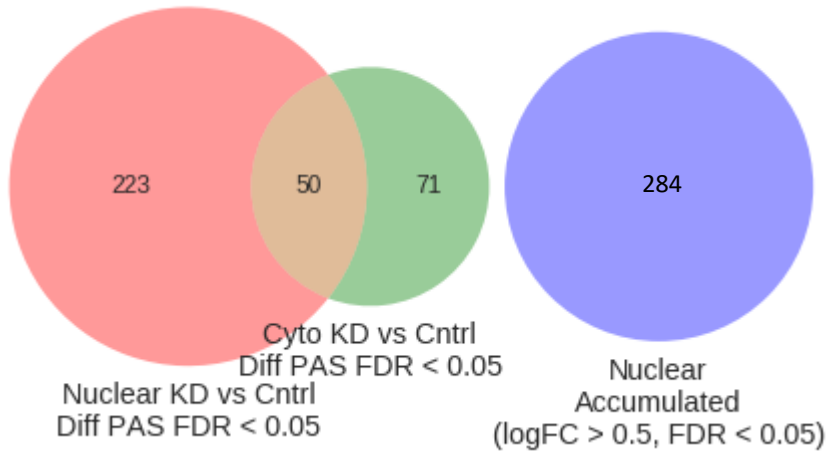

B.

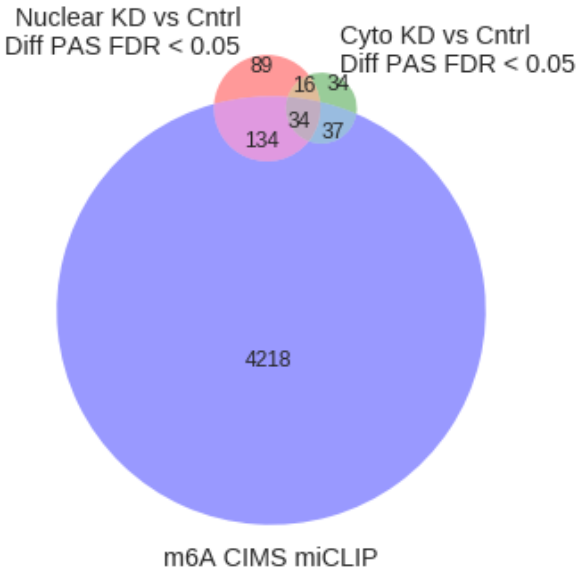

Figure 5.7 DaPars analysis revealed alternative polyadenylation of 294 transcripts upon Wtap/Kiaa1429 knockdown. A. Transcripts undergoing alternative polyadenylation do not overlap with the identified nuclear accumulated and m^{6}A targeted. **B**. 58% of transcripts undergoing alternative polyadenylation events also contain m^{6}A.

5.5 TREX deposition is altered on m^{6}A targeted transcripts upon knockdown of the methylation writer machinery.

To establish the basis for the nuclear retention of transcripts targeted for m^{6}A, we conducted Alyref RNA immune precipitation (RIP) experiments in both Mettl3/Kiaa1429 and Wtap/Kiaa1429 knockdown conditions. siRNA was transfected every 48 hour for a 72 hour knockdown period. Figure 5.8a is the resulting qPCR analysis from Mettl3/Kiaa1429 and Wtap/Kiaa1429 knockdown Alyref RIP, normalised to input and Control siRNA. Interestingly the knockdown conditions did not result in similar phenotypes. A significant increase of Alyref was observed compared to control in Mettl3/Kiaa1429 on all methylated transcripts (*Taf7* p=0.018, *Dicer1 e23* p=0.0073, *Dicer1 e3-e4* p=0.1, *Ptpn12 e13* p=0.013, *Ptpn12 e5-e8* p=0.021 and *Gstp1* p=0.76). Not only did we see an increase in Alyref at our 3' m^{6}A site of *Dicer1* and *Ptpn12* but also at the 5' end of the transcript (see Figure 5.2a for a primer map). This suggests knockdown of Mettl3/Kiaa1429 could increase the deposition of Alyref all along a transcript. Upon Mettl3/Kiaa1429 knockdown Wtap levels increase (Figure 5.8b).

Upon knockdown of Wtap/Kiaa1429, Figure 5.8a indicates a significant loss of Alyref on all methylated transcripts (*Taf7* p=0.0026, *Dicer1 e23* p=0.0023, *Dicer1 e3-e4* p=0.0023, *Ptpn12 e13* p=0.000001, *Ptpn12 e5-e8* p=0.00015 and *Gstp1* p=0.24). As with Mettl3/Kiaa1429 the phenotype occurs at the 5' and 3' end of Dicer1 and Ptpn12 not just at the identified 3' long exon methylation site. The loss of Alyref upon Wtap/Kiaa1429 indicates Wtap is required for the recruitment of TREX to certain methylated transcripts.

To build on the observation of Alyref loss upon Wtap/Kiaa1429 knockdown we conducted a Uap56 RIP, since Uap56 is the key RNA helicase which drives TREX assembly on mRNA. This was to identify if it was a loss of Alyref or a loss of TREX deposition. The bar chart presented in Figure 5.8c depicts the resulting qPCR, normalised to input and Control RNAi. We observed a significant decrease of Uap56 upon all methylated transcripts. Again we noted the loss of Uap56 was not just at the predicted 3' methylation sites for *Ptpn12* and *Dicer1* but also at the 5'

terminus. The Uap56 and Alyref RIPs in Wtap/Kiaa1429 indicate the reason for nuclear accumulation of the methylated transcripts is the inability to deposit TREX upon the mRNA.

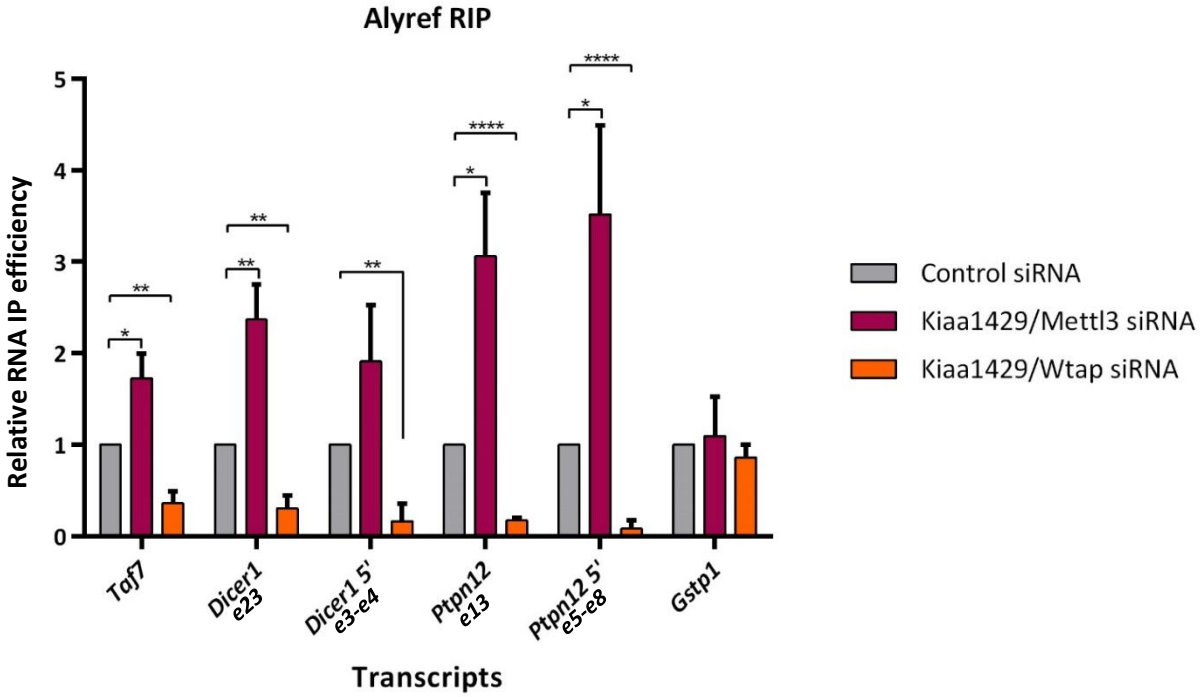

Figure 5.8a Alyref RIP in a Kiaa1429/Mettl3 and Kiaa1429/Wtap knockdown. Alyref deposition significantly increased upon m^{6}A containing transcripts within Kiaa1429/Mettl3 knockdown (*Taf7* p=0.018, *Dicer1 e23* p=0.0073, *Dicer1 e3-e4* p=0.1, *Ptpn12 e13* p=0.013, *Ptpn12 e5-e8* p=0.021 and *Gstp1* p=0.76). Alyref deposition upon the mRNA significantly decreased upon Kiaa1429/Wtap knockdown (*Taf7* p=0.0026, *Dicer1 e23* p=0.0023, *Dicer1 e3-e4* p=0.0023, *Ptpn12 e13* p=0.000001, *Ptpn12 e5-e8* p=0.00015 and *Gstp1* p=0.24).

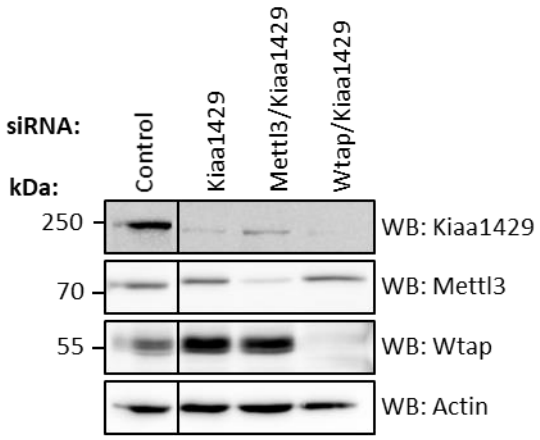

Figure 5.8b Wtap protein levels increase upon Kiaa1429/Mettl3 knockdown. Western blot illustrating the increase in expression of Wtap upon Kiaa1429/Mettl3 knockdown compared with Control siRNA.

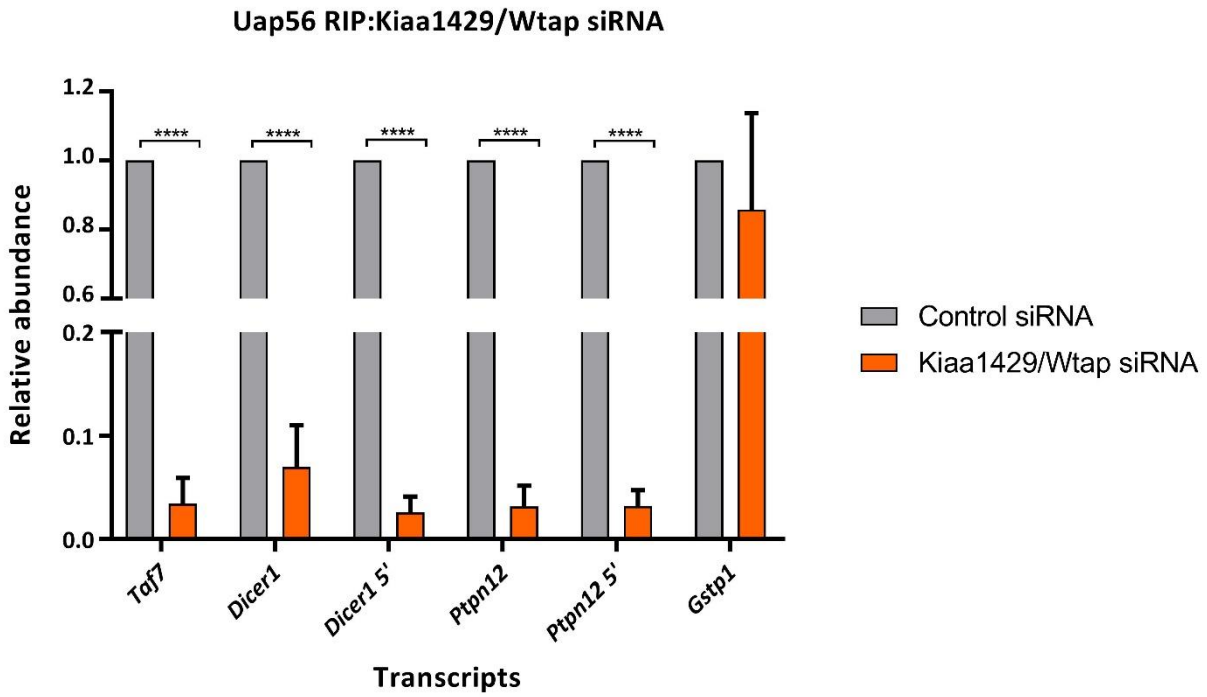

Figure 5.8c Uap56 deposition significantly decreased upon Kiaa1429/Wtap knockdown. Uap56 RIP indicating the reduced deposition upon transcripts targeted for m^6A addition.

5.9 Chapter 5: Summary

We did not observe any export phenotype upon the knockdown of individual methyltransferase complex members. This may be due to the redundancy with the m^{6}A writer pathway. However, upon knockdown of two core members of the methyltransferase complex we observed an export defect for a subset of m^{6}A containing transcripts. In both Wtap/Kiaa1429 and Mettl3/Kiaa1429 knockdown our selected transcripts showed an increase nuclear/cytoplasmic ratio. The double knockdowns indicated the deposition of m6A or the presence of a complete methyltransferase Writer complex is required for efficient nuclear export of some transcripts.

RNA sequencing of the nuclear and cytoplasmic fractions from Control and Wtap/Kiaa1429 siRNA revealed transcripts that are nuclear accumulated and of these 73% had been identified to contain an m^{6}A site. The nuclear accumulated transcripts appear to be involved in the cell cycle, RNA metabolism and DNA repair. Further analysis revealed that nuclear accumulated transcripts tend to have an increased number of m6A sites compared to non-nuclear accumulated. It was also revealed that the nuclear accumulated transcripts contained longer exons, with a greater final exon compared with non-nuclear accumulated. This suggests transcripts with larger exons require Wtap/Kiaa1429 for optimal export. We also identified a subset of transcripts that were alternatively polyadenylated upon knockdown of Wtap/Kiaa1429, with 60% of these transcripts also containing at least one m^{6}A site. Interestingly the transcripts undergoing alternative polyadenylation did not overlap with the nuclear accumulated and methylated transcripts.

Finally we identified that upon Wtap/Kiaa1429 knockdown our methylated transcripts lost Alyref and Uap56 deposition. This would result in an export block. However, we also identified that upon Mettl3/Kiaa1429 knockdown an increase of Alyref deposition upon methylated transcripts. We can speculate on the reasoning for increased Alyref, firstly, it may simply be due to the increase in Wtap upon Mettl3/Kiaa1429 knockdown. This is because we identified loss of Alyref

upon knockdown of Wtap/Kiaa1429. Secondly it may be due to the loss of Mettl3s enzymatic activity to continue the mRNA maturation process.

This chapter demonstrates a close relationship between the m^6A writers and the TREX complex. It builds on out biochemical data from Chapter 3. We can now see Wtap is required for TREX recruitment and knockdown of Wtap/Kiaa1429 results in nuclear accumulation of methylated transcripts with a long exon, specifically a larger 3' long exon. It is currently excepted TREX deposition is dependent on splicing/EJC deposition and capping of an mRNA (Masuda *et al.*, 2005; Andersen *et al.*, 2013). However the long exons of *Ptpn12* and *Dicer* contain TREX at distal position from the EJC. We noted these TREX binding sites align with the m^6A peaks. Following the data presented above we may hypothesise m^6A/writer machinery could act as an EJC surrogate facilitating the deposition of TREX within long exons. This may also apply to intronless transcripts that do not undergo splicing, such as *Taf7*.

Chapter 6: Ythdc1 associates with TREX

Ythdc1 is a nuclear reader of m^6A that preferentially binds to GGm^6A motif via two tryptophan residues within an aromatic cage. It binds primarily to the CDS of its target mRNAs (Xu *et al.*, 2014). Ythdc1 is currently defined in exon inclusion mechanisms employing a cooperative mRNA binding relationship with Srsf3 and a competitive mRNA binding relationship with Srsf10 (Xiao *et al.*, 2016). Further evidence of the dynamic relationship between m^6A readers was presented in Ythdc1 PAR-CLIP indicating a 20% overlap in target transcripts with the cytoplasmic Ythdf2 (Xu *et al.*, 2014). Due to our previous finding of TREX associating with the methyltransferase complex, we set out to investigate a possible relationship between the nuclear reader and the export machinery. In this chapter we explore the association of Ythdc1 and TREX/Nxf1. We gathered evidence linking Ythdc1 the writers and the export machinery.

6.1 Cellular location of Ythdc1 compared to TREX and the methyltransferase complex.

To begin our investigation into Ythdc1 and its possible export role we aimed to characterise the protein in greater detail. Therefore we set out to identify where Ythdc1 resides. It must be noted previous work pin pointed Ythdc1 localisation to specialised structures named YT bodies. These structures reside within close proximity to nuclear speckles (Rafalska *et al.*, 2004).

Protein fractionation was conducted on HEK293T cells then subject to western blot analysis, presented in Figure 6.1. The majority of Ythdc1 is located within the chromatin fraction and trace amount in the nucleoplasm. Interestingly the methyltransferase complex does not follow the same pattern. Kiaa1429 and Wtap are predominantly located in the nucleoplasm with trace amounts also in the chromatin. Mettl3 however, is present in all three fractions, with its highest

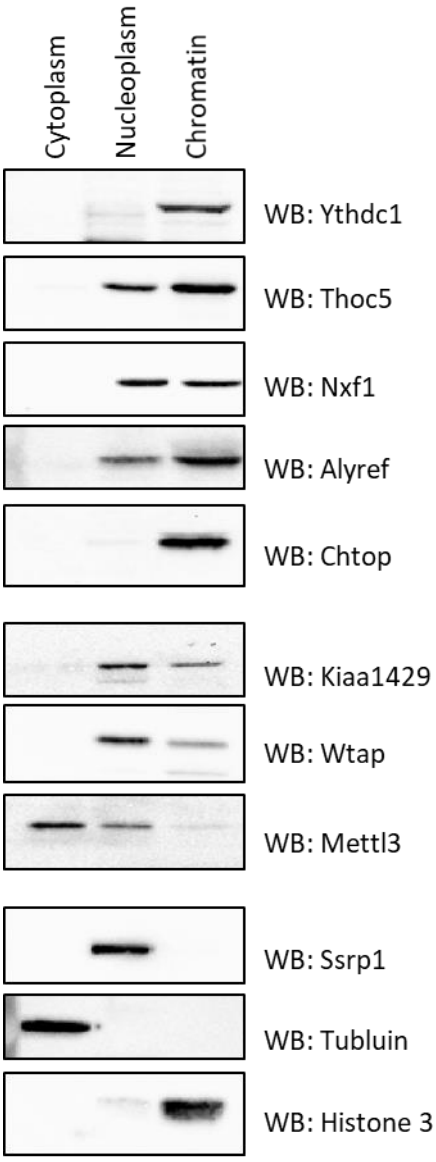

Figure 6.1 Fractionation of proteins from the cytoplasm, nucleoplasm and chromatin. Western blot indicating the location of each TREX member and methylation machinery member. Separation was controlled by probing Ssrp1 (nucleoplasm), Tubulin (cytoplasm and Histone 3 (chromatin).

concentration in the cytoplasm. The TREX complex was situated in the chromatin and nucleoplasm, with a bias towards the chromatin, consistent with co-transcriptional recruitment. The lower panels of the western blot suggest a clean separation of each fraction, indicated by the positioning of Ssrp1 (nucleoplasm), Tubulin (cytoplasm) and Histone 3 (chromatin).

6.2 Ythdc1 associates with TREX and Nxf1.

As with the m^6A writes we set out to identify any interaction between Ythdc1 and TREX using Co-IP experiments. However our initial attempts to Co-IP endogenous Ythdc1 were not successful (Figure 6.2a). The Ythdc1 antibody did not enrich Ythdc1 over input; the pulldown of Ythdc1 was to the same extent as anti-Alyref CO-IP Figure 6.2a. Therefore to further study Ythdc1 interactions we constructed a Flag-Ythdc1 (p3x-Flag-MYC, Sigma-Aldrich) expression vector. Figure 6.2b depicts the result of a Flag-Ythdc1 and Flag-GFP HEK293T overexpression followed by a Flag IP. All core TREX complex components (Uap56, ThoC5, Chtop and Alyref) pulldown with Flag-Ythdc1 but not Flag-GFP. HnrnpA1 western blot was included to indicate the IP was specific. All conditions were supplemented with RNase and DNase.

To confirm our Flag-Ythdc1 results we conducted the reverse endogenous CO-IP using Alyref and Chtop, Figure 6.2c. The western blot in Figure 6.2c shows Ythdc1 associates with both Alyref and Chtop. Uap56 was employed as a positive control and was present in both Alyref and Chtop CO-IP. HnrnpA1 probe indicated the pulldown was specific. A further endogenous pulldown of Nxf1 (Figure 6.2d) indicates Ythdc1 is associated. This CO-IP was controlled with Uap56 (not bound to Nxf1 in current mRNA export model (Viphakone, Guillaume M Hautbergue, *et al.*, 2012)), indicating a specific pulldown.

The final CO-IP experiment conducted indicated a possibility for mutually exclusive binding of Alyref and Chtop upon Ythdc1 (Figure 6.2e). Equal amounts of Flag-Ythdc1 was transfected into Control, Thoc5, Chtop and Alyref stable inducible

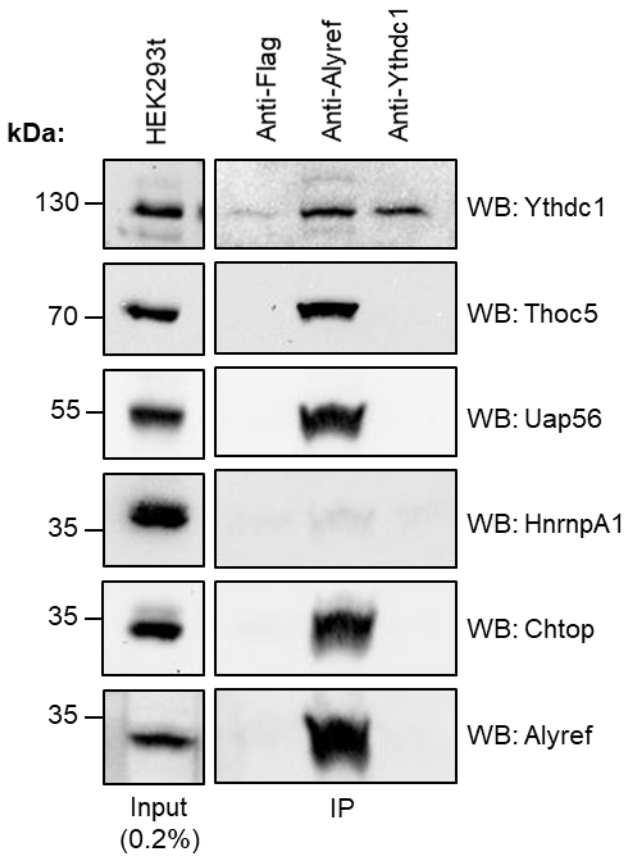

Figure 6.2a Endogenous Ythdc1 Co-IP. The resulting western blot of an Alyref and Ythdc1 Co-IP. The Ythdc1 antibody was not suitable for Co-IP experiments. Alyref pulled down the reader Ythsc1. HnrnpA1 was probed to demonstrate the IP was specific.

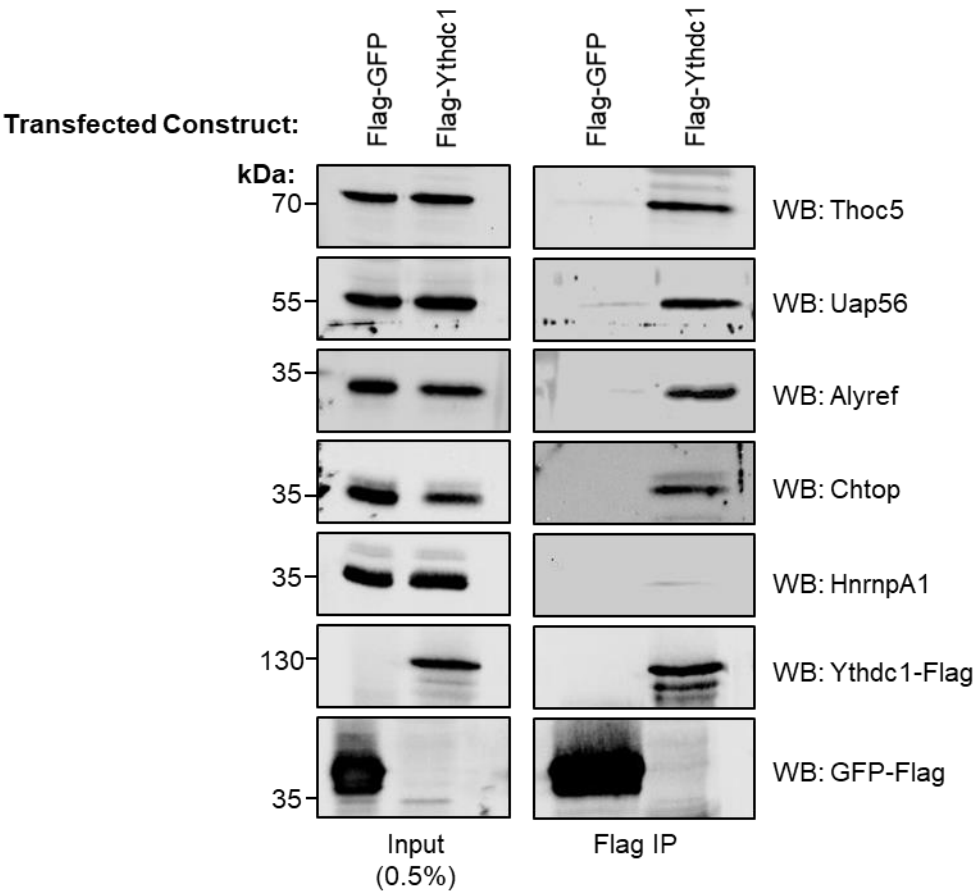

Figure 6.2b Flag-Ythdc1 pulls down the TREX complex. Flag-GFP and Flag-Ythdc1 were overexpressed in HEK293t cells. The resulting CO-IP indicated a specific association of Flag-Ythdc1 and core members of the TREX complex. Flag-GFP indicated there was not background binding, HnrnpA1 indicated the IP was specific.

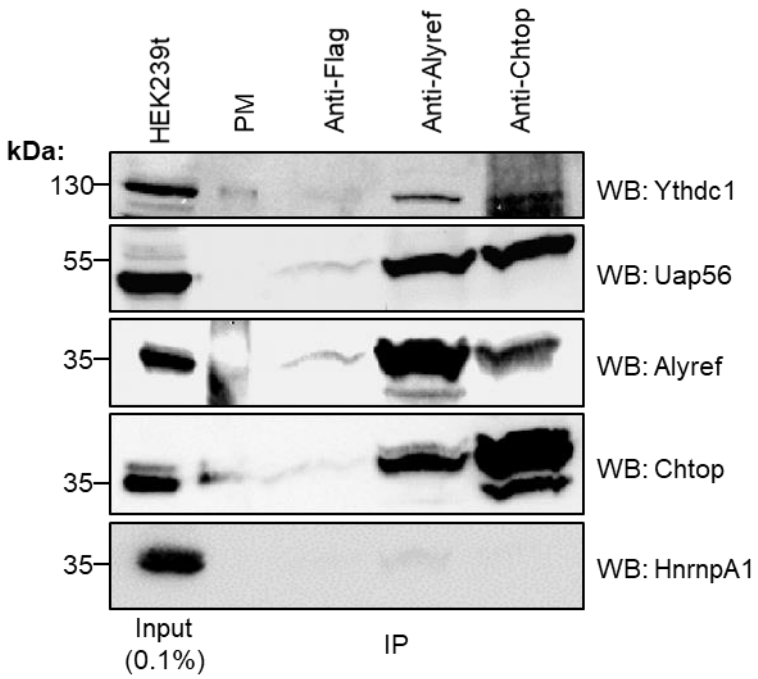

Figure 6.2c Alyref and Chtop associate with Ythdc1. Endogenous CO-IP of Alyref and Chtop with Ythdc1. HnrnpA1 was a specificity control, Uap56 employed as a positive control.

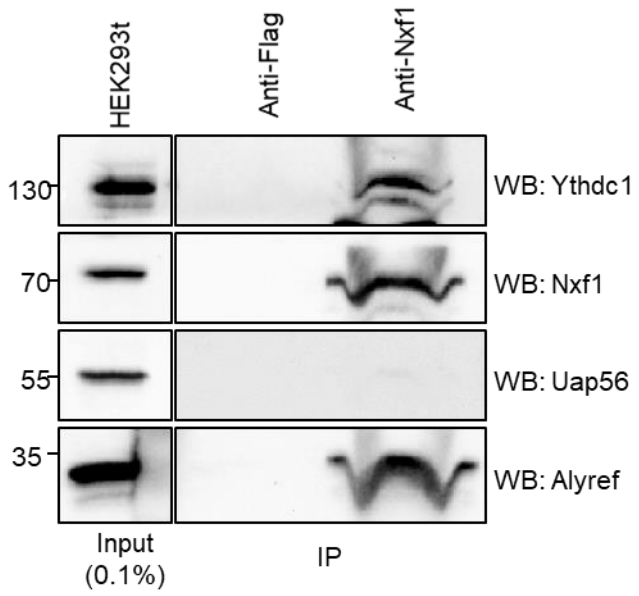

Figure 6.2d Nxf1 associates with Ythdc1. An endogenous Nxf1 CO-IP with Ythdc1. Uap56 was probed as a negative control, Alyref as a positive.

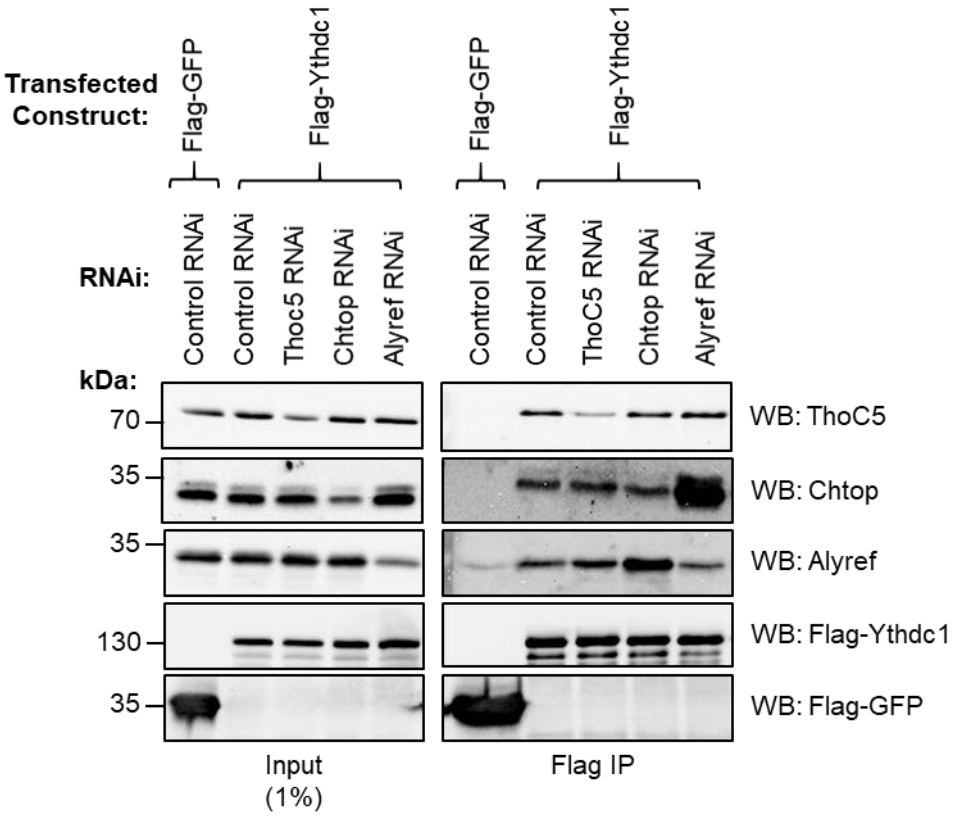

Figure 6.2e mutually exclusive binding of Alyref and Chtop to Flag-Ythdc1. Flag-Ythdc1 CO-IP in Thoc5, Chtop and Alyref RNAi. Removal of Alyref increases Chtop association with Flag-Ythdc1. The RNAi of Chtop results in an increase association of Chtop with Flag-Ythdc1.

RNAi cell lines. The aim was to identify any singular interaction that maybe vital for Ythdc1:TREX association. Flag-Ythdc1 associates with Thoc5 to the same degree in Alyref and Chtop RNAi when compared with Control RNAi, suggesting an Alyref/Chtop independent interaction. An increase of Alyref binding upon Chtop RNAi was observed, a similar increase was observed for Chtop upon Alyref RNAi. The input levels of Alyref do not change in Chtop RNAi suggesting the enrichment of IP is indeed due to the removal of Chtop. However Chtop levels did increase upon Alyref RNAi, although this increase was modest, the CO-IP will potentially magnify small changes present in the input. The increase of Chtop upon Alyref RNAi was previously shown by Chang *et al.,* 2013. We can therefore not confidently conclude increased Chtop binding is a result of removal of Alyref. Control RNAi transfected with Flag-GFP was included as a negative control. Finally the IP efficiency of Flag-Ythdc1 was consistent throughout all RNAi conditions. Together these results show an association between Ythdc1 and TREX/Nxf1 and Alyref/Chtop may bind a mutually exclusive site on Ythdc1.

6.3 Ythdc1-MS2 tethering assay.

With the identification of a TREX/Ythdc1 interaction we sort to identify any functional export properties Ythdc1 may harbour. We employed an MS2-tethered export assay (Hautbergue *et al.,* 2009). The assay system is diagrammatically illustrated in Figure 6.3a. A luciferase coding sequence and MS2-RNA operator sites are flanked by an inefficiently spliced intron derived from the HIV-1 ENV region. This unspliced pre-mRNA fusion is retained in the nucleus under normal conditions. If spliced the luciferase CDS is removed and therefore not exported into the cytoplasm. The MS2 coat protein binds to the operators. Therefore if an MS2 coat protein export factor fusion is created and over expressed we would anticipate export and expression of the luciferase construct. The cytoplasmic luciferase activity was measured via a luminometer. Figure 6.3b indicates the system is functional as we measure greater luciferase activity within MS2-Alyref (8-fold) and

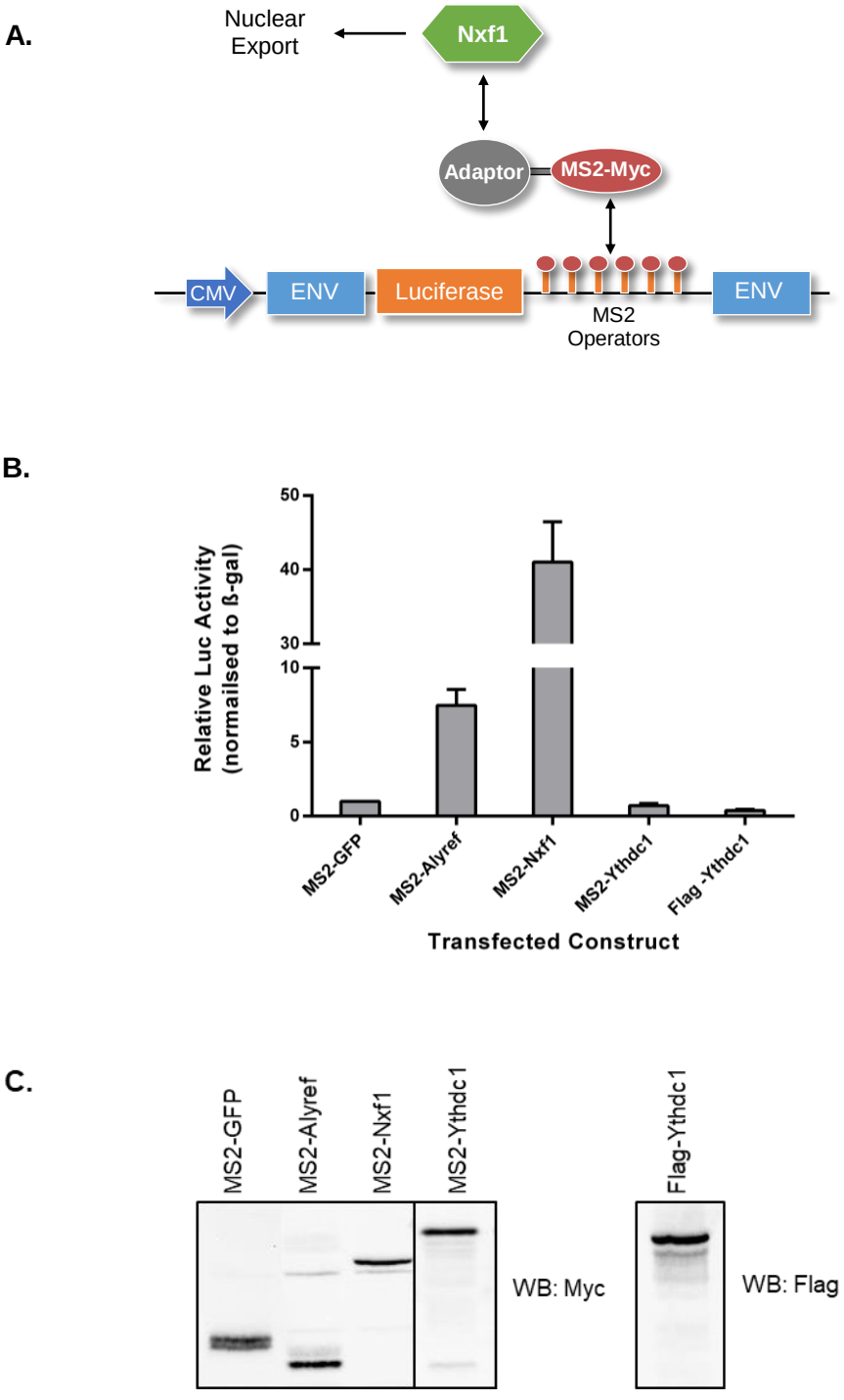

Figure 6.3 MS2-tethered luciferase export assay comparing export activity of Ythdc1, Alyref and Nxf1. A. schematic of the reporter assay, the C terminal MS2 tether was attached to either Ythdc1, Alyref or Nxf1. **B.** Resulting luciferase activity upon MS2-tether binding operators. Nxf1 gave 40 fold greater than control. Ythdc1 did not induce luciferase activity above control. **C.** Expression levels of tethered MS2 constructs.

MS2-Nxf1 (40-fold) when compared to MS2-GFP upon equal transfections and a 48 hour incubation in HEK293T. MS2-Ythdc1 did not yield an increase in luciferase activity compared to control MS2-GFP and Flag-Ythdc1. Figure 6.3c is a western blot of the constructs used in the assay.

6.4 Interplay between m^{6}A writers, TREX and Ythdc1.

The next stage of our study was to dissect the interactions between m^{6}A writers, TREX and Ythdc1. Results presented in Figure 3.6a displayed Ythdc1 association with Wtap but not with other writers such as Kiaa1429. The literature does not currently mention any interaction between the writers and readers, therefore we set out to investigate this relationship. Confirmation of the IP is presented in Figure 6.4a, an endogenous CO-IP of all m^{6}A writers. The results match that of the previous CO-IP, Wtap is the only writer to enrich Ythdc1. Mettl3 appears to show a very weak IP, this suggests it maybe a distant part of the complex with no direct interaction with Ythdc1. Interestingly Figure 6.4a does not show an association between Kiaa1429 and Mettl3/Mett14. HnrnpA1 indicated the IP was specific for Kiaa1429 and Wtap but did pulldown with Mettl3/Mett14, however the lack of Kiaa1429 in these conditions indicates specificity.

Moving forward we aimed to dissect the interaction between Ythdc1, TREX and Wtap aiming to build upon the observed compensatory mechanism from Figure 6.2d. Therefore using the siRNAs and conditions presented in Chapter 5 (72 hour incubation with a second transfections of 10 nM siRNA at 48 hours) we conducted an Alyref CO-IP in a number of knockdown backgrounds, Control, Mettl3, Wtap and Kiaa1429 siRNA. The resulting western blot in Figure 6.4b indicates greater Ythdc1 association with Alyref upon Mettl3 and Wtap knockdown but not with a Kiaa1429 knockdown. Interestingly the two conditions to give a phenotype, Mettl3 and Wtap, are the CO-IP partners of Ythdc1. The IP of Alyref is consistent throughout the conditions as is the pulldown of Uap56, ruling out a difference in IP efficacies as a contributor to the Ythdc1 variance. Also of

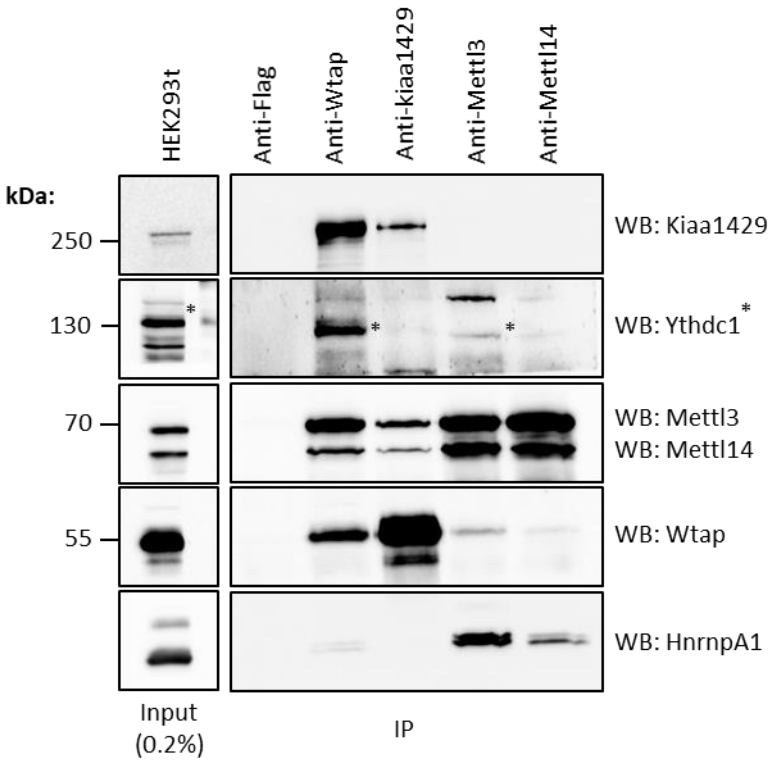

*identifies Ythdc1 signal

Figure 6.4a Wtap and Mettl3 associate with Ythdc1. CO-IP of all members of the methyltransferase complex Mettl3. Mett14, Kiaa1429 and Wtap (Abcam). Ythdc1 associates with Wtap and weakly with Mettl3.

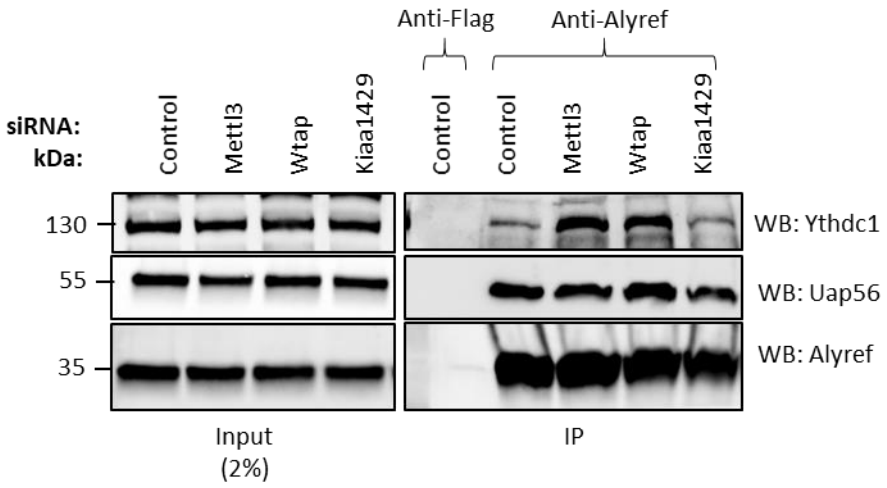

Figure 6.4b Increased association between Alyref and Ythdc1 upon Mettl3 or Wtap knockdown. Alyref CO-IP in Mettl3, Wtap (Abcam) and Kiaa1429 backgrounds. Equal amounts of Alyref and Uap56 were associated.

note the input levels of Ythdc1 remain constant throughout each knockdown condition.

The results of Figure 6.4b opened up the question of how Ythdc1 is associating with the mRNA. As we observed removal of the Writers Mettl3/Wtap leads to increased Alyref and Ythdc1 association, indicating a possible Ythdc1/TREX pre methylation association. Therefore with the data of TREX association we conducted an mRNP capture in an Alyref/Chtop and Nxf1 RNAi background, induced for 48 hours. The decision for Alyref/Chtop RNAi was based upon Figure 6.2d, as removing one allows greater binding of the other, therefore removing both will reduce any redundant functions. The choice of Nxf1 RNAi was to decipher if Ythdc1 association with the mRNA is at a late stage in the export pathway. Surprisingly Figure 6.4c indicates reduced Ythdc1 PolyA+ association in an Alyref/Chtop RNAi background but not Nxf1 RNAi. The Uap56 probe indicates a comparable level of PolyA+ pulldown in each condition. This result was not present in a single Alyref (48 hour induction) RNAi mRNP capture, Figure 6.2d. It appears Ythdc1 deposition on the mRNA maybe dependent on multiple members of the TREX complex. To add merit to the global result indicated via the mRNP capture we conducted an Ythdc1 RIP in the Alyref/Chtop RNAi background using the identical conditions as the mRNP capture. Figure 6.2e graphically displays the results of the Ythdc1 RIP. Each transcript from both conditions was normalised to input followed by normalisation to the null IP and finally compared to the Control RNAi RIP. All methylated transcripts showed a significant decreased (*Taf7* p value =0.002, *Dicer1* p= 0.01 and *Ptpn12* p= 0.019) in Ythdc1 deposition. Targets from Chapter 5 were employed as we have previously demonstrated their involvement in the m^6A pathway with Wtap and Kiaa1429 data. This result adds value to the mRNP capture presented in figure 6.4d.

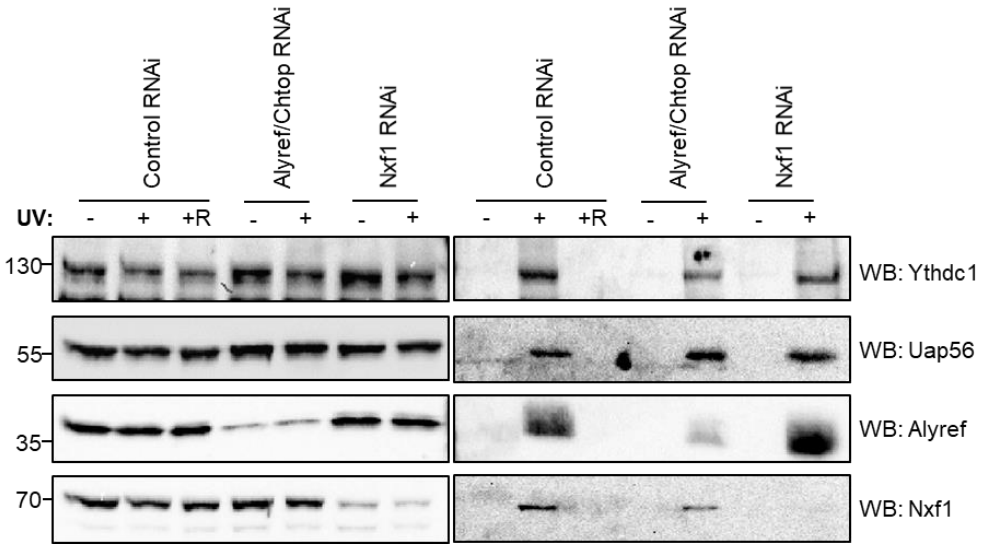

Figure 6.4c Reduced Ythdc1 Association with PolyA+ RNA upon Alyref/Chtop RNAi. An mRNP capture conducted in Alyref/Chtop and Nxf1 RNAi, post 48 hour induction. Ythdc1 Probe indicated a reduced association with the PolyA+ RNA.

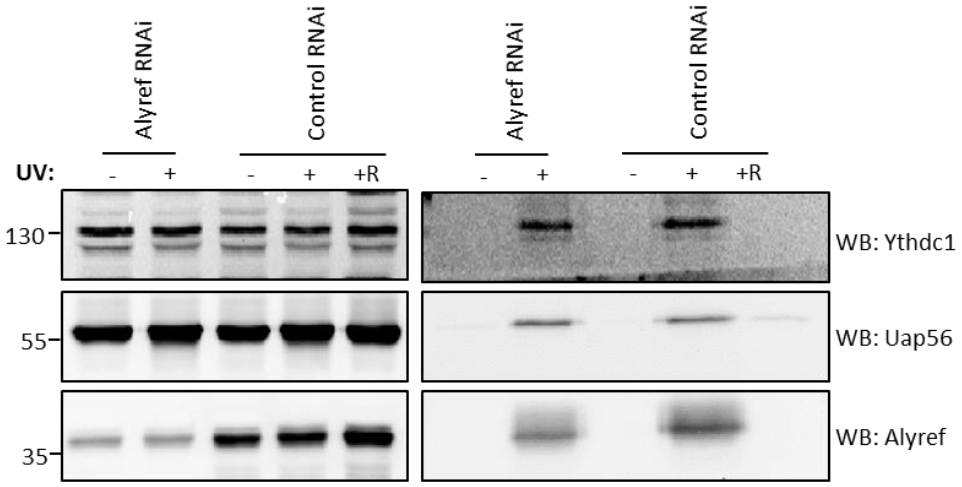

Figure 6.4d Alyref RNAi does not reduce YThdc1 deposition upon PolyA+ RNA. An mRNP capture conducted in 48 hour induced Alyref RNAi. Ythdc1 deposition was unchanged compared to Control RNAi.

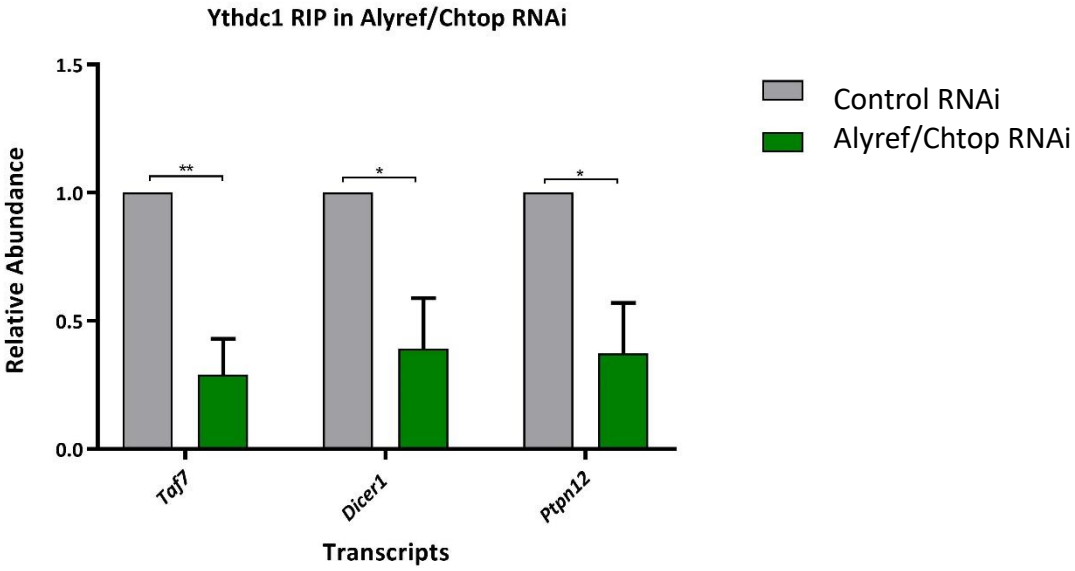

Figure 6.4e Ythdc1 association with mRNA is reduced upon Alyref/Chtop RNAi. A Ythdc1 RIP in a 48 hour induced Alyref/Chtop RNAi background. All transcripts have been shown to be methylated and result in a significant decrease in Ythdc1 binding. (*Taf7* p value =0.002, *Dicer1* p= 0.01 and *Ptpn12* p= 0.019)

6.5 Construction of a TET-inducible Ythdc1 RNAi HEK Flpin cell line.

To further characterise the role for Ythdc1 in mRNA export, we constructed a stable inducible Ythdc1 RNAi cell line. The cell line was constructed using two targeting hairpins and the BLOCK-iT Pol II mir expression vector system (Invitrogen). Initial validation of the hairpins was carried out using transiently transfected vectors and the previously constructed Flag-Ythdc1 construct (data not shown), allowing for selection of the most potent hairpin combination. The selected hairpin was sub cloned into the FRT integration vector and subsequently transfected allowing integration. The colony displaying the greatest knockdown was selected and expanded. Validation of the resulting stable cell line can be seen in Figure 6.5a. At 72 hours post induction the protein levels of Ythdc1 have reduced to roughly 50% of the Control RNAi.

An early observation when testing extended time points indicated Ythdc1 RNAi can reduce cell growth. An MTT assay was carried out measuring viable cell growth over a period of 120 hours (Figure 6.5b). An MTT assay is a colour metric assay measuring the activity of mitochondrial oxidoreductase enzymes as a marker for cell viability. Post 72 hour induction Ythdc1 RNAi cells begin to reduce in viability. At 96 hours ~40% reductions has occurred when compared to control, at 120 hours ~80% of Ythdc1 RNAi cells are no longer viable.

A.

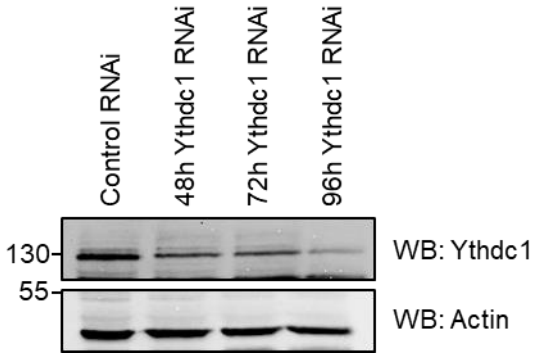

B.

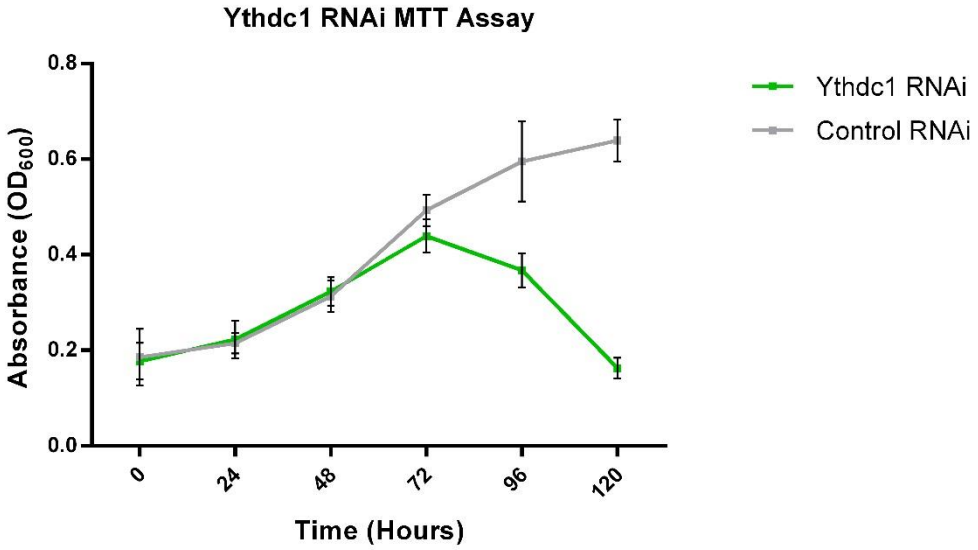

Figure 6.5 Validation of a Ythdc1 RNAi stable cell line. A. Western blot showing multiple time points of induced Ythdc1 RNAi compared to Control RNAi. **B.** Colorimetric MTT assay indicating a reduction in viability for Ythdc1 RNAi stable cell line post 72 hours.

6.6 Ythdc1 RNAi does not disrupt TREX on a global level.

To identify a cause for the cell death occurring upon prolonged Ythdc1 RNAi we conducted a number of experiments based on previous results linking Ythdc1 and TREX. We postulated upon the observed strong and dynamic interplay with TREX, Ythdc1 RNAi may result in a block of export. We initially attempted a global approach but would have to become more targeted in later studies. FISH was the first experiment conducted with the Ythdc1 RNAi cell line. The reasoning for this was to identify a global mRNA export block. Figure 6.6a presents Ythdc1 RNAi compared with Nxf1 RNAi having undergone a 72 hour induction prior to fixing. The nucleus (DNA) is DAP1 stained (blue) and Cye3 probe bound to the PolyA+ tail of mRNA (red). As published Nxf1 RNAi produced a PolyA+ nuclear accumulation (Viphakone *et al.*, 2012). Ythdc1 RNAi gave no nuclear accumulation of PolyA+ RNA when compared to Control RNAi.

The second phase of our TREX/Ythdc1 study looked upon the formation of the TREX complex within Ythdc1 RNAi. The rationale behind this experiment came from the previously observed dynamics in Ythdc1 Co-IP (Figure 6.2d and 6.4b). An Alyref Co-IP in Ythdc1 RNAi was undertaken in the presence of RNase/DNase. Figure 6.6b is the resulting western blot and depicts no change in Alyref IP with other TREX members. Interestingly it also indicated there is no change in Alyref and Wtap association within Ythdc1 RNAi. This implies the association of TREX and the methylation writers is independent of Ythdc1.

The final attempt at assessing a disruption within the TREX complex was an mRNP capture in a Ythdc1 RNAi background. The results presented in Figure 6.6c indicate there is no change in Alyref of Nxf1 deposition upon the mRNA detectable with an mRNP capture at 72 hours of Ythdc1 RNAi. Again the capture was control for background bead binding (-U.V) and PolyA+ dependent pulldown (+U.V and RNase). The culmination of these experiments indicated Ythdc1 does not change export machinery/characteristic at the global cellular level.

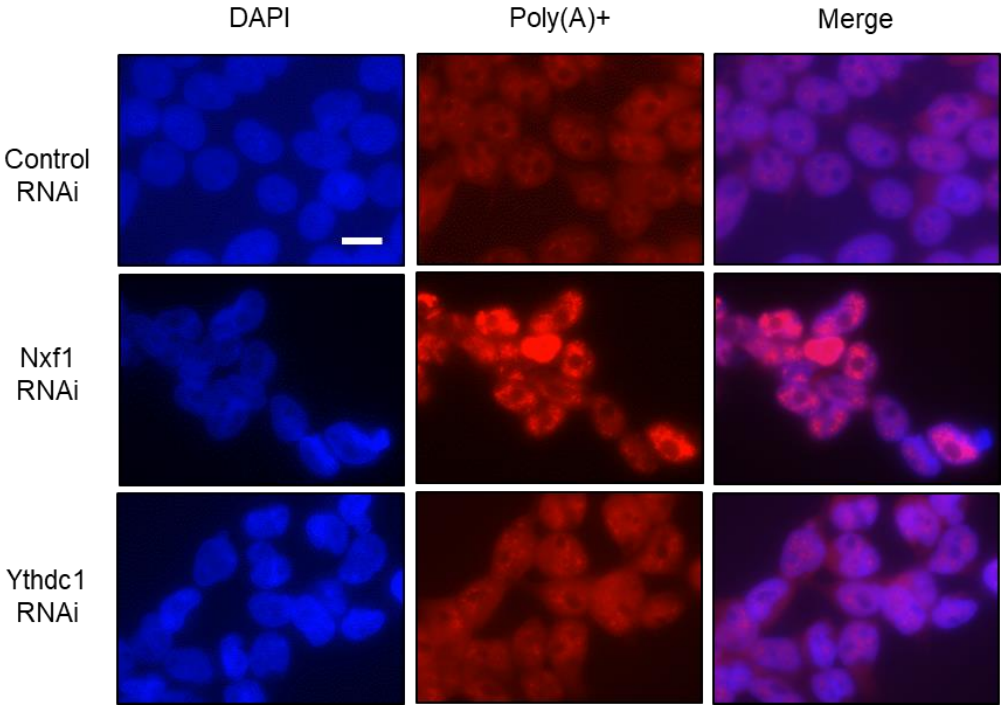

Figure 6.6a Ythdc1 RNAi does not induce nuclear accumulation of mRNA. F.I.S.H was conducted on 72 hour induced Control, Ythdc1 and Nxf1 RNAi. As indicated accumulation of the PolyA+ signal is observed in Nxf1 RNAI (Red) but not Ythdc1 RNAi.

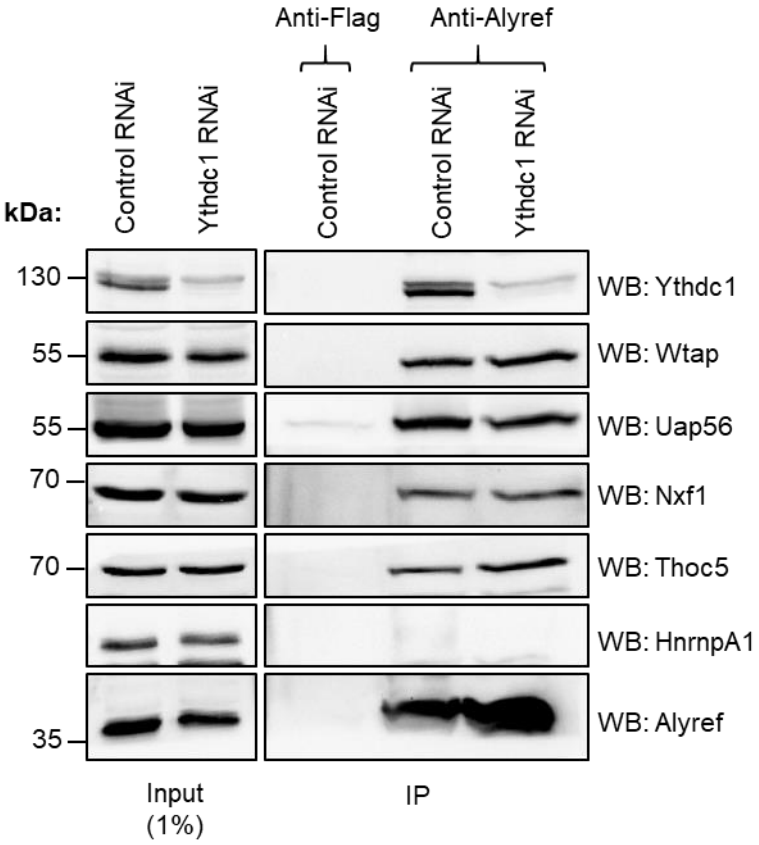

Figure 6.6b Ythdc1 depletion does not alter TREX composition. Endogenous Alyref CO-IP in a Ythdc1 RNAi background. Alyref association with other TREX members did not differ compared to control. Alyref and Wtap association was unchanged by Ythdc1 RNAi.

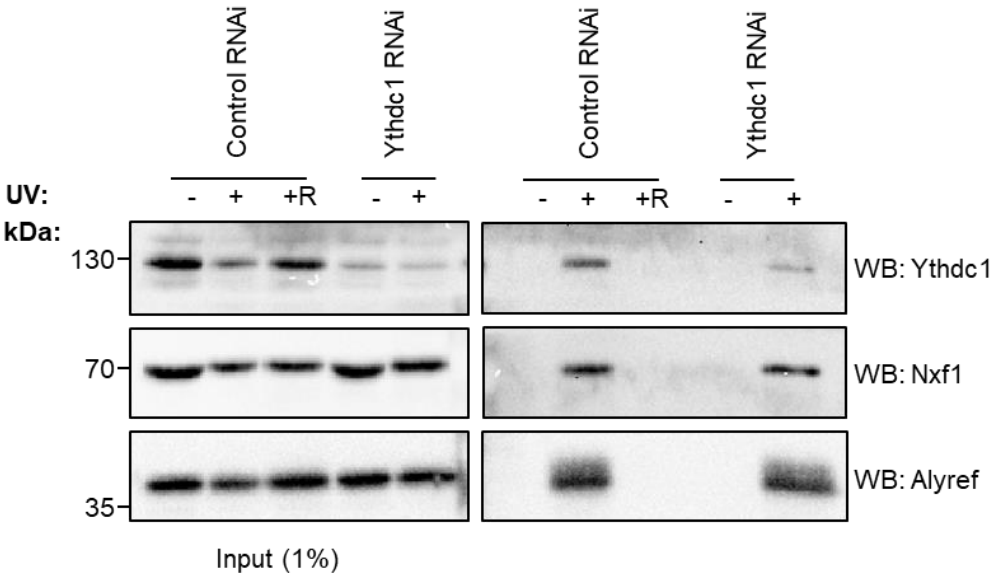

+R = UV cross linked and RNAseA Treated

Figure 6.6c Ythdc1 RNAi does not alter Alyref of Nxf1s association with mRNA. mRNP capture in a Ythdc1 RNAi background. The levels of Alyref and Nxf1 upon PolyA+ RNA do not change.

6.7 Ythdc1 RNAi results in an export block for a subset of transcripts.

The null results presented above indicate Ythdc1 does not illicit a global mRNA export block. Therefore we became more targeted whilst reflecting on our previous work involving the m^6A writers (Chapter 5). We selected the same methylated transcripts *Taf7, Dicer1 3'* and *Ptpn12 3'* with our non-methylated transcript *Mc1r.* The methylated transcripts also appear to be bound by Ythdc1 in recent PAR-CLIP studies (Xu *et al.*, 2014). *Taf7* is an intronless transcript whilst *Dicer1* and *Ptpn12* both contain long 3' exons with multiple m^6A sites (Dominissini *et al.*, 2012). The primers employed were the same as previous work (Chapter 5) spanning the long 3' methylated exon. The initial experiment was to identify any export block of these transcripts upon 72 hour Ythdc1 RNAi. The export of these transcripts was measured via nuclear/cytoplasmic RNA extraction. The resulting RNA was subject to cDNA synthesis and qPCR analysis. Figure 6.7a depicts the controls from the nuclear/cytoplasmic fractionation. Figure 6.7a western blot indicated no leakage of proteins between fractions; a good indicator of a clean preparation, Ssrp1 is only present in the nucleus and tubulin only present in the cytoplasm. Further confirmation of the fractionation is presented (Figure 6.7b) by measuring the levels of pre mRNA HnrnpA2B1 in each fraction per condition. As graphically depicted no HnrnpA2B1 pre-mRNA is present in the cytoplasm of each condition, all experiments were conducted in biological triplicate.

Taf7, Dicer1 and *Ptpn12* result in a positive nuclear/cytoplasmic ratio upon Ythdc1 RNAi when normalised to Control RNAi indicating an mRNA export block (Figure 6.8a). However only *Taf7* ($p=0.00033$) and *Ptpn12* 3' ($p=0.00082$) gave a significant increase over control, not *Dicer1 3'* ($p=0.166$). *Mc1r,* our non-methylated transcript, did not significantly change compared to Control RNAi. The nuclear levels of each transcript depicted in Figure 6.8b show an accumulation of *Ptpn12 3'* but not *Taf7* or *Dicer.* This could be due to nuclear RNA degradation. The cytoplasmic levels of all methylated transcripts are reduced, Figure 6.8c. In both

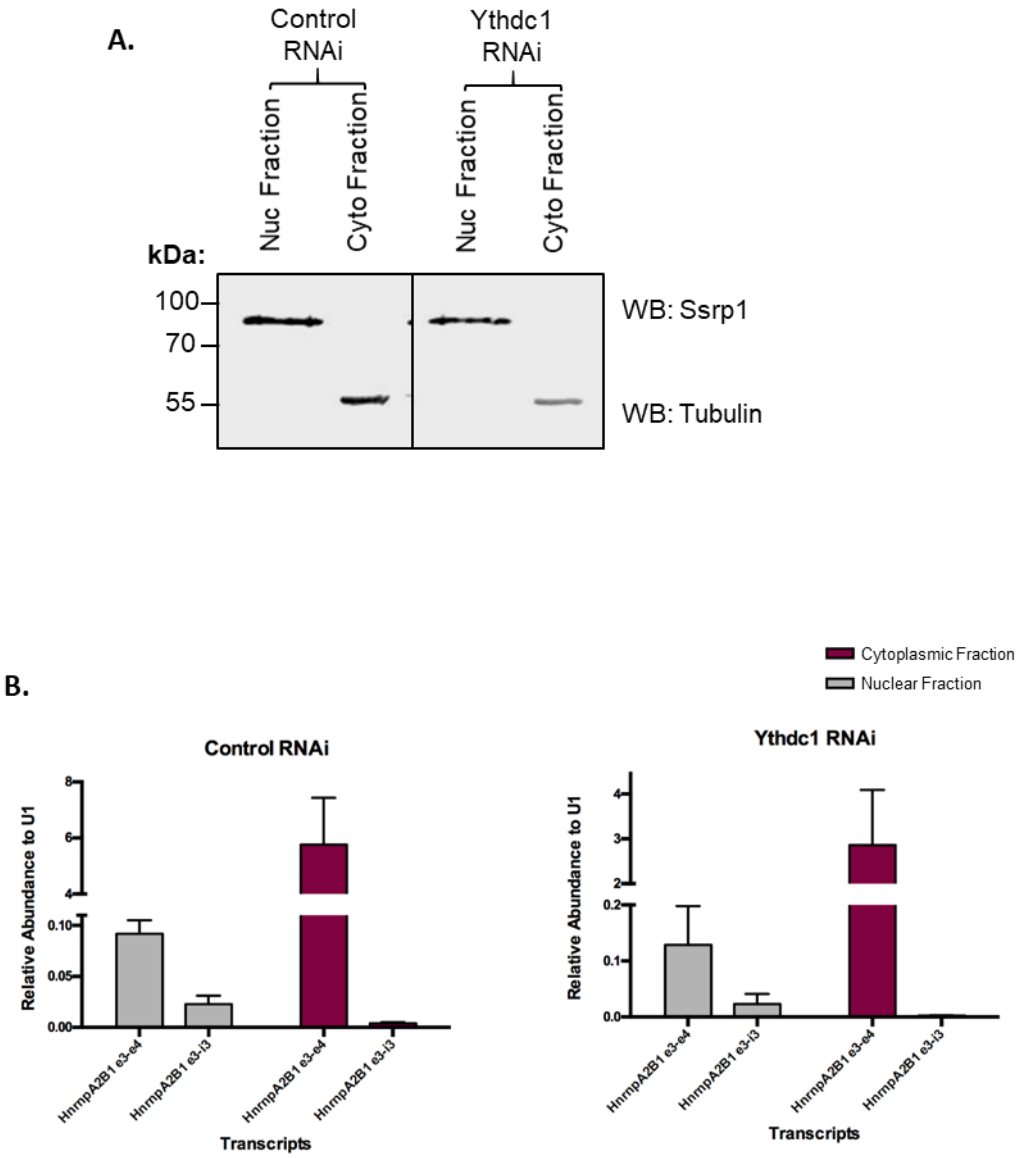

Figure 6.7 Ythdc1 RNAi nuclear/cytoplasmic fractionation was clean. A. Western blot indicating no leakage between compartments, Ssrp1 located in the nucleus and Tubulin in the cytoplasm. **B.** The graphs depict levels of pre/mRNA HnrnpA2B1 in Control and Ythdc1 RNAi nucleolus and cytoplasm. There was no pre-mRNA in the Cytoplasm.

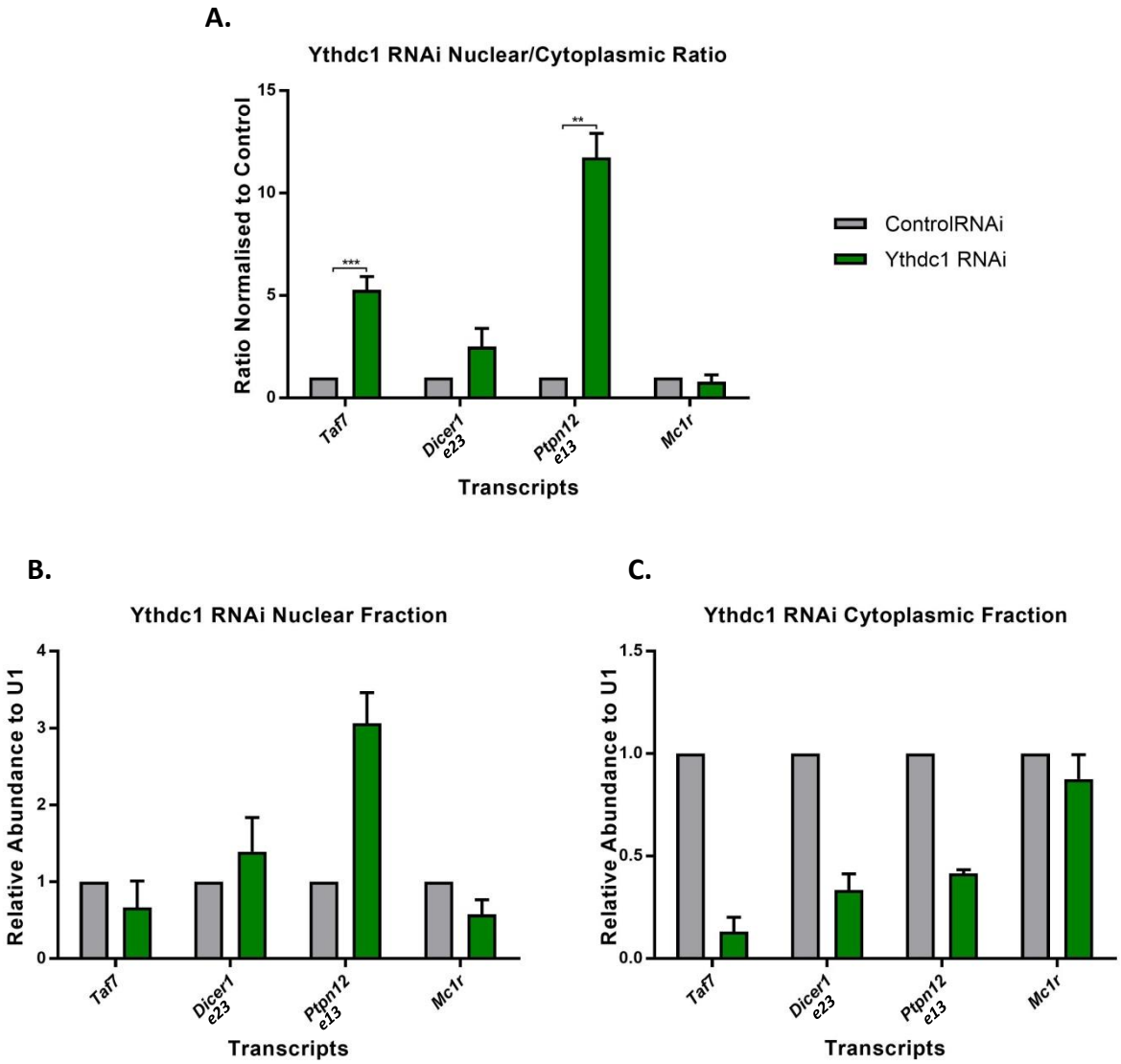

Figure 6.8 Ythdc1 RNAi results in an export block of methylated transcripts. **A.** Nuclear cytoplasmic ration of Ythdc1 RNAi fractionation normalised to Control RNAi. Methylated transcripts *Taf7* and *Ptpn13 3'* resulted in a significant increase in ratio (p=0.00033 and 0.000824 respectively). Although *Dicer 3'* increased it was not significant (p=0.166). **B.** Nuclear levels of transcripts normalised to control. *Dicer 3'* and *Ptpn12 3'* increase. **C.** Cytoplasmic levels of Ythdc1 RNAi transcripts normalised to control. All methylated transcripts decrease.

the nuclear and cytoplasmic fraction *Mc1r* does not differ greatly when normalised to Control RNAi.

As with the writer nuclear/cytoplasmic (Mettl3/Kiaa1429 and Wtap/Kiaa1429) experiments we assessed the nuclear fraction to identify if the accumulated mRNA had undergone splicing. Figure 6.8d depicts qPCR of Ythdc1 RNAi nuclear fractions normalised to Control RNAi nuclear fractions. The primers were designed to cover the exon:exon boundary adjacent to the methylation site (*Dicer* e24-e25 and *Ptpn12* e14-e15) therefore only giving a product if the transcripts has been spliced. Indeed the accumulated transcripts in Ythdc1 RNAi are spliced. This corresponds with the observed increase in nuclear transcripts levels when employing primers spanning the 3' long exon (Figure 6.8b).

6.8 Increased deposition of Alyref upon target mRNAs within Ythdc1 RNAi.

The results presented above match that of the writer complex double knockdowns (Kiaa1429/Wtap and Kiaa1429/Mettl3 siRNA). Therefore our next step was to assess the levels of TREX upon these specific transcripts, as we have previously conducted in Chapter 5. An Alyref RIP was performed in a Control and Ythdc1 RNAi background. Control/Ythdc1 RNAi was induced for 72 hours to ensure conditions were comparable to the nuclear cytoplasmic experiments. The resulting RNA was subject to DNase treatment and subsequent cDNA synthesis. Figure 6.9 graphically represents the qPCR analysis conducted on the cDNA. Primers from previous experiments (Chapter 5) were employed. Each RIP was normalised to input and to the Null IP and displayed relative to Control RNAi. We observed a significant increase of Alyref on all m^6A containing targets, *Taf7* (p=0.014), *Dicer1 5' e3-e4* (p=0.0072) and *3' e23* (p=0.0055) and *Ptpn12 5' e5-e8* (p=0.00027) and *3' e13* (p=0.00034). There was no significant change in Alyref deposition for our non-methylated transcript *Mc1r* (p=0.072). Again we saw a deposition increase all along the transcript of *Ptpn12* and *Dicer1* not just at the reported 3' site of methylation. These findings match that of Mettl3/Kiaa1429

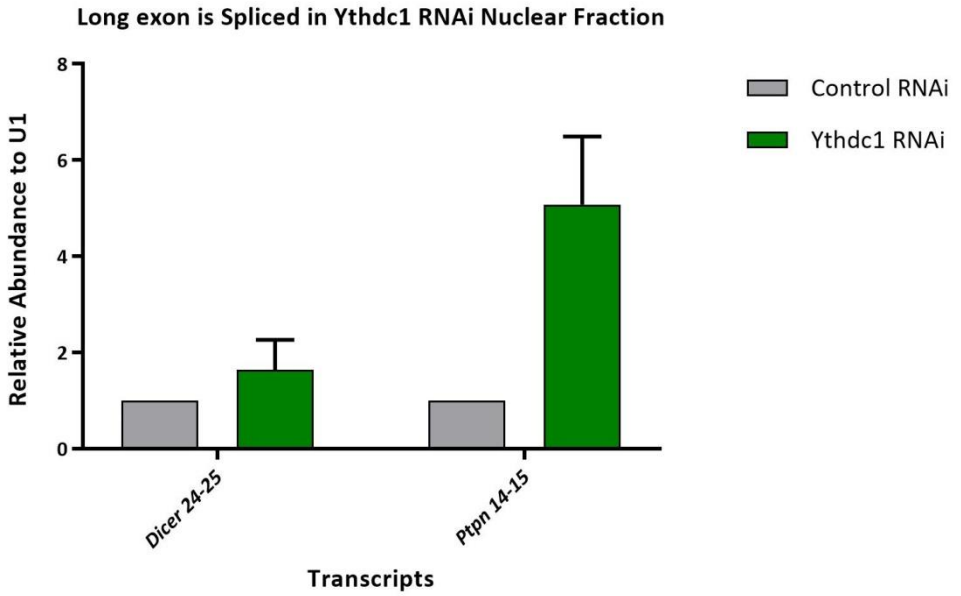

Figure 6.8d Nuclear accumulating mRNAs for Dicer1 and Ptpn12 are spliced. qPCR of nuclear Control and Ythdc1 RNAi fractions. Primers spanning exon-exon junctions resulted in similar levels of nuclear accumulation as the 3' long exon internal primers employed in Figure 6.8b.

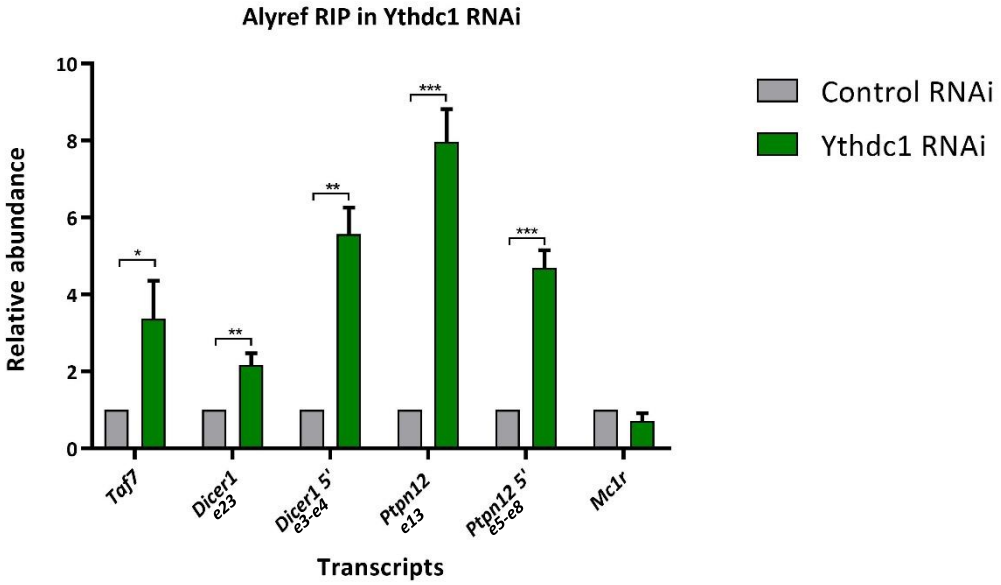

Figure 6.9 Ythdc1 RNAi results in accumulation of Alyref upon m^{6}A **containing transcripts.** Alyref RIP in Ythdc1 RNAi. Normalised to input and null IP. Results displayed relative to Control RNAi. All m^{6}A transcripts gave a significant increase in Alyref deposition , *Taf7* (p=0.014), *Dicer1 5'* (p=0.0072) and *3*' (p=0.0055) and *Ptpn12 5'* (p=0.00027) and *3*' (p=0.00034).

siRNA treated cells but not Wtap/Kiaa1429. This suggest the observed export block is not a result of reduced TREX deposition.

6.9 Ythdc1 shares homology with cleavage and polyadenylation factors.

Nuclear/cytoplasmic fractionation of Ythdc1 RNAi revealed transcripts are down in the nucleus and cytoplasm compared with control RNAi (Taf7 and Dicer1). However we identified no loss of Alyref upon the transcripts within the nucleus. Results presented above allow us to hypothesise Ythdc1 RNAi affects Nxf1 association with TREX resulting in the export block of certain m^6A containing transcripts. With the evidence of Ythdc1s 3' terminal exon binding (Xiao *et al.*, 2016) we looked into the possibility of a polyadenylation/cleavage defect. Analysis of Ythdc1 in the STRING association data base revealed homology to the *Arabidopsis* homologue Cpsf30 (Figure 6.10). Interestingly Cpsf30 is a known cleavage and polyadenylation factor containing a YTH domain (Fray and Simpson, 2015). The STRING database revealed Ythdc1 may associate with other cleavage and polyadenylation machinery (Cpsf2, Cpsf1 and Pcf11) depicted in Figure 6.11. However we currently have no experimental evidence linking Ythdc1 with polyadenylation with mammalian cells. With this observation we can speculate a further cause of the export defect in Ythdc1 RNAi, this maybe defective cleavage and polyadenylation of certain m^6A containing transcripts.

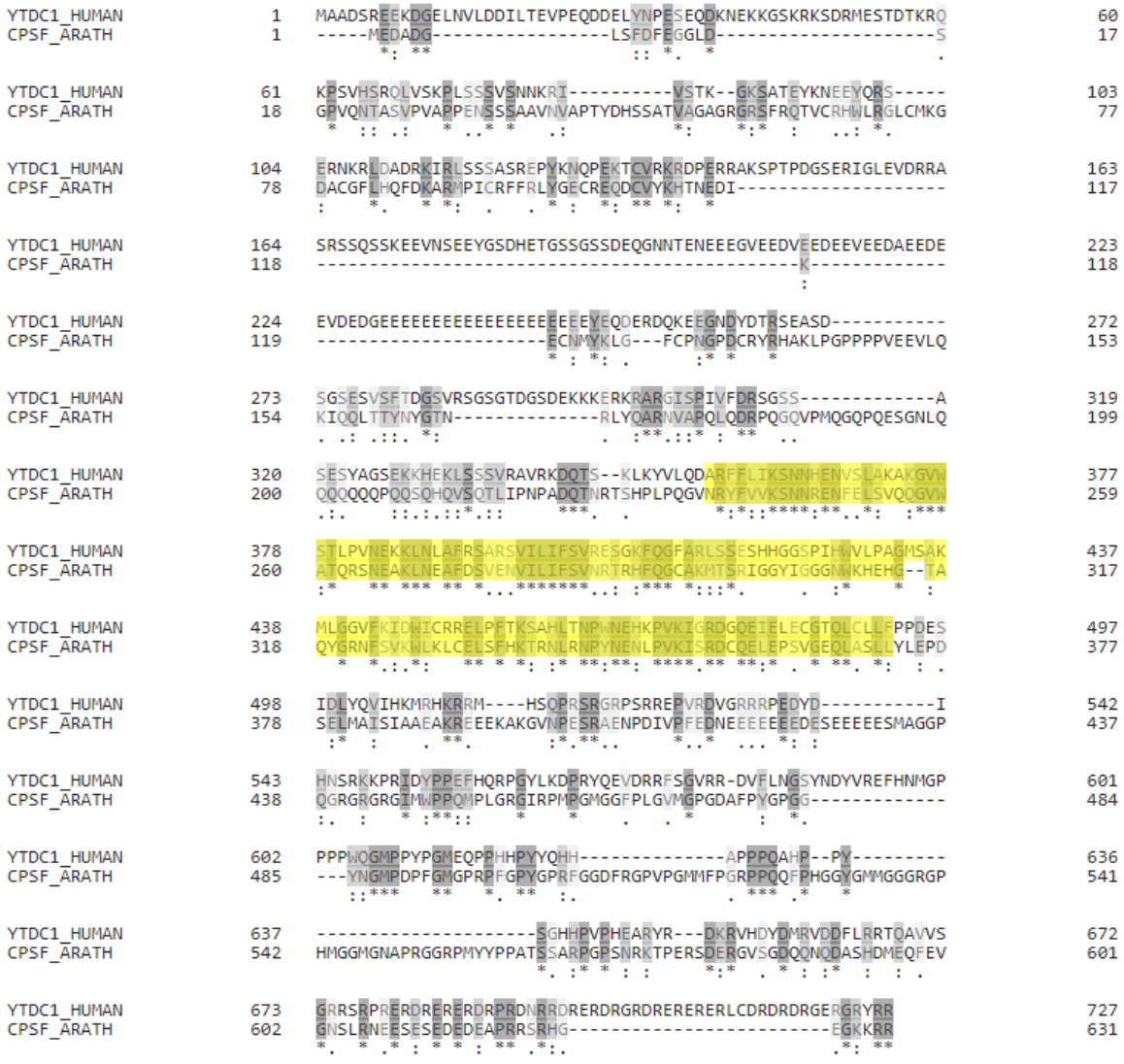

Figure 6.10 Aliment of Ythdc1 primary amino acid sequence with Cpsf30 (*Arabidopsis*). Similarity highlighted in grey. YTG domain highlighted in yellow.

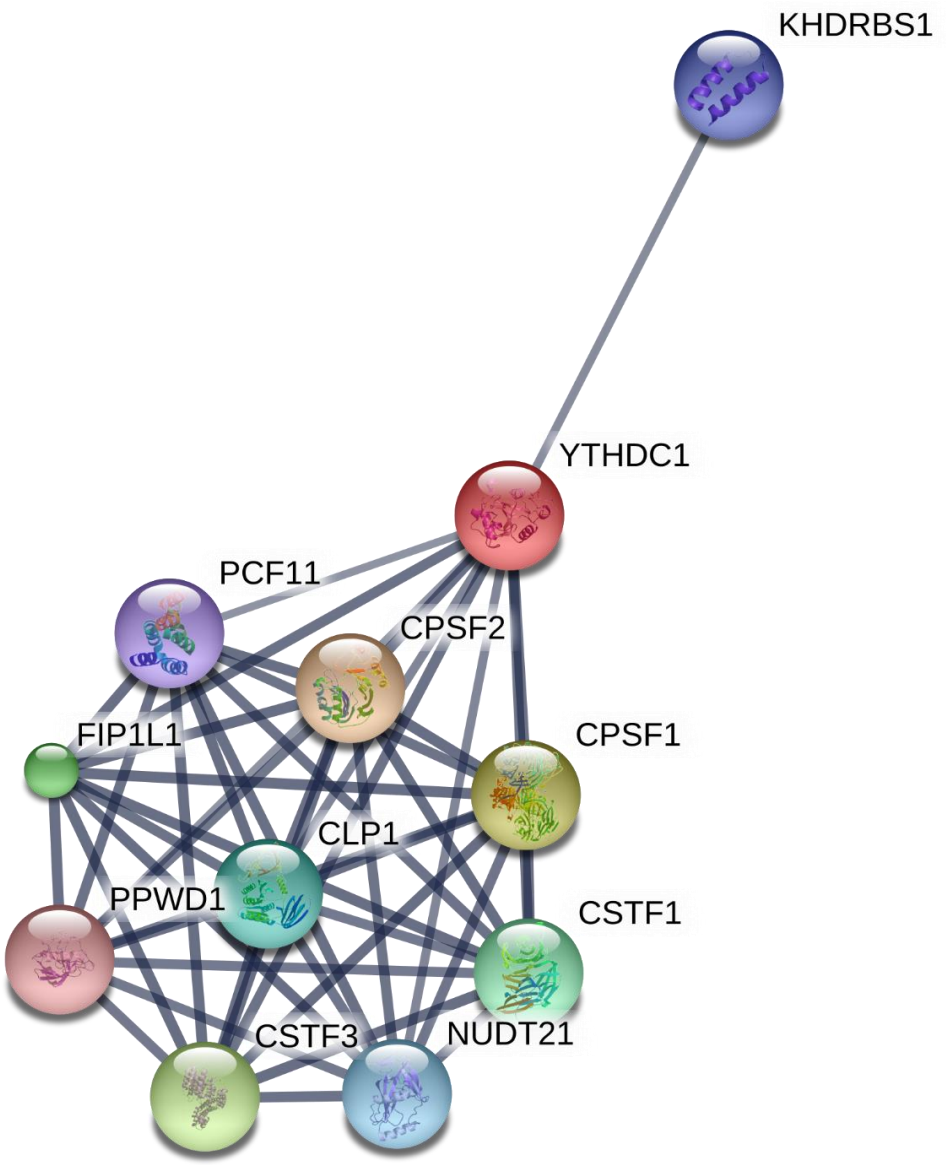

Figure 6.11 Interaction map for Ythdc1 from STRING data base. Ythdc1 has a high level of homology with *Arabidopsis* Cpsf30. Ythdc1 is predicted to interact with the cleavage and polyadenylation machinery.

6.10 Chapter 6: Summary

Ythdc1 appears to be localised in the chromatin whereas the methyltransferase complex resides predominantly in the nucleoplasm. This suggests Ythdc1 may carry out other functions prior to methylation. Interestingly Ythdc1 and the TREX complex showed a similar fractionation pattern. Further data suggested an association between the TREX complex/Nxf1 and Ythdc1. Furthermore there appears to be a compensatory mechanism in place for Alyref/Chtop binding Ythdc1, removal of one induced increased association of the other to Ythdc1. This may indicate a possible redundancy mechanism in the observed cross talk between pathways. Removal of Alyref/Chtop, but not Alyref, results in a decrease deposition of Ythdc1 upon methylated transcripts, indicating a TREX dependent recruitment of Ythdc1 to the mRNA. Although Ythdc1 associates with the TREX complex and Nxf1 it does not act as a classical export component in our MS2-tethering assay.

Wtap and Mettl3 of the methyltransferase complex interact with Ythdc1 but Kiaa1429 does not. Wtap being associated to a greater degree when compared with Mettl3, suggesting a distal relationship between Mettl3 and Ythdc1. This is the first evidence linking the m^6A writers and reader in the same complex. Further data revealed an increase accumulation of Alyref upon Ythdc1 in a Wtap and Mettl3 knockdown. If we were to speculate on the data presented we may contrive Ythdc1 associates with TREX prior to the methyltransferase complex.

Ythdc1 RNAi results in reduced cell growth and ultimately lethality over a 120 hour induction time period. Although Ythdc1 RNAi results in call death it does not appear to be as the result of a global mRNA export block or disruption of the TREX complex. However targeted analysis of methylated transcripts based of published iCLIP data (Xu *et al.*, 2014) revealed, Ythdc1 bound transcripts do indeed accumulate in the nucleus upon 72 hours of Ythdc1 RNAi. The nuclear accumulated transcripts appear to have undergone splicing. Finally the knockdown of Ythdc1 yields an increase in Alyref deposition upon m^6A/Ythdc1 bound transcripts. This is a phenocopy of the results presented in chapter 5 for

Mettl3/Kiaa1429. We can again hypothesise that the increased Alyref levels are due to a defect in handover to Nxf1. We can rule out the increased Alyref being a result of increased Alyref protein expression as throughout our data the proteins levels of Alyref do not changed upon Ythdc1 RNAi. A second possibility could be a defect in cleavage and polyadenylation of the m^6A containing transcripts. However further experimental evidence is required to confirm an interaction and role of Ythdc1 with the cleavage and polyadenylation machinery.

Chapter 7: Discussion

7.1 Hypophosphorylated Wtap may act as an export adaptor.

Investigation into Wtap revealed it is heavily phosphorylated in its C-terminus and also contains a number of SR repeats. Removing the C-terminus results in a loss of RNA binding (Figure 4.7a) but does not changes Wtap cellular localisation pattern (Figure 4.6). Wtap interacting partners may associate via the N-terminus keeping it in situ. Dephosphorylating Wtap resulted in a reduced IP of Mettl3/Mettl14, but increases the IP with export receptor Nxf1, illustrated in Figure 7.1. This is counter to the current published Co-IP data indicating Mettl3/Mettl14 bind to only the N-terminus (1-250aa) of Wtap (Ping et al, 2014). It is difficult to conclude dephosphorylation of Wtap inhibits Mettl3 binding as our experimental design treats the entire lysate with alkaline phosphatase, therefore many other proteins will be dephosphorylated. It has been reported phosphorylation is required for heterodimeric Mettl3/Mettl14 complex formation (Wang *et al.,* 2016), therefore disrupting this may indirectly affect Wtap/Mettl3/Mettl14 complex formation. Identification of four SR repeats in the C-terminus and Co-IP experiments with hypophosphorylated Wtap (Figure 4.8a,b,c) revealed it may act in a similar fashion to other SR proteins (Muller et al., 2016) working as an export adaptor with Nxf1. The Hypophosphorylated Wtap interaction with Nxf1 appears to be independent of Kiaa1429 (Figure 4.8b) suggesting it's also not an m^6A dependent process. Figure 4.8c displays Kiaa1429 and Nxf1 Co-IP with Wtap, this may be due to incomplete dephosphorylation of Wtap, and therefore the IP is of a mixed phosphostate population.

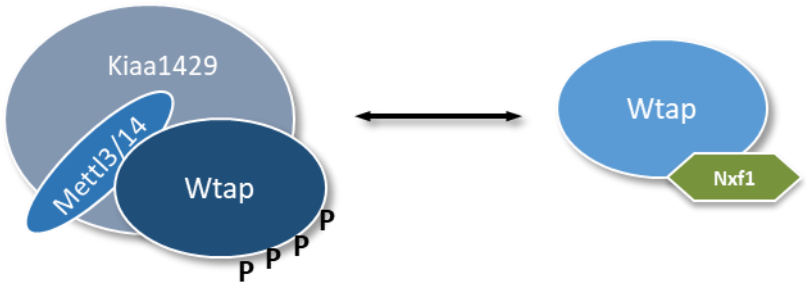

Figure 7.1 Wtap exists in multiple complex's depending in its phosphorylation state. Our data indicated Wtap associates with Mettl3/Mettl14 and Kiaa1429 in a phosphorylated state. On the other hand hypophosphorylated Wtap associates with export receptor Nxf1.

7.2 TREX associates with the m^{6}A writer machinery and Ythdc1.

We identified interactions between the m^{6}A machinery (Wtap, Kiaa1429, Mettl3/Mettl14 and Ythdc1) and TREX/Nxf1 through Co-IP experiments. This builds on previous results indicating an overlap between the two complexes (Masuda *et al.,* 2005; Horiuchi *et al.,* 2013; Zheng *et al.,* 2013; Bansal *et al.,* 2014). It appears Kiaa1429 is the central component linking both complexes (TREX and writers) together, as knockdown of Kiaa1429 results in a decrease Co-IP between Wtap, TREX and Mettl3 (Figure 3.7). However, we do not observe any export phenotype upon Kiaa1429 knockdown (Figure 3.8 and Figure 5.3b). The reasoning behind the lack of a phenotype maybe due to the upregulation of Wtap, at the protein (Figure 3.7) and RNA level (Figure 5.1e), compensating for the loss of Kiaa1429.

Ythdc1 Co-IP data revealed an association with the TREX complex and Nxf1 similar to the writers Kiaa1429 and Wtap. We observed possible mutually exclusive binding of Chtop/Alyref to Ythdc1 (Figure 6.2d). Removing Chtop resulted in an increase of Alyref associating with Ythdc1. This adds confidence to our Co-IP data. Furthermore we identified Wtap, and to some extent Mettl3, associate with Ythdc1, Figure 6.4a. An interaction between m^{6}A readers and writers has not yet been published. Knockdown of Wtap or Mettl3 resulted in an increased Co-IP between Ythdc1 and Alyref (Figure 6.4b) whereas Kiaa1429 knockdown did not increase Alyref-Ythdc1 association. This suggests the interaction between Ythdc1 and Alyref does not require the regulatory or enzymatic element of the m^{6}A writer complex and said interaction may be independent, and possibly prior, to methylation.

7.3 A novel mechanism for TREX deposition.

Building on our association data between the three elements TREX, m^6A writers and Ythdc1 we conducted nuclear cytoplasmic fractionation and RIP experiments. Firstly, we required the simultaneous knockdown of two writers to observe an mRNA export block, implying redundancy within the system. However, this was not the case for Ythdc1, suggesting no redundancy for the actions of Ythdc1. This may also explain the cell death observed post 72 hours of Ythdc1 RNAi (Figure 6.5).

Nuclear cytoplasmic experiments on Mettl3/Kiaa1429, Wtap/Kiaa1429 and Ythdc1 knockdown resulted in a block of export for select m^6A targeted transcripts (*Taf7, Dicer1* and *Ptpn12*). However, our initial observation was on a small select group. The sequencing of poly A+ RNA from nuclear and cytoplasmic fractions from both Control and Wtap/Kiaa1429 siRNA revealed 73% of all nuclear accumulated transcripts were impaired by m^6A depletion. Interestingly the nuclear fraction of Wtap/Kiaa1429 contained an overrepresentation of transcripts containing long exons (1000bp+), more importantly long terminal 3' exons, and a high number of m^6A sites (5+) (see Figures 5.6c-e). Although not confirmed by sequencing analysis we predict, due to recent publications, that the majority of nuclear accumulated transcripts have undergone splicing (Ke *et al.,* 2017). With these findings in mind we can begin to consider the possibility of an m^6A writer and TREX dependent export mechanism for transcripts with long exons. The current models of mRNA export indicates TREX deposition is completed post splicing, therefore being deposited close to the EJC, TREX is also recruited via the CBC (Cheng *et al,.* 2006; Gromadzka *et al.,* 2016). With this in mind we do not currently have an explanation of how TREX is deposited 1000bp away from the EJC within long exons, see Figure 5.2b (unpublished iCLIP). The above observations of our nuclear accumulated transcripts inply the possibility of an m^6A writer, and by extension the m^6A mark, dependent mechanism for TREX deposition upon long exons and intronless transcripts.

RIP experiments were conducted in all knockdown background to give merit to the statement above. Too our surprise we observed a number of different phenotypes depending upon what writer/reader or TREX member was knocked down. To put our results into context we constructed a simplified idealist model in Figure 7.2. Initial recruitment of TREX to certain mRNAs is dependent on Wtap/Kiaa1429 (Figure 5.8a and b), as knocking them down results in a decrease of Alyref and Uap56 upon target mRNAs. This is not just at the m^6A position but throughout the transcript. Further evidence for Wtap dependent TREX deposition is presented upon knockdown of Mettl3/Kiaa1429, we observed no loss of Alyref but instead, an increase. Our explanation for this is twofold, Wtap levels increase upon Mettl3/Kiaa1429 knockdown. Simply put if, as we suggest, Wtap is responsible for recruiting TREX (specifically Alyref) more Wtap upon the mRNA may result in more Alyref upon select transcripts. Secondly we hypothesise the enzymatic addition of m^6A via Mettl3 is required for the continued maturation of the complex. Therefore removing Mettl3 hinders progression of the complex, leading to a build-up of TREX. As well as a methyltransferase and TREX complex association, our data suggests an early Ythdc1 recruitment prior to the addition of m^6A. We observed decreased Ythdc1 upon the mRNA in a TREX knockdown (Figure 6.4e-d). We only observe a reduction of Ythdc1 when we knockdown two major components of TREX (Alyref/Chtop) and the deposition of other factors was unchanged on the mRNA. We do not see a loss of Ythdc1 on the mRNA when knocking down the export receptor Nxf1. We did not see a change in Wtap mRNA deposition upon TREX knockdown. Suggesting TREX may be required for Ythdc1s recruitment to the mRNP. The final experiments leading to the construction of the schematic of Step 1 was the association between Wtap/Mettl3 and Ythdc1. Ythdc1 associates with Wtap (and partially with Mettl3), knockdown of Wtap culminates in an increase of Ythdc1-Alyref association. We believe this is indicative of another complex maturation defect. We would predict a reduction of m^6A upon Wtap/Mettl3 knockdown, therefore a reduction of Ythdc1 bound to the mRNA. Ythdc1 has a very low affinity for unmodified mRNA (Zhang et al., 2010). We can hypothesise a

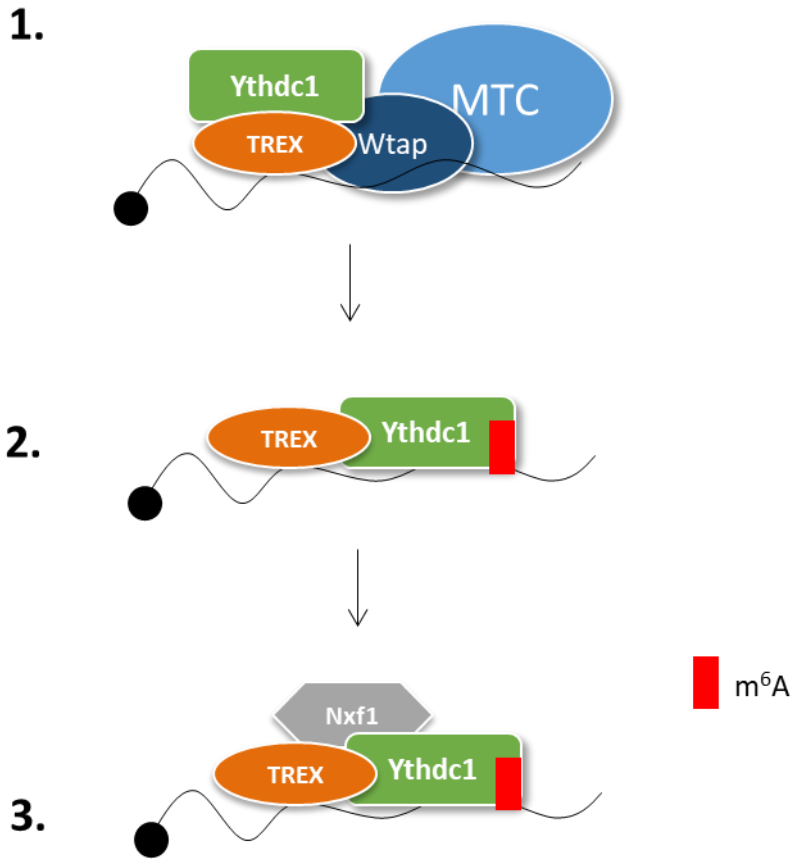

Figure 7.2 Simplistic model of TREX and m^{6}A machinery working in a cooperative mRNA nuclear export pathway. Step 1 consists of the reader Ythdc1 bound to TREX and Wtap. Our data suggests Wtap is responsible for initial TREX recruitment to the mRNA. Step two is post methylations. The writer complex dissociates allowing Ythdc1 to bind the m^{6}A modification. Step 3 is the interaction of export receptor Nxf1 with TREX and Ythdc1. It must be noted that we propose this only occurs on a small subset of m^{6}A containing transcripts with long 3' terminal exons.

Ythdc1 association with TREX/Wtap prior to the addition of m^{6}A. We have TREX-Ythdc1 bound to the methyltransferase complex primarily via Kiaa1429 and Wtap. The enzymatic addition of m^{6}A results in the disassociation of the writers and Ythdc1 binding the m^{6}A mark, Step 2. We assume the methyltransferase complex dissociates from the mRNP post m^{6}A addition due to Ythdc1 mRNA binding having the same footprint. Finally Step 3 was constructed from the Nxf1-Ythdc1 Co-IP data (Figure 6.2d). We observed an increase of Alyref bound to select transcripts when we knockdown Ythdc1. With this knowledge and our current data we can predict the knockdown of Ythdc1 results in a late stage export block. In Ythdc1 RNAi conditions, mRNA will be loaded with TREX but not exported, implying a possible defect in Nxf1 recruitment. Unfortunately we were unable to obtain RIP data for Nxf1 in Ythdc1 RNAi possibly due to its transient RNA binding mechanism.

We believe we have evidence to suggest the m^{6}A writer complex and reader (Ythdc1) play a role in the nuclear export of a subset of m^{6}A containing transcripts. This pathway appears to aid in the deposition of TREX upon long exon containing transcripts. Our simplified model in Figure 7.2 is constructed from our current data and we aim to reinforce this with future studies.

7.4 Ythdc1 cell death and export block.

The published GO analysis of Ythdc1 targets (Xu *et al.*, 2014) is consistent of the categories for our nuclear accumulated/m^{6}A containing transcripts within Wtap/Kiaa1429 knockdown (Figure 5.6b). Cell cycle, gene expression and DNA repair are over represented. We believe the export block induced by Ythdc1 RNAi is responsible for the cell death post 72 hours (Figure 6.5b). We predict transcripts required for cell growth/protein expression are trapped in the nucleus.

Furthermore the literature indicates Srsf3 and Ythdc1 are associated, and involved in alternative splicing of a transcript subset (Xiao *et al.*, 2016). Srsf3 was also found to act as an export adaptor to the receptor Nxf1 (Muller-McNicoll *et al.*, 2016). It is feasible to assume Srsf3 and Ythdc1 are present in the final mature

configuration of the export complex with Nxf1 based of our Co-IP data. Both Srsf3 and Ythdc1 have a 3' preference within their targets with evidence of Nxf1 3' recruitment being partially down to the action of Srsf3. Moreover this also overlaps with the 3'deposition of Ythdc1. We believe Ythdc1 plays an important role in the final licencing of a transcript for Nxf1 dependent nuclear export.

Finally we discovered a possible link indicating Ythdc1 could have a role in the cleavage and polyadenylation pathway. Ythdc1 shares homology with *Arabidopsis* Cpsf30, a YTH-domain containing polyadenylation factor (Fray and Simpson, 2015). Analysis of Ythdc1 association partners within the STRING database revealed multiple Cpsf proteins. Although we only tested a limited number of transcripts in Ythdc1 RNAi, we predict Ythdc1 would only act in the cleavage/polyadenylation of a subset of methylated transcripts. Further experimental evidence is required to solidify this hypothesis, if true our model presented above would still be valid. The association of TREX and writers would be unchanged but an addition step of Ythdc1 and TREX facilitating the polyadenylation of specific transcripts would occur. This may also explain the alternative polyadenylation identified within our Wtap/Kiaa1429 knockdown, Figure 5.7.

7.5 Conclusion

We believe we have identified a cooperative pathway for the deposition of TREX upon long exons and intronless transcripts. Our evidence indicates a dynamic complex consisting of TREX, m^6A writers and readers and as the transcripts mature the complex may alter. Furthermore, we have discovered Ythdc1 may also play a role in the cleavage and polyadenylation of a subset of transcripts.

7.6 Future Work

To increase our understanding of the C-terminus of Wtap we would aim to do a more in-depth analysis. Mass spectrometry should be conducted on Flag-Wtap and Flag-ΔC to identify differences in its association profile. Mutations should be introduced converting each and all of the SR region to an alanine followed by pulldowns with Nxf1. This will enable a more targeted look at the possible SR interactions with Nxf1.

Further analysis is required on our Wtap/Kiaa1429 sequencing data set. We aim to confirm no splicing defect is present. It would also be desirable to construct a Wtap knockout cell line and repeat the Wtap/Kiaa1429 experiments. To confirm if a siRNA efficiency was not the result of no identifying a phenotype upon knockdown of individual members.

To confirm our hypothesis of more Wtap in Mettl3/Kiaa1429 knockdown is responsible for the increase of Alyref on the mRNA we will over express Flag-Wtap and Flag-GFP in Hek293t and conduct an Alyref RIP. If we observe more Alyref upon the mRNA this will confirm our hypothesis. Alternatively the idea of Mettl3 catalytic activity being required for complex progression can be tested via mutational analyse. Point mutations in either of Mettl3s CCCH motifs result in the loss of m^6A catalytic ability of (Wang *et al*., 2016). Expression of the Mettl3 mutants followed by an Alyref RIP would allow us to identify if the catalytic activity is required for complex progression.

The mutations mentioned above would also be a bases for further Ythdc1 studies. Switching one or all of the tryptophan residues in the Ythdc1 aromatic m^6A binding cage results in no mRNA binding (Xu *et al*>, 2015b). This would allow us to confirm if the initial binding of Ythdc1 to TREX is dependent on m^6A, building on evidence of a prior association with Wtap and TREX. As we observed Ythdc1 binding Nxf1 it would be interesting to assess where on Nxf1, Ythdc1 binds. Using truncated Nxf1 constructs from previous studies (Viphakone, Guillaume M Hautbergue, *et al.*, 2012) and Flag-Ythdc1 pulldowns can easily be done to identify

the specific binding site. Comparing data sets already published in an Ythdc1 knockdown will allow us to look for any polyadenylation/termination defect (Xiao *et al.*, 2016). Experimental confirmation of a termination defect can then be established using qPCR with primers upstream and downstream of the polyadenylation site. Further sequencing should be conducted using our nuclear/cytoplasmic fractionation method in an Ythdc1 RNAi background. This will allow us to compare the transcripts sensitive and cross reference with our Wtap/Kiaa1428 data sets. Furthermore computational analysis of Ythdc1 PAR CLIP (Xu *et al.*, 2014) and Alyref, Chtop and Nxf1 iCLIP (unpublished) can be used to construct further experimental questions and confirm if Ythdc1 3' binding correlates with that of Alyref.

References

Aguilo, F., Zhang, F., Sancho, A., Fidalgo, M., Di Cecilia, S., Vashisht, A., Lee, D. F., Chen, C. H., Rengasamy, M., Andino, B., Jahouh, F., Roman, A., Krig, S. R., Wang, R., Zhang, W., Wohlschlegel, J. A., Wang, J. and Walsh, M. J. (2015) 'Coordination of m6A mRNA Methylation and Gene Transcription by ZFP217 Regulates Pluripotency and Reprogramming', *Cell Stem Cell*. Elsevier Inc., 17(6), pp. 689–704. doi: 10.1016/j.stem.2015.09.005.

Alarcón, C. R., Goodarzi, H., Lee, H., Liu, X., Tavazoie, S. and Tavazoie, S. F. (2015) 'HNRNPA2B1 Is a Mediator of m(6)A-Dependent Nuclear RNA Processing Events.', *Cell*, 162(6), pp. 1299–308. doi: 10.1016/j.cell.2015.08.011.

Alarcón, C. R., Lee, H., Goodarzi, H., Halberg, N. and Tavazoie, S. F. (2015) 'N6-methyladenosine marks primary microRNAs for processing', *Nature*, 519(7544), pp. 482–5. doi: 10.1038/nature14281.

Amlacher, S., Sarges, P., Flemming, D., van Noort, V., Kunze, R., Devos, D. P., Arumugam, M., Bork, P. and Hurt, E. (2011) 'Insight into Structure and Assembly of the Nuclear Pore Complex by Utilizing the Genome of a Eukaryotic Thermophile', *Cell*, 146(2), pp. 277–289. doi: 10.1016/j.cell.2011.06.039.

Andersen, P. R., Domanski, M., Kristiansen, M. S., Storvall, H., Ntini, E., Verheggen, C., Schein, A., Bunkenborg, J., Poser, I., Hallais, M., S, R., Sandberg, R., berg, Hyman, A., LaCava, J., Rout, M. P., Andersen, J. S., Bertrand, E., Bertr, E. and Jensen, T. H. (2013) 'The human cap-binding complex is functionally connected to the nuclear RNA exosome.', *Nature structural {&} molecular biology*, 20(12), pp. 1367–1376. doi: 10.1038/nsmb.2703.

Arts, G.-J., Fornerod, M. and Mattaj, lain W. (1998) 'Identification of a nuclear export receptor for tRNA', *Current Biology*, 8(6), pp. 305–314. doi: 10.1016/S0960-9822(98)70130-7.

Bartel, D. P. (2004) 'MicroRNAs: Genomics, Biogenesis, Mechanism, and

Function', *Cell*, 116(2), pp. 281–297. doi: 10.1016/S0092-8674(04)00045-5.

Baßler, J., Klein, I., Schmidt, C. and Kallas, M. (2012) 'The conserved Bud20 zinc finger protein is a new component of the ribosomal 60S subunit export machinery', *and cellular biology*, pp. 1–16. Available at: http://mcb.asm.org/content/32/24/4898.short.

Batista, P. J., Molinie, B., Wang, J., Qu, K., Zhang, J., Li, L., Bouley, D. M., Lujan, E., Haddad, B., Daneshvar, K., Carter, A. C., Flynn, R. A., Zhou, C., Lim, K. S., Dedon, P., Wernig, M., Mullen, A. C., Xing, Y., Giallourakis, C. C. and Chang, H. Y. (2014) 'M^{6}A RNA modification controls cell fate transition in mammalian embryonic stem cells', *Cell Stem Cell*. Elsevier Inc., 15(6), pp. 707–719. doi: 10.1016/j.stem.2014.09.019.

Bayliss, R., Leung, S. W., Baker, R. P., Quimby, B. B., Corbett, A. H. and Stewart, M. (2002) 'Structural basis for the interaction between NTF2 and nucleoporin FxFG repeats.', *The EMBO Journal*, 21(12), pp. 2843–2853. doi: 10.1093/emboj/cdf305.

Beck, M. and Hurt, E. (2016) 'The nuclear pore complex: understanding its function through structural insight', *Nature Reviews Molecular Cell Biology*. Nature Publishing Group, 18(2), pp. 73–89. doi: 10.1038/nrm.2016.147.

Berulava, T., Rahmann, S., Rademacher, K., Klein-Hitpass, L. and Horsthemke, B. (2015) 'N6-Adenosine Methylation in MiRNAs.', *PloS one*, 10(2), p. e0118438. doi: 10.1371/journal.pone.0118438.

Bradatsch, B., Katahira, J., Kowalinski, E., Bange, G., Yao, W., Sekimoto, T., Baumgärtel, V., Boese, G., Bassler, J., Wild, K., Peters, R., Yoneda, Y., Sinning, I. and Hurt, E. (2007) 'Arx1 Functions as an Unorthodox Nuclear Export Receptor for the 60S Preribosomal Subunit', *Molecular Cell*, 27(5), pp. 767–779. doi: 10.1016/j.molcel.2007.06.034.

Braun, I. C., Herold, A., Rode, M., Conti, E. and Izaurralde, E. (2001) 'Overexpression of TAP/p15 Heterodimers Bypasses Nuclear Retention and

Stimulates Nuclear mRNA Export', *Journal of Biological Chemistry*, 276(23), pp. 20536–20543. doi: 10.1074/jbc.M100400200.

Brennan, C. M., Gallouzi, I. E. and Steitz, J. A. (2000) 'Protein ligands to HuR modulate its interaction with target mRNAs in vivo', *The Journal of Cell Biology*. Available at: http://jcb.rupress.org/content/151/1/1.abstract.

Calado, A., Treichel, N., Müller, E. C., Otto, A. and Kutay, U. (2002) 'Exportin-5-mediated nuclear export of eukaryotic elongation factor 1A and tRNA', *EMBO Journal*, 21(22), pp. 6216–6224. doi: 10.1093/emboj/cdf620.

Chang, C.-T., Hautbergue, G. M., Viphakone, N., Dijk, T. B., Philipsen, S., Wilson, S. A., van Dijk, T. B., Chang, C.-T., Hautbergue, G. M., Viphakone, N., Dijk, T. B., Philipsen, S., Wilson, S. A. and Dijk, T. (2013) 'Chtop is a component of the dynamic TREX mRNA export complex', *The EMBO Journal*, 32(3), pp. 473–486. doi: 10.1038/emboj.2012.342.

Cheng, H., Dufu, K., Lee, C.-S., Hsu, J., Dias, A. and Reed, R. (2006) 'Human mRNA Export Machinery Recruited to the 5' End of mRNA', *Cell*, 127(7), pp. 1389–1400.

Chi, B., Wang, Q., Wu, G., Tan, M., Wang, L., Shi, M., Chang, X. and Cheng, H. (2013) 'Aly and THO are required for assembly of the human TREX complex and association of TREX components with the spliced mRNA.', *Nucleic acids research*, 41(2), pp. 1294–1306.

Cook, A., Fernandez, E., Lindner, D., Ebert, J., Schlenstedt, G. and Conti, E. (2005) 'The structure of the nuclear export receptor Cse1 in its cytosolic state reveals a closed conformation incompatible with cargo binding', *Molecular Cell*, 18(3), pp. 355–367. doi: 10.1016/j.molcel.2005.03.021.

Cronshaw, J. M. (2002) 'Proteomic analysis of the mammalian nuclear pore complex', *The Journal of Cell Biology*, 158(5), pp. 915–927. doi: 10.1083/jcb.200206106.

Desrosiers, R., Friderici, K. and Rottman, F. (1974) 'Identification of Methylated

Nucleosides in Messenger RNA from Novikoff Hepatoma Cells', *Proceedings of the National Academy of Sciences*, 71(10), pp. 3971–3975. doi: 10.1073/pnas.71.10.3971.

Dominissini, D., Moshitch-Moshkovitz, S., Schwartz, S., Salmon-Divon, M., Ungar, L., Osenberg, S., Cesarkas, K., Jacob-Hirsch, J., Amariglio, N., Kupiec, M., Sorek, R. and Rechavi, G. (2012) 'Topology of the human and mouse m6A RNA methylomes revealed by m6A-seq.', *Nature*, 485(7397), pp. 201–206. doi: 10.1038/nature11112.

Du, H., Zhao, Y., He, J., Zhang, Y., Xi, H., Liu, M., Ma, J. and Wu, L. (2016) 'YTHDF2 destabilizes m6A-containing RNA through direct recruitment of the CCR4–NOT deadenylase complex', *Nature Communications*, 7, p. 12626. doi: 10.1038/ncomms12626.

Dufu, K., Livingstone, M. J., Seebacher, J., Gygi, S. P., Wilson, S. a and Reed, R. (2010) 'ATP is required for interactions between UAP56 and two conserved mRNA export proteins, Aly and CIP29, to assemble the TREX complex.', *Genes & development*, 24(18), pp. 2043–53. doi: 10.1101/gad.1898610.

Dunin-Horkawicz, S. (2006) 'MODOMICS: a database of RNA modification pathways', *Nucleic Acids Research*, 34(90001), pp. D145–D149. doi: 10.1093/nar/gkj084.

Fahrenkrog, B. and Aebi, U. (2003) 'The nuclear pore complex: nucleocytoplasmic transport and beyond', *Nature Reviews Molecular Cell Biology*, 4(10), pp. 757–766. doi: 10.1038/nrm1230.

Faza, M. B., Chang, Y., Occhipinti, L., Kemmler, S., Panse, V. G., Faza, M. B., Chang, Y., Occhipinti, L., Kemmler, S. and Panse, V. G. (2012) 'Role of Mex67-Mtr2 in the nuclear export of 40S pre-ribosomes', *PLoS genetics*. Available at: http://dx.plos.org/10.1371/journal.pgen.1002915.g011.

Finkel, D. and Groner, Y. (1983) 'Methylations of adenosine residues (m6A) in pre-mRNA are important for formation of late simian virus 40 mRNAs', *Virology*, 131(2), pp. 409–425. doi: 10.1016/0042-6822(83)90508-1.

Floer, M., Blobel, G. and Rexach, M. (1997) 'Disassembly of RanGTP karyopherinb complex, an intermediate in nuclear protein import', *Journal of Biological Chemistry*, 272(31), pp. 19538–19546.

Fornerod, M., Van Deursen, J., Van Baal, S., Reynolds, A., Davis, D., Murti, K. G., Fransen, J. and Grosveld, G. (1997) 'The human homologue of yeast CRM1 is in a dynamic subcomplex with CAN/Nup214 and a novel nuclear pore component Nup88', *EMBO Journal*, 16(4), pp. 807–816. doi: 10.1093/emboj/16.4.807.

Fornerod, M., Ohno, M., Yoshida, M. and Mattaj, I. W. (1997) 'CRM1 is an export receptor for leucine-rich nuclear export signals', *Cell*, 90(6), pp. 1051–1060. doi: 10.1016/S0092-8674(00)80371-2.

Fray, R. G. and Simpson, G. G. (2015) 'The Arabidopsis epitranscriptome', *Current Opinion in Plant Biology*. Elsevier Ltd, 27, pp. 17–21. doi: 10.1016/j.pbi.2015.05.015.

Fustin, J.-M., Doi, M., Yamaguchi, Y., Hida, H., Nishimura, S., Yoshida, M., Isagawa, T., Morioka, M. S., Kakeya, H., Manabe, I. and Okamura, H. (2013) 'RNA-Methylation-Dependent RNA Processing Controls the Speed of the Circadian Clock', *Cell*, 155(4), pp. 793–806. doi: 10.1016/j.cell.2013.10.026.

Fribourg, S., Braun, I. C., Izaurralde, E. and Conti, E. (2001) 'Structural basis for the recognition of a nucleoporin FG repeat by the NTF2-like domain of the TAP/p15 mRNA nuclear export factor', *Molecular Cell*, 8, pp. 645–656. doi: 10.1016/S1097-2765(01)00348-3.

Fustin, J.-M., Doi, M., Yamaguchi, Y., Hida, H., Nishimura, S., Yoshida, M., Isagawa, T., Morioka, M. S., Kakeya, H., Manabe, I. and Okamura, H. (2013) 'RNA-

Methylation-Dependent RNA Processing Controls the Speed of the Circadian Clock', *Cell*, 155(4), pp. 793–806. doi: 10.1016/j.cell.2013.10.026.

Gebhardt, A., Habjan, M., Benda, C., Meiler, A., Haas, D. A., Hein, M. Y., Mann, A., Mann, M., Habermann, B. and Pichlmair, A. (2015) 'mRNA export through an additional cap-binding complex consisting of NCBP1 and NCBP3.', *Nature communications*. Nature Publishing Group, 6, p. 8192. doi: 10.1038/ncomms9192.

Geula, S., Moshitch-Moshkovitz, S., Dominissini, D., Mansour, A. A., Kol, N., Salmon-Divon, M., Hershkovitz, V., Peer, E., Mor, N., Manor, Y. S., Ben-Haim, M. S., Eyal, E., Yunger, S., Pinto, Y., Jaitin, D. A., Viukov, S., Rais, Y., Krupalnik, V., Chomsky, E., Zerbib, M., Maza, I., Rechavi, Y., Massarwa, R., Hanna, S., Amit, I., Levanon, E. Y., Amariglio, N., Stern-Ginossar, N., Novershtern, N., Rechavi, G. and Hanna, J. H. (2015) 'm6A mRNA methylation facilitates resolution of naive pluripotency toward differentiation', *Science*, 347(6225), pp. 1002–1006. doi: 10.1126/science.1261417.

Görlich, D., Dabrowski, M., Bischoff, F. R., Kutay, U., Bork, P., Hartmann, E., Prehn, S. and Izaurralde, E. (1997) 'A novel class of RanGTP binding proteins.', *The Journal of Cell Biology*, 138(1), pp. 65–80. Available at: s.

Gromadzka, A. M., Steckelberg, A. L., Singh, K. K., Hofmann, K. and Gehring, N. H. (2016) 'A short conserved motif in ALYREF directs cap- and EJC-dependent assembly of export complexes on spliced mRNAs', *Nucleic Acids Research*, 44(5), pp. 2348–2361. doi: 10.1093/nar/gkw009.

Güttler, T. and Görlich, D. (2011) 'Ran-dependent nuclear export mediators: a structural perspective.', *The EMBO journal*, 30(17), pp. 3457–74. doi: 10.1038/emboj.2011.287.

Han, S. P., Tang, Y. H. and Smith, R. (2010) 'Functional diversity of the hnRNPs: past, present and perspectives.', *The Biochemical journal*, 430(3), pp. 379–392. doi: 10.1042/BJ20100396.

Hartmann, A. M., Nayler, O., Schwaiger, F. W., Obermeier, A. and Stamm, S. (1999) 'The interaction and colocalization of Sam68 with the splicing-associated factor YT521-B in nuclear dots is regulated by the Src family kinase p59(fyn).', *Molecular biology of the cell*, 10(11), pp. 3909–26. doi: 10.1091/mbc.10.11.3909.

Haussmann, I. U., Bodi, Z., Sanchez-Moran, E., Mongan, N. P., Archer, N., Fray, R. G. and Soller, M. (2016) 'm6A potentiates Sxl alternative pre-mRNA splicing for robust Drosophila sex determination', *Nature*. Nature Publishing Group. doi: 10.1038/nature20577.

Hautbergue, G., Hung, M., Golovanov, A., Lian, L. and Wilson, S. (2008) 'Mutually exclusive interactions drive handover of mRNA from export adaptors to TAP', *Proceedings of the National Academy of Sciences*, 105(13), pp. 5154–5159.

Hautbergue, G. M., Lian, L.-Y., Clayton, J., Wilson, S. A., Phelan, M. M., Phelan, M., Goult, B., Goult, B. T., Clayton, J. C., Hautbergue, G. M., Wilson, S. A. and Lian, L.-Y. (2012) 'The structure and selectivity of the SR protein SRSF2 RRM domain with RNA.', *Nucleic acids research*, 40(7), pp. 3232–3244. doi: 10.1093/nar/gkr1164.

Hellmuth, K., Lau, D. M., Bischoff, F. R., Künzler, M., Hurt, E. and Simos, G. (1998) 'Yeast Los1p has properties of an exportin-like nucleocytoplasmic transport factor for tRNA.', *Molecular and cellular biology*, 18(11), pp. 6374–86. doi: 10.1128/MCB.18.11.6374.

Herold, A., Klymenko, T., Izaurralde, E., Herold, A., Klymenko, T. and Izaurralde, E. (2001) 'NXF1 / p15 heterodimers are essential for mRNA nuclear export in NXF1 / p15 heterodimers are essential for mRNA nuclear export in Drosophila', *Spring*, pp. 1768–1780.

Horiuchi, K., Kawamura, T., Iwanari, H., Ohashi, R., Naito, M., Kodama, T. and Hamakubo, T. (2013) 'Identification of Wilms' tumor 1-associating protein complex and its role in alternative splicing and the cell cycle.', *The Journal of biological chemistry*. American Society for Biochemistry and Molecular Biology,

288(46), pp. 33292–33302. doi: 10.1074/jbc.M113.500397.

Horiuchi, K., Umetani, M., Minami, T., Okayama, H., Takada, S., Yamamoto, M., Aburatani, H., Reid, P. C., Housman, D. E., Hamakubo, T. and Kodama, T. (2006) 'Wilms' tumor 1-associating protein regulates G2/M transition through stabilization of cyclin A2 mRNA', *Proceedings of the National Academy of Sciences of the United States of America*. National Acad Sciences, 103(46), pp. 17278–17283. doi: 10.1073/pnas.0608357103.

Huang, Y., Yan, J., Li, Q., Li, J., Gong, S., Zhou, H., Gan, J., Jiang, H., Jia, G.-F., Luo, C. and Yang, C.-G. (2015) 'Meclofenamic acid selectively inhibits FTO demethylation of m6A over ALKBH5.', *Nucleic acids research*. Oxford University Press, 43(1), pp. 373–384. doi: 10.1093/nar/gku1276.

Hülsmann, B. B., Labokha, A. A. and Görlich, D. (2012) 'The permeability of reconstituted nuclear pores provides direct evidence for the selective phase model.', *Cell*, 150(4), pp. 738–751. doi: 10.1016/j.cell.2012.07.019.

Hung, M.-L., Walsh, M. J., Snijders, A. P. L., Chang, C.-T., Jones, R., Ponting, C. P. and Dickman, M. J. (2009) 'UIF, a New mRNA Export Adaptor that Works Together with REF/ALY, Requires FACT for Recruitment to mRNA', *Current Biology*, 19(22), pp. 1918–1924. doi: 10.1016/j.cub.2009.09.041.

Hung, M. L., Hautbergue, G. M., Snijders, A. P. L., Dickman, M. J. and Wilson, S. A. (2010) 'Arginine methylation of REF/ALY promotes efficient handover of mRNA to TAP/NXF1', *Nucleic Acids Research*, 38(10), pp. 3351–3361. doi: 10.1093/nar/gkq033.

Katahira, J., Yoneda, Y., Katahira, J. and Yoneda, Y. (2009) 'Roles of the TREX complex in nuclear export of mRNA.', *RNA biology*, 6(2), pp. 149–152. Available at: http://eutils.ncbi.nlm.nih.gov/entrez/eutils/elink.fcgi?dbfrom=pubmed&id=19229134&retmode=ref&cmd=prlinks.

Ke, S., Alemu, E. A., Mertens, C., Gantman, E. C., Fak, J. J., Mele, A., Haripal, B.,

Zucker-Scharff, I., Moore, M. J., Park, C. Y., Vågbø, C. B., Kuśnierczyk, A., Klungland, A., Darnell, J. E. and Darnell, R. B. (2015) 'A majority of m6A residues are in the last exons, allowing the potential for 3' UTR regulation', *Genes and Development*, 29(19), pp. 2037–2053. doi: 10.1101/gad.269415.115.

Ke, S., Pandya-jones, A., Saito, Y., Fak, J. J., Vågbø, C. B., Geula, S., Hanna, J. H., Black, D. L., Jr, J. E. D. and Darnell, R. B. (2017) 'm 6 A mRNA modifications are deposited in nascent pre-mRNA and are not required for splicing but do specify cytoplasmic turnover', pp. 990–1006. doi: 10.1101/gad.301036.117.

Kennedy, E. M., Bogerd, H. P., Kornepati, A. V. R., Kang, D., Ghoshal, D., Marshall, J. B., Poling, B. C., Tsai, K., Gokhale, N. S., Horner, S. M. and Cullen, B. R. (2016) 'Posttranscriptional m6A Editing of HIV-1 mRNAs Enhances Viral Gene Expression', *Cell Host and Microbe*. Elsevier Inc., 19(5), pp. 675–685. doi: 10.1016/j.chom.2016.04.002.

Kutay, U., Ralf Bischoff, F., Kostka, S., Kraft, R. and Görlich, D. (1997) 'Export of importin α from the nucleus is mediated by a specific nuclear transport factor', *Cell*, 90(6), pp. 1061–1071. doi: 10.1016/S0092-8674(00)80372-4.

Lacadie, S. A. and Rosbash, M. (2005) 'Cotranscriptional spliceosome assembly dynamics and the role of U1 snRNA:5???ss base pairing in yeast', *Molecular Cell*, 19(1), pp. 65–75. doi: 10.1016/j.molcel.2005.05.006.

Lee, M., Kim, B. and Kim, V. N. (2014) 'Emerging roles of RNA modification: M6A and U-Tail', *Cell*. Elsevier Inc., 158(5), pp. 980–987. doi: 10.1016/j.cell.2014.08.005.

Lence, T., Akhtar, J., Bayer, M., Schmid, K., Spindler, L., Ho, C. H., Kreim, N., Andrade-Navarro, M. A., Poeck, B., Helm, M. and Roignant, J.-Y. (2016) 'm6A modulates neuronal functions and sex determination in Drosophila', *Nature*. Nature Publishing Group. doi: 10.1038/nature20568.

Li, F., Zhao, D., Wu, J. and Shi, Y. (2014) 'Structure of the YTH domain of human YTHDF2 in complex with an m6A mononucleotide reveals an aromatic cage for

m6A recognition', *Cell Research*, 24, pp. 1490–1492. doi: 10.1038/cr.2014.153.

Libri, D., Dower, K., Boulay, J., Thomsen, R., Rosbash, M. and Jensen, T. H. (2002) 'Interactions between mRNA export commitment, 3'-end quality control, and nuclear degradation.', *Molecular and cellular biology*, 22(23), pp. 8254–66. doi: 10.1128/MCB.22.23.8254.

Lichinchi, G., Zhao, B. S., Wu, Y., Lu, Z., Qin, Y., He, C. and Rana, T. M. (2016) 'Dynamics of Human and Viral RNA Methylation during Zika Virus Infection', *Cell Host & Microbe*. Elsevier Inc., 20(5), pp. 666–673. doi: 10.1016/j.chom.2016.10.002.

Liker, E., Fernandez, E., Izaurralde, E. and Conti, E. (2000) 'The structure of the mRNA export factor TAP reveals a cis arrangement of a non-canonical RNP domain and an LRR domain.', *The EMBO journal*, 19(21), pp. 5587–5598. doi: 10.1093/emboj/19.21.5587.

Linder, B., Grozhik, A. V, Olarerin-George, A. O., Meydan, C., Mason, C. E. and Jaffrey, S. R. (2015) 'Single-nucleotide-resolution mapping of m6A and m6Am throughout the transcriptome', *Nature Methods*. Nature Publishing Group, 12(8), pp. 767–772. doi: 10.1038/nmeth.3453.

Lipowsky, G., Bischoff, F. R., Izaurralde, E., Kutay, U., Schäfer, S., Gross, H. J., Beier, H. and Görlich, D. (1999) 'Coordination of tRNA nuclear export with processing of tRNA.', *RNA (New York, N.Y.)*, 5(4), pp. 539–49. doi: 10.1017/S1355838299982134.

Little, N. A., Hastie, N. D. and Davies, R. C. (2000) 'Identification of WTAP, a novel Wilms' tumour 1-associating protein', *Human Molecular Genetics*. Oxford University Press, 9(15), pp. 2231–2239.

Liu, J., Yue, Y., Han, D., Wang, X., Fu, Y., Zhang, L., Jia, G., Yu, M., Lu, Z., Deng, X., Dai, Q., Chen, W. and He, C. (2014) 'A METTL3-METTL14 complex mediates mammalian nuclear RNA N6-adenosine methylation.', *Nature chemical biology*, 10(2), pp. 93–5. doi: 10.1038/nchembio.1432.

Liu, N., Dai, Q., Zheng, G., He, C., Parisien, M. and Pan, T. (2015) 'N(6)-methyladenosine-dependent RNA structural switches regulate RNA-protein interactions.', *Nature*, 518(7540), pp. 560–564. doi: 10.1038/nature14234.

Lund, E., Güttinger, S., Calado, A., Dahlberg, J. E. and Kutay, U. (2004) 'Nuclear export of microRNA precursors.', *Science*, 303(5654), pp. 95–98. doi: 10.1126/science.1090599.

Luo, M. L., Zhou, Z., Magni, K., Christoforides, C., Rappsilber, J., Mann, M. and Reed, R. (2001) 'Pre-mRNA splicing and mRNA export linked by direct interactions between UAP56 and Aly.', *Nature*, 413(6856), pp. 644–7. doi: 10.1038/35098106.

Luo, M., Zhou, Z., Magni, K., Christoforides, C., Rappsilber, J., Mann, M. and Reed, R. (2001) 'Pre-mRNA splicing and mRNA export linked by direct interactions between UAP56 and Aly.', *Nature*, 413(6856), pp. 644–647.

M??ller-McNicoll, M., Botti, V., de Jesus Domingues, A. M., Brandl, H., Schwich, O. D., Steiner, M. C., Curk, T., Poser, I., Zarnack, K. and Neugebauer, K. M. (2016) 'SR proteins are NXF1 adaptors that link alternative RNA processing to mRNA export', *Genes and Development*, 30(5), pp. 553–566. doi: 10.1101/gad.276477.115.

Masuda, S. (2005) 'Recruitment of the human TREX complex to mRNA during splicing', *Genes & Development*, 19(13), pp. 1512–1517.

Masuda, S., Das, R., Cheng, H., Hurt, E., Dorman, N. and Reed, R. (2005a) 'Recruitment of the human TREX complex to mRNA during splicing', *Genes and Development*, 19(13), pp. 1512–1517. doi: 10.1101/gad.1302205.

Masuda, S., Das, R., Cheng, H., Hurt, E., Dorman, N. and Reed, R. (2005b) 'Recruitment of the human TREX complex to mRNA during splicing.', *Genes & development*, 19(13), pp. 1512–7. doi: 10.1101/gad.1302205.

Mauer, J., Luo, X., Blanjoie, A., Jiao, X., Grozhik, A. V., Patil, D. P., Linder, B.,

Pickering, B. F., Vasseur, J. J., Chen, Q., Gross, S. S., Elemento, O., Debart, F., Kiledjian, M. and Jaffrey, S. R. (2017) 'Reversible methylation of m6Amin the 5' cap controls mRNA stability', *Nature*. Nature Publishing Group, 541(7637), pp. 371–375. doi: 10.1038/nature21022.

Meyer, K. D., Saletore, Y., Zumbo, P., Elemento, O., Mason, C. E. and Jaffrey, S. R. (2012) 'Comprehensive analysis of mRNA methylation reveals enrichment in 3' UTRs and near stop codons', *Cell*, 149(7), pp. 1635–1646. doi: 10.1016/j.cell.2012.05.003.

Moindrot, B., Cerase, A., Coker, H., Masui, O., Grijzenhout, A., Pintacuda, G., Schermelleh, L., Nesterova, T. B. and Brockdorff, N. (2015) 'A Pooled shRNA Screen Identifies Rbm15, Spen, and Wtap as Factors Required for Xist RNA-Mediated Silencing', *Cell Reports*. The Authors, 12(4), pp. 562–572. doi: 10.1016/j.celrep.2015.06.053.

Moore, M. S. and Blobel, G. (1994) 'Purification of a Ran-interacting protein that is required for protein import into the nucleus.', *Proceedings of the National Academy of Sciences of the United States of America*, 91(October), pp. 10212–10216. doi: 10.1073/pnas.91.21.10212.

Nayler, O., Hartmann, A. M. and Stamm, S. (2000) 'The ER repeat protein YT521-B localizes to a novel subnuclear compartment', *Journal of Cell Biology*, 150(5), pp. 949–961. doi: 10.1083/jcb.150.5.949.

Okada, C., Yamashita, E., Lee, S. J., Shibata, S., Katahira, J., Nakagawa, A., Yoneda, Y. and Tsukihara, T. (2009) 'A high-resolution structure of the pre-microRNA nuclear export machinery.', *Science (New York, N.Y.)*, 326(5957), pp. 1275–9. doi: 10.1126/science.1178705.

Patil, D. P., Chen, C.-K., Pickering, B. F., Chow, A., Jackson, C., Guttman, M. and Jaffrey, S. R. (2016) 'm6A RNA methylation promotes XIST-mediated transcriptional repression', *Nature*. Nature Publishing Group, 537(7620), pp. 1–25. doi: 10.1038/nature19342.

Pemberton, L. F., Blobel, G. and Rosenblum, J. S. (1998) 'Transport routes through the nuclear pore complex', *Current Opinion in Cell Biology*, 10(3), pp. 392–399. doi: 10.1016/S0955-0674(98)80016-1.

Ping, X.-L., Sun, B.-F., Wang, L., Xiao, W., Yang, X., Wang, W.-J., Adhikari, S., Shi, Y., Lv, Y., Chen, Y.-S., Zhao, X., Li, A., Yang, Y., Dahal, U., Lou, X.-M., Liu, X., Huang, J., Yuan, W.-P., Zhu, X.-F., Cheng, T., Zhao, Y.-L., Wang, X., Danielsen, J. M. R., Liu, F. and Yang, Y.-G. (2014) 'Mammalian WTAP is a regulatory subunit of the RNA N6-methyladenosine methyltransferase', *Cell research*, 24(2), pp. 177–189. doi: 10.1038/cr.2014.3.

Proudfoot, N. J. (1977) 'Complete 3' noncoding region sequences of rabbit and human β-globin messenger RNAs', *Cell*, 10(4). doi: 10.1016/0092-8674(77)90089-7.

Rafalska, I., Zhang, Z., Benderska, N., Wolff, H., Hartmann, A. M., Brack-Werner, R. and Stamm, S. (2004) 'The intranuclear localization and function of YT521-B is regulated by tyrosine phosphorylation.', *Human Molecular Genetics*. Oxford University Press, 13(15), pp. 1535–1549. doi: 10.1093/hmg/ddh167.

Reed, R. and Hurt, E. (2002) 'A conserved mRNA export machinery coupled to pre-mRNA splicing', *Cell*. Available at: http://www.sciencedirect.com/science/article/pii/S009286740200627X.

Reed, R. and Hurt, E. (2002) 'A conserved mRNA export machinery coupled to pre-mRNA splicing.', *Cell*, 108(4), pp. 523–531.

Roundtree, I. A. and He, C. (2016) 'Nuclear m6A Reader YTHDC1 Regulates mRNA Splicing', *Trends in Genetics*. Elsevier Ltd, 32(6), pp. 320–321. doi: 10.1016/j.tig.2016.03.006.

Schwartz, S., Mumbach, M. R., Jovanovic, M., Wang, T., Maciag, K., Bushkin, G. G., Mertins, P., Ter-Ovanesyan, D., Habib, N., Cacchiarelli, D., Sanjana, N. E., Freinkman, E., Pacold, M. E., Satija, R., Mikkelsen, T. S., Hacohen, N., Zhang, F., Carr, S. A., Lander, E. S. and Regev, A. (2014) 'Perturbation of m6A writers reveals

two distinct classes of mRNA methylation at internal and 5' sites', *Cell Reports*. The Authors, 8(1), pp. 284–296. doi: 10.1016/j.celrep.2014.05.048.

Segref, A., Mattaj, I. W. and Ohno, M. (2001) 'The evolutionarily conserved region of the U snRNA export mediator PHAX is a novel RNA-binding domain that is essential for U snRNA export.', *RNA (New York, N.Y.)*, 7(3), pp. 351–60. doi: 10.1017/S1355838201002278.

Shatkin, a and Manley, J. (2000) 'The ends of the affair: capping and polyadenylation.', *Nature structural biology*, 7(10), pp. 1–5. doi: 10.1038/79583.

Shi, H., Wang, X., Lu, Z., Zhao, B. S., Ma, H., Hsu, P. J. and He, C. (2017) 'YTHDF3 facilitates translation and decay of N6-methyladenosine-modified RNA', *Cell Research*. Nature Publishing Group, 27(3), pp. 315–328. doi: 10.1038/cr.2017.15.

Small, T. W. and Pickering, J. G. (2009) 'Nuclear degradation of Wilms tumor 1-associating protein and survivin splice variant switching underlie IGF-1-mediated survival.', *The Journal of biological chemistry*. American Society for Biochemistry and Molecular Biology, 284(37), pp. 24684–24695. doi: 10.1074/jbc.M109.034629.

Sträßer, K. and Hurt, E. (2000) 'Yra1p, a conserved nuclear RNA-binding protein, interacts directly with Mex67p and is required for mRNA export', *The EMBO journal*, 19(3), pp. 410–420. doi: 10.1093/emboj/19.3.410.

Strässer, K., Masuda, S., Mason, P., Pfannstiel, J., Oppizzi, M., Rodriguez-Navarro, S., Rondón, A., Aguilera, A., Struhl, K., Reed, R. and Hurt, E. (2002) 'TREX is a conserved complex coupling transcription with messenger RNA export.', *Nature*, 417(6886), pp. 304–308.

Tran, E. J. (2006) 'Dynamic Nuclear Pore Complexes: Life on the Edge', *Cell*, 125(6), pp. 1041–1053. doi: 10.1016/j.cell.2006.05.027.

Trotta, C. R., Lund, E., Kahan, L., Johnson, A. W. and Dahlberg, J. E. (2003) 'Coordinated nuclear export of 60s ribosomal subunits and NMD3 in

vertebrates', *EMBO Journal*, 22(11), pp. 2841–2851. doi: 10.1093/emboj/cdg249.

Viphakone, N., Cumberbatch, M. G., Livingstone, M. J., Heath, P. R., Dickman, M. J., Catto, J. W. and Wilson, S. A. (2015) 'Luzp4 defines a new mRNA export pathway in cancer cells', *Nucleic Acids Research*, 43(4), pp. 2353–2366. doi: 10.1093/nar/gkv070.

Viphakone, N., Hautbergue, G. M., Walsh, M., Chang, C.-T., Holland, A., Folco, E. G., Reed, R. and Wilson, S. A. (2012) 'TREX exposes the RNA-binding domain of Nxf1 to enable mRNA export', *Nature Communications*, p. 1006. doi: 10.1038/ncomms2005.

Viphakone, N., Hautbergue, G. M., Walsh, M., Chang, C.-T., Holland, A., Folco, E. G., Reed, R. and Wilson, S. A. (2012) 'TREX exposes the RNA-binding domain of Nxf1 to enable mRNA export.', *Nature communications*. Nature Publishing Group, 3, p. 1006. doi: 10.1038/ncomms2005.

Wang, X., Zhao, B. S., Roundtree, I. A., Lu, Z., Han, D., Ma, H., Weng, X., Chen, K., Shi, H. and He, C. (2015) 'N^6-methyladenosine modulates messenger RNA translation efficiency', *Cell*, 161(6), pp. 1388–1399. doi: 10.1016/j.cell.2015.05.014.

Wang, P., Doxtader, K. A. and Nam, Y. (2016) 'Structural Basis for Cooperative Function of Mettl3 and Mettl14 Methyltransferases', *Molecular Cell*. Elsevier Inc., 63(2), pp. 306–317. doi: 10.1016/j.molcel.2016.05.041.

Wang, X., Feng, J., Xue, Y., Guan, Z., Zhang, D., Liu, Z., Gong, Z., Wang, Q., Huang, J., Tang, C., Zou, T. and Yin, P. (2016) 'Structural basis of N6-adenosine methylation by the METTL3–METTL14 complex', *Nature*, 534(7608), pp. 575–578. doi: 10.1038/nature18298.

West, S., Gromak, N. and Proudfoot, N. J. (2004) 'Human 5' to 3' exonuclease Xrn2 promotes transcription termination at co-transcriptional cleavage sites', *Nature*, 432(7016), pp. 522–525. doi: 10.1038/nature03035.

Wu, J., Bao, A., Chatterjee, K., Wan, Y. and Hopper, A. K. (2015) 'Genome-wide screen uncovers novel pathways for tRNA processing and nuclear–cytoplasmic dynamics', *Genes and Development*, 29(24), pp. 2633–2644. doi: 10.1101/gad.269803.115.

Xiang, Y., Laurent, B., Hsu, C.-H., Nachtergaele, S., Lu, Z., Sheng, W., Xu, C., Chen, H., Ouyang, J., Wang, S., Ling, D., Hsu, P.-H., Zou, L., Jambhekar, A., He, C. and Shi, Y. (2017) 'RNA m6A methylation regulates the ultraviolet-induced DNA damage response', *Nature*. Nature Publishing Group, 543(7646), pp. 573–576. doi: 10.1038/nature21671.

Xiao, W., Adhikari, S., Wang, X.-J., Zhao, Y.-L., Yang, Y.-G., Dahal, U., Chen, Y.-S., Hao, Y.-J., Sun, B.-F., Sun, H.-Y., Li, A., Ping, X.-L., Lai, W.-Y., Wang, X., Ma, H.-L., Huang, C.-M., Yang, Y., Huang, N., Jiang, G.-B., Wang, H.-L., Zhou, Q. and Yang, Y.-G. (2016) 'A Reader YTHDC1 Regulates mRNA Splicing', *Molecular Cell*, 61, pp. 1–13. doi: 10.1016/j.molcel.2016.01.012.

Xu, C., Wang, X., Liu, K., Roundtree, I. A., Tempel, W., Li, Y., Lu, Z., He, C. and Min, J. (2014) 'Structural basis for selective binding of m6A RNA by the YTHDC1 YTH domain.', *Nature Chemical Biology*, 10(11), pp. 927–929. doi: 10.1038/nchembio.1654.

Xu, C., Liu, K., Ahmed, H., Loppnau, P., Schapira, M. and Min, J. (2015a) ' Structural Basis for the Discriminative Recognition of N 6 -Methyladenosine RNA by the Human YT521-B Homology Domain Family of Proteins ', *Journal of Biological Chemistry*, 290(41), p. 24902. doi: 10.1074/jbc.m115.680389.

Xu, C., Liu, K., Ahmed, H., Loppnau, P., Schapira, M. and Min, J. (2015b) 'Structural basis for the discriminative recognition of N6-Methyladenosine RNA by the human YT521-B homology domain family of proteins', *Journal of Biological Chemistry*, 290(41), pp. 24902–24913. doi: 10.1074/jbc.M115.680389.

Yi, R., Qin, Y., Macara, I. G. and Cullen, B. R. (2003) 'Exportin-5 mediates the

nuclear export of pre-microRNAs and short hairpin RNAs', *Genes and Development*, 17(24), pp. 3011–3016. doi: 10.1101/gad.1158803.

Yue, Y., Liu, J. and He, C. (2015) 'RNA N6-methyladenosine methylation in post-transcriptional gene expression regulation.', *Genes {&} Development*. Cold Spring Harbor Lab, 29(13), pp. 1343–1355. doi: 10.1101/gad.262766.115.

Zemp, I. and Kutay, U. (2007) 'Nuclear export and cytoplasmic maturation of ribosomal subunits', *FEBS letters*. Available at: http://www.sciencedirect.com/science/article/pii/S0014579307005376.

Zhang, Z., Theler, D., Kaminska, K. H., Hiller, M., De La Grange, P., Pudimat, R., Rafalska, I., Heinrich, B., Bujnick, J. M., Allain, F. H. T. and Stamm, S. (2010) 'The YTH domain is a novel RNA binding domain', *Journal of Biological Chemistry*, 285(19), pp. 14701–14710. doi: 10.1074/jbc.M110.104711.

Zhao, B. S., Roundtree, I. A. and He, C. (2016) 'Post-transcriptional gene regulation by mRNA modifications', *Nature Reviews Molecular Cell Biology*. Nature Publishing Group, 18(1), pp. 31–42. doi: 10.1038/nrm.2016.132.

Zhao, X., Yang, Y., Sun, B.-F., Shi, Y., Yang, X., Xiao, W., Hao, Y.-J., Ping, X.-L., Chen, Y.-S., Wang, W.-J., Jin, K.-X., Wang, X., Huang, C.-M., Fu, Y., Ge, X.-M., Song, S.-H., Jeong, H. S., Yanagisawa, H., Niu, Y., Jia, G.-F., Wu, W., Tong, W.-M., Okamoto, A., He, C., Danielsen, J. M. R., Wang, X.-J. and Yang, Y.-G. (2014) 'FTO-dependent demethylation of N6-methyladenosine regulates mRNA splicing and is required for adipogenesis.', *Cell research*, 24(12), pp. 1403–1419. doi: 10.1038/cr.2014.151.

Zheng, G., Dahl, J. A., Niu, Y., Fedorcsak, P., Huang, C. M., Li, C. J., Vågbø, C. B., Shi, Y., Wang, W. L., Song, S. H., Lu, Z., Bosmans, R. P. G., Dai, Q., Hao, Y. J., Yang, X., Zhao, W. M., Tong, W. M., Wang, X. J., Bogdan, F., Furu, K., Fu, Y., Jia, G., Zhao, X., Liu, J., Krokan, H. E., Klungland, A., Yang, Y. G. and He, C. (2013) 'ALKBH5 Is a Mammalian RNA Demethylase that Impacts RNA Metabolism and Mouse Fertility', *Molecular Cell*, 49(1), pp. 18–29. doi: 10.1016/j.molcel.2012.10.015.

Zhou, J., Wan, J., Gao, X., Zhang, X., Jaffrey, S. R. and Qian, S.-B. (2015) ‘Dynamic m(6)A mRNA methylation directs translational control of heat shock response.’, *Nature*. doi: 10.1038/nature15377.

Zolotukhin, A. S., Tan, W., Bear, J., Smulevitch, S. and Felber, B. K. (2002) ‘U2AF participates in the binding of TAP (NXF1) to mRNA.’, *The Journal of biological chemistry*, 277(6), pp. 3935–42. doi: 10.1074/jbc.M107598200.